Anderson's considerations on the flow of superfluid helium: Some offshoots

Eric Varoquaux*

CNRS-UMR 3680 and CEA-IRAMIS, Service de Physique de l'État Condensé, Centre d'Études de Saclay, 91191 Gif-sur-Yvette Cedex, France

(published 17 August 2015)

Nearly five decades have elapsed since the seminal 1966 paper of P. W. Anderson on the flow of superfluid helium, ^{4}He at that time. Some of his "considerations"—the role of the quantum phase as a dynamical variable, the interplay between the motion of quantized vortices and potential superflow, its incidence on dissipation in the superfluid and the appearance of critical velocities, the quest for the hydrodynamic analogs of the Josephson effects in helium—and the way they have evolved over the past half century are recounted in this review. But it is due to key advances on the experimental front that phase slippage could be harnessed in the laboratory, leading to a deeper understanding of superflow, vortex nucleation, the various intrinsic and extrinsic dissipation mechanisms in superfluids, macroscopic quantum effects, and the superfluid analog of both ac and dc Josephson effects—pivotal concepts in superfluid physics—have been performed. Some of the experiments that have shed light on the more intimate effect of quantum mechanics on the hydrodynamics of the dense heliums are surveyed, including the nucleation of quantized vortices both by Arrhenius processes and by macroscopic quantum tunneling, the setting up of vortex mills, and superfluid interferometry.

DOI: 10.1103/RevModPhys.87.803 PACS numbers: 67.25.dk, 67.30.ef, 03.75.Lm, 03.75.Dg

CONTENTS

Superfluids display quantum properties over large distances. Superfluid currents may persist indefinitely unlike those of ordinary fluids (Reppy and Lane, 1965); the circulation of flow velocity has been found quantized over meter-size paths (Verbeek *et al.*, 1974). These manifestations of macroscopic quantum phenomena have constituted one of the early hallmarks of experimental condensed matter physics as reviewed over the years by a number of authors.[1] They are viewed as

*eric.varoquaux@cea.fr

[1]Among these reviews, see, in particular, Vinen (1963, 1966, 1968), Khalatnikov (1965), Andronikashvili and Mamaladze (1966), Putterman and Rudnick (1971), Nozières and Pines (1990), Vollhardt and Wölfle (1990), Volovik (2003), and Sonin (2015).

supporting the concept of a macroscopic wave function extending over the whole superfluid sample as put forward by London (1954). Together with Landau's views on the irrotational nature of superfluid motion (Landau, 1941), these ideas form the basis of the two-fluid model, summarized in Sec. I, which not only describes the hydrodynamics of superfluids (Khalatnikov, 1965) but has been extended to other fields of physics such as superconductivity, the Bose-Einstein condensed gases, etc. (Enz, 1974).

Hydrodynamics, and superfluid hydrodynamics in its wake, is expected to break down at small scale when the typical lengths of the problem at hand are no longer much larger than the interatomic separation or other microscopic lengths characteristic of the internal structure of the fluid, the "size" of Cooper pairs in superfluid ^{3}He, for instance. It has however been known for a long time, notably from the ion propagation measurements of Rayfield and Reif (1964), that the relevant scale in superfluid ^{4}He is surprisingly small, of the order of angstroms. In these experiments, the velocity of vortex rings could be measured in a direct way and compared to the usual outcome of classical hydrodynamics (see Sec. II). Rayfield and Reif found that hydrodynamics remains valid down to atomic sizes. Their result holds for ^{4}He, which is a dense fluid of bosons. The relevant scale is much larger in superfluid ^{3}He, a Bardeen-Cooper-Schrieffer (BCS)-type p-wave superfluid in which the characteristic length is fixed by the size of the Cooper pair. This article aims at reviewing how the hydrodynamics of superfluid ^{4}He and ^{3}He evolves from large to small scale and ultimately breaks down at close distance, revealing the more intimate quantum properties of these fluids. This is no mean feat, as noted long ago by Uhlenbeck, who is quoted to have said "One must watch like a hawk to see Planck's constant appear in hydrodynamics" (Putterman, 1974).

The main object of study in the following is the time and space evolution of the phase of the macroscopic wave function, often simply referred to as "the phase," in so-called aperture flow. This concept of phase with wave-mechanical properties governing the evolution of macroscopic quantities has become so well known that its meaning is, wrongly perhaps, taken for granted. It was put forward by P. W. Anderson in 1966, following the lead of Feynman (1953a, 1953b, 1954, 1955), mainly by the recognition of the phase as the quantity commandeering in superfluids both the putative Josephson-type effects and dissipation caused by vortex motion. The dynamics of quantized vortices, central to Anderson's ideas, is outlined in Sec. II. A detailed understanding of these phenomena is of fundamental importance as they govern the breakdown of viscousless flow, the most noteworthy feature of superfluidity, and the appearance of an entirely new class of phenomena, the hydrodynamic analogs of the Josephson effects, that underpin the sort of interferometry that can be performed with the superfluid wave function.

These ideas were put forward in the mid-1960s, in particular, at the Sussex Meeting in 1965, by Anderson (1966a), and by a number of prominent physicists, notably Nozières and Vinen. Reliable experimental observations were performed 20 years later only, as recalled in Sec. III, giving a host of new results and insights on superfluid hydrodynamics, notably an improved understanding of critical velocities and of the nucleation of vortices, topics discussed in Secs. IV and V, of possible mechanisms for formation of vortex tangles, described in Sec. VI, of the appearance of the Josephson regime of superflow through tiny apertures, described in Sec. VII.

Presented here is a coverage of some of the ramifications of Anderson's ideas on phase slippage in superfluids. It is intended to provide a gangway between the many excellent monographs[2] that provide the background material on this subject and the more specialized research publications in the literature that give the full, raw, sometimes arcane, coverage. As such, it does not constitute a comprehensive review (space and time constraining) but touches on a few selected issues that provide the backbone of this subfield of superfluid hydrodynamics. Reviews with different flavors span over a quarter of a century and show how this field has evolved.[3]

Particularly worthy of notice are the reviews of closely related subjects, Sonin's description of vortex dynamics (Sonin, 1987, 2015), the Landau critical velocity in superfluid ^{4}He by McClintock and Bowley (1995) and in superfluid ^{3}He-B by Dobbs (2000), and vortex formation and dynamics in superfluid ^{3}He by Salomaa and Volovik (1987), Volovik (2003), and Eltsov, Krusius, and Volovik (2005). The later references also cover the exciting field of exotic topological defects in superfluid ^{3}He under rotation, not considered here.

I. THE BASIC SUPERFLUID: He-4

Helium-4 undergoes an ordering transition toward a superfluid state at $T \sim 2.17$ K under its saturated vapor pressure (SVP), which is now commonly viewed as a form of Bose-Einstein condensation. A similar transition occurs in helium-3 at $T \lesssim 2.7$ mK when Cooper pairing in a state with parallel spin $S = 1$ and relative orbital momentum $l = 1$ occurs.

A. The two-fluid hydrodynamics

The flowing superfluid helium must obey some form of hydrodynamic equations given by the general conservation laws, Galilean invariance, and the thermodynamic equation of state that should also include its superfluid properties. These equations were written down for ^{4}He by Landau (1941) (Landau and Lifshitz, 1959; Khalatnikov, 1965) who made the key assumption that in order to describe the viscousless fluid flow the independent hydrodynamical variables must include a velocity field $\mathbf{v}_s$, to which is associated a fraction ρ_s/ρ of the total density of the liquid, $\rho = m_4/v_4$ being the ^{4}He atomic mass divided by the volume occupied by one atom. This ideal inviscid fluid velocity field conforms to the Euler equation for ideal fluid flow. As a consequence, it also obeys the Kelvin-Helmholtz theorem, which states that the vorticity $\nabla \times \mathbf{v}_s$ remains constant along the fluid flow lines.[4]

[2]See, for example, Nozières and Pines (1990), Tilley and Tilley (1990), and Vollhardt and Wölfle (1990).

[3]The reviews include the work of Avenel and Varoquaux (1987, 1989), Varoquaux, Avenel, and Meisel (1987), Varoquaux, Zimmermann, and Avenel (1991), Bowley, Kirk, and King (1992), Varoquaux *et al.* (1992, 1999, 2001), Avenel, Ihas, and Varoquaux (1993), Varoquaux and Avenel (1994), Zimmermann (1996), Packard (1998, 2004), Varoquaux (2001), Davis and Packard (2002), and Sato and Packard (2012).

[4]See Landau and Lifshitz (1959), Sec. 8.

In addition to vorticity conservation, a more stringent condition was assumed by Landau (1941), namely, that the superfluid velocity field be at any instant irrotational at all points in the superfluid[5]:

$$\nabla \times \mathbf{v}_s = 0. \tag{1}$$

The superfluid fraction velocity therefore derives from a velocity potential. This property will be shown to be related to the microscopic description of the superfluid and to have far-reaching consequences.

The remainder of the fluid, the normal fraction $\rho_n = \rho - \rho_s$, to which is associated a "normal" velocity $\mathbf{v}_n$, obeys an equation similar to the Navier-Stokes equation of viscous flow. The total momentum density of the helium liquid is the sum of the contributions of these two fluids:

$$\mathbf{j} = \rho_s \mathbf{v}_s + \rho_n \mathbf{v}_n. \tag{2}$$

The superfluid part of the flow is assumed to be ideal. Therefore, it carries no entropy. The fluid entropy is transported by the normal fluid described by Landau as a gas of thermally excited elementary excitations, the phonons, or sound quanta, at long wavelengths and the rotons at wavelengths of the order of interatomic spacing, as sketched in Fig. 1. Landau attributed the nonviscous property of ^{4}He flow to the intrinsic shape of this spectrum. There exists no elementary excitation with a finite momentum $\mathbf{p} = \hbar\mathbf{k}$ and a small enough energy $\epsilon(\mathbf{p})$ to couple to a solid obstacle or a wall at rest while conserving energy and momentum at least for small enough superflow velocities. This requirement sets the Landau criterion for dissipationless flow $v_s < v_L$. The intricate problem of critical velocities above which dissipation arises in superfluid flow is dealt with in Sec. IV.

When ρ_n and ρ_s can be assumed incompressible, i.e., for small flow velocities, the separation between potential flow for $\mathbf{v}_s$ and a Poiseuille flow for $\mathbf{v}_n$ becomes exact.[6] In this approximation, superflow is effectively decoupled from normal fluid motion. It has become customary to talk somewhat loosely of the motion of the superfluid as fully distinct from that of the normal fluid. This simplified view is adopted here but, occasionally, it fails (Idowu, Kivotides *et al.*, 2000; Idowu, Willis *et al.*, 2000).

Landau's two-fluid hydrodynamics, based on early experiments on superfluids and preceded by the original suggestion of Tisza (1938a, 1938b, 1938c), accounts remarkably well for a whole class of thermodynamical and hydrodynamical properties, notably for the existence of second sound and for the nonclassical rotational inertia in Andronikashvili oscillating-disks experiments (Andronikashvili and Mamaladze, 1966). It features full internal consistency; it assumes that the motion of ρ_s is pure potential (irrotational) flow and carries no entropy, and it reaches the conclusion that, below v_L, this motion is indeed fully inviscid. It has been universally adopted.

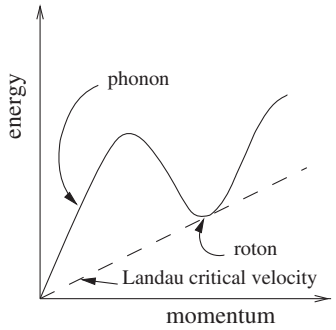

FIG. 1. Dispersion curve of the elementary excitations in superfluid ^{4}He as devised by Landau (1947).

The two-fluid hydrodynamics has been extended to the superfluid phases of ^{3}He. A number of new features appear owing to the anisotropy introduced by the Cooper pairing in a $l = 1$ state of orbital momentum. Some of these features are discussed in Sec. VII.B, but the separation of the hydrodynamics between a superfluid component and a normal component still holds as well as the existence of a Landau critical velocity.

However, this model has a number of shortcomings as pointed out by London (1954). In particular, for the purpose of this review, it does not discuss the roots of the irrotationality condition, Eq. (1), which are to be found in the existence of a complex scalar order parameter arising from the transition to a Bose-condensed state, as recognized at a very early stage of the study of superfluids by London (1938).[7] It gives no clue as to when the hydrodynamics of the superfluid fails at close distance as any macroscopic approach to hydrodynamic is bound to. Namely, it provides no way of estimating the superfluid coherence length or healing length of the macroscopic wave function. It also completely disregards the existence of quantized vorticity,[8] which, as recognized by Feynman (1953a, 1953b, 1954, 1955), and Anderson (1965), is responsible for dissipation of the superfluid motion and for different, and more commonly met in practice, critical velocity mechanisms than that of v_L.

As already noted, the Landau criterion for critical velocities rests on the fact that the elementary excitation energy spectrum is sharply defined, that is, it rises linearly as $\epsilon = cp$ with no spread in energy: there are no excitations with low energy and small moment capable of exchanging momentum

[5]This fundamental assumption, which sets an important difference between superfluids and ideal Euler fluids, is discussed later in this section. It is best justified by its consequences, the subject matter of the principal part of this review.

[6]See Landau and Lifshitz (1959), Chap. XVI.

[7]Landau and Lifshitz (1959), Sec. 128, trace its roots to the property of the energy spectrum for the low energy excitations of the superfluid, constituted by sound quanta or phonons. The Landau school (Khalatnikov, 1965, Chap. 8, and Abrikosov, Gorkov, and Dzyaloshinski, 1961, Sec. 1.3) merely states the irrotationality condition as an assumption justified by its experimental implications. London (1954), Sec. 19, actually derives this condition from a peculiar variation principle devised by Eckart (1938) but the actual significance of this principle has not been clarified, nor, as it seems, that of Eq. (1) [see, for example, the pedagogical review of Essèn and Fiolhais (2012) and the references therein on the similar problem of the Meissner effect in superconductivity].

[8]This question was nonetheless treated by the Landau school (Khalatnikov, 1965).

with the superfluid in slow motion, thus causing dissipation. This sharpness of the energy spectrum $\epsilon(p)$ has been checked directly by neutron scattering measurements of the dynamic structure factor as discussed, in particular, by Glyde (1993, 2013).

It should be pointed out that ^{3}He in the normal Fermi liquid state displays an elementary excitation spectrum with a phonon branch and a roton minimum in neutron diffraction experiments (Stirling *et al.*, 1976; Griffin, 1987). However, that spectrum is broad; ^{3}He does not exhibit superfluid properties until Cooper pairs of fermions form and Bose condense. As stressed by Feynman (1972), it really is the lack, the "scarcity" in Feynman's words, of low-lying energy levels at finite momenta, a property of the N-boson ground state with a macroscopic number of particles in it and the nonexistence of particle states with vanishing energy that results in superfluidity.

B. The superfluid order parameter

A different approach to superfluidity in which a central role was attributed to the phase of the order parameter (assumed to describe this superfluidity) was sketched by Onsager in 1948, as reported by London (1954).[9] London himself did not make much use of this concept of phase; although, on the one hand, he was the first to propose that superfluidity arises from Bose-Einstein condensation and the appearance of a "macroscopic wave function," and, on the other hand, he had earlier realized the important significance of the phase factor in quantum-mechanical wave functions.

Indeed, as soon as wave functions are considered, the concept of quantum phase becomes relevant. Its early origin can be found in a formalization of electrodynamics by Weyl (Yang, 2003), in which a gauge transformation explicitly introduces a factor e^{θ} in the theory. A change of gauge $\mathbf{A}' \rightarrow \mathbf{A} + \nabla\theta$ combined with a change of the wave function $\psi' \rightarrow \psi \exp\{ie\theta/\hbar c\}$ leaves the Schrödinger equation unchanged. The application of Weyl's prescription to quantum-mechanical systems led London to turn the exponent θ into a purely imaginary quantity $i\varphi$, φ then having the significance of an actual phase (Yang, 2003). These historical developments explain the somewhat inadequate terminology that refers to changes of the phase as gauge transformations (Greiter, 2005).[10]

But the unifying power of quantum field gauge theories ultimately carried the day. The fact that a droplet of superfluid randomly picks up a (well-defined) quantum phase when it nucleates out of vapor or out of normal fluid in a confined geometry is referred to as the breaking of gauge symmetry. The term "Bose broken symmetry" promoted, in particular, by Griffin (1987) to describe the appearance of a macroscopic number of particles in the ground state of a Bose system with the same one-particle wave function exhibiting the same phase factor gained only limited acceptance.

The ground state wave function of a homogeneous system of structureless bosons such as superfluid ^{4}He at rest can be shown quite generally to have no node[11]; it reduces to a complex scalar with a constant phase and a modulus that remains finite at every point in the sample. Atomic motion results in small-scale, small-amplitude fluctuations of this complex scalar. Averaging these fluctuations over finite, but still small, volume elements leaves a "coarse-grained" average wave function. If the system is inhomogeneous on a scale much larger than the coarse-graining volume, the modulus and phase are slowly varying functions of the position $\mathbf{r}$,

$$\Psi(\mathbf{r}) = f(\mathbf{r})e^{i\varphi(\mathbf{r})}. \tag{3}$$

This in essence is the macroscopic wave function considered by London (1938, 1954), Onsager (1949), and Feynman (1953a, 1953b, 1954, 1955, 1972). The detailed information on the localization of the bosons at $\mathbf{r}_1, \mathbf{r}_2, \ldots, \mathbf{r}_N$ and on their short-range correlations is not contained in Eq. (3). This equation is not an exact many-body ground state wave function.[12] However, considered as a "macroscopic matter field" in Anderson's own words, it has provided a lot of mileage in describing the properties of superfluids.

C. The superfluid velocity

The particle density $n(\mathbf{r})$ at point $\mathbf{r}$ of the N-boson system is given in terms of this macroscopic wave function, Eq. (3), by

$$n(\mathbf{r}) = \int d^3\mathbf{r}_1 \ldots d^3\mathbf{r}_N \Psi^\star(\mathbf{r})\Psi(\mathbf{r}) \sum_{i=1}^{N} \delta(\mathbf{r} - \mathbf{r}_i), \tag{4}$$

and the particle current density by

$$\begin{aligned}
\mathbf{j}(\mathbf{r}) &= \int d^3\mathbf{r}_1 \cdots d^3\mathbf{r}_N \\
&\quad \times \sum_{i=1}^{N} \frac{\hbar}{2im_4} [\Psi^\star(\mathbf{r})\delta(\mathbf{r} - \mathbf{r}_i)\nabla_{\mathbf{r}}\Psi(\mathbf{r}) \\
&\quad + \Psi(\mathbf{r})\nabla_{\mathbf{r}}\delta(\mathbf{r} - \mathbf{r}_i)\Psi^\star(\mathbf{r})] \\
&= \int d^3\mathbf{r}_1 \cdots d^3\mathbf{r}_N \\
&\quad \times \sum_{i=1}^{N} \frac{\hbar}{2im_4} \delta(\mathbf{r} - \mathbf{r}_i)[\Psi^\star(\mathbf{r})\nabla_{\mathbf{r}}\Psi(\mathbf{r}) - \Psi(\mathbf{r})\nabla_{\mathbf{r}}\Psi^\star(\mathbf{r})] \\
&= n(\mathbf{r}) \frac{\hbar}{m_4} \nabla\varphi(\mathbf{r}).
\end{aligned} \tag{5}$$

Equation (5) leads as a matter of course to the definition of the local mean velocity of the bosons as

[9] As implied in a footnote of a paper by Onsager (1949) and mentioned in the footnote in page 151 of London's book.

[10] In the words of Yang (2003) "Weyl in 1929 came back with an important paper that really launched what was called, and is still called, gauge theory of electromagnetism, a misnomer. (It should have been called phase theory of electromagnetism.)"

[11] See Feynman (1953a, 1953b, 1954, 1955), Penrose (1951), Penrose and Onsager (1956), or Landau and Lifshitz (1958), Sec. 61.

[12] A useful discussion of this topic can be found in Nozières and Pines (1990), Chap. 5, and also in Feynman (1972). The more rigorous approach discussed in Sec. I.D, based on the density matrix formalism, shows how such an exact wave function can be constructed.

$$\mathbf{v}_s = \frac{\hbar}{m_4}\nabla\varphi(\mathbf{r}). \tag{6}$$

According to this definition, the quantity $\mathbf{v}_s$ derives from the velocity potential $(\hbar/m_4)\varphi(\mathbf{r})$ and is identified as the quantity introduced in the two-fluid hydrodynamics under the same notation. This identification implies that the quantity $n(\mathbf{r})$ given by Eq. (4) stands for the superfluid number density ρ_s/m_4. The strong correlations between bosons in the dense system, in particular, the hard-core interactions, are averaged out in the coarse-graining procedure.

Equation (6) for the superfluid velocity and the identification of $f(\mathbf{r})$ in Eq. (3) with $(\rho_s/m_4)^{1/2}$ thus appears as a necessary formal construction that reproduces, in the classical limit, the quantity postulated by Landau to set up the two-fluid hydrodynamic model. At finite temperature, the number of atoms involved in Eqs. (4) and (5) is simply proportional to $\rho_s(T)/\rho$. The macroscopic wave function thus takes the following form:

$$\Psi(\mathbf{r}) = n_s(\mathbf{r})^{1/2}e^{i\varphi(\mathbf{r})}. \tag{7}$$

D. A more microscopic approach

So far, the discussion has been based on the general properties of the ground state wave function of N-boson systems, turned into a macroscopic wave function by coarse-grained averaging. No precise prescription on how this averaging can be carried out in practice, no clue as to the suspected relationship between Bose-Einstein condensation and superfluidity at the microscopic level have been given. Off-diagonal long-range order (ODLRO) represents the commonly acknowledged fundamental concept that achieves this connection, underlying both superconductivity and superfluidity. It defines the kind of order that prevails in a superfluid or a superconductor as put forward by Yang (1962), extending earlier work by Penrose (1951) and Penrose and Onsager (1956) while a parallel route was taken by Bogolyubov and other representatives of the Russian school,[13] and, in particular, Beliaev (1958) for the system of interacting bosons.[14]

ODLRO stands for the correlation that exists between atoms in Bose-Einstein condensates (BEC). In its simplest form, for a gas of N noninteracting Bose particles in a box of volume V, it is expressed by the single-particle density matrix

$$\rho_1(\mathbf{r},\mathbf{r}') = (N/V)\int d\mathbf{r}_2\cdots d\mathbf{r}_N\ \Psi_N^\star(\mathbf{r},\mathbf{r}_2,\ldots,\mathbf{r}_N)\Psi_N \times(\mathbf{r}',\mathbf{r}_2,\ldots,\mathbf{r}_N), \tag{8}$$

where Ψ_N is the eigenfunction of the ground state of the N-boson system at $T=0$ satisfying the boundary conditions at the box wall (rigid walls or periodic). As the particles of an ideal gas do not interact, the many-body wave function Ψ_N is simply the product of N identical single-particle wave functions $\psi(\mathbf{r})$ evaluated at $\mathbf{r}=\mathbf{r}_i$, the particle locations, suitably normalized and symmetrized. Upon integration over the $N-1$ particles $\mathbf{r}_2\cdots\mathbf{r}_N$, all that is left is the product

$$\rho_1(\mathbf{r},\mathbf{r}') = (N/V)\psi^\star(\mathbf{r})\psi(\mathbf{r}') \tag{9}$$

of single-particle wave functions, which is quite simple but highly anomalous in that it does not vanish when the two locations $\mathbf{r}$ and $\mathbf{r}'$ become far apart as it would do for a classical ideal gas. This simple remark has startling consequences. Even though the boson particles are assumed not to interact in the ideal gas, they still show a large degree of correlation. These correlations of statistical origin[15] preclude the use of the grand canonical ensemble because two widely separated parts of the system cannot be assumed to behave independently (Ziff, Uhlenbeck, and Kac, 1977).

The extension of the anomalous result Eq. (9) to nonideal Bose gases is nontrivial; one may remember for instance that a minute attractive interaction between bosons destabilizes the gas. And yet a further extension to nonequilibrium situations is mandatory to describe superflow.

Such an extension to the weakly repulsive Bose gas is implicit in the pioneering work of Bogolyubov (1947) who showed how second quantization techniques could be used to derive the property of linearity of the energy spectrum at long wavelengths $\epsilon = cp$ as asserted for the dense superfluid helium by Landau. Further progress was carried out by Beliaev (1958) using field-theoretical techniques to express the relationship between the particle number density n, the chemical potential μ, and the particle number density in the condensate n_0, which differs from n because the interaction between particles prevents all of them from falling into the lowest energy state.

Various refinements have led to what now constitutes the conventional way[16] to describe the nearly ideal BEC gas with a number density of atoms n, the Bose order parameter being written as a complex number $\sqrt{n_0}\exp(i\varphi)$ involving the number density of atoms in the ground state n_0, as expounded, for instance, by Dalfovo *et al.* (1999). This description is well grounded only for a small depletion of the condensate, i.e., for n_0/n not too far from unity. For a dense, strongly interacting Bose system, such as liquid ^{4}He, this condition is not fulfilled. The zero-momentum ground state is strongly depleted.

The spirit of the definition of the order parameter for helium was given by Penrose (1951) and Penrose and Onsager (1956), based on an analysis of the large-scale correlations in the various terms of the single-particle density matrix.

In a usual fluid, the on-diagonal elements $\rho_1(\mathbf{r},\mathbf{r})$ are of the order of the particle number density $n(\mathbf{r})$. Particle correlations decrease rapidly as $\mathbf{r}-\mathbf{r}'$ increases and so do the off-diagonal terms with $\mathbf{r}\neq\mathbf{r}'$. By contrast, a superfluid can sustain a persistent current: large-scale correlations should be strong so that, when a particle is deflected at $\mathbf{r}$ by an obstacle and kicked out of the condensate, a twin-sister particle is immediately relocated in the condensate at $\mathbf{r}'$ with no loss of order in

[13] See Abrikosov, Gorkov, and Dzyaloshinski (1961).

[14] See Kadanoff (2013) for an account of the historical genesis of the idea of ODLRO and a discussion of the role of the condensate in superfluidity and superconductivity.

[15] Further discussion on these correlations is given in Sec. VIII.B.

[16] See, for example, Griffin (1993) and his historical note (Griffin, 1999).

momentum space. Such correlations should be described in the density matrix by a term embodying the condensate of the same "structure" as the product in Eq. (9), supplemented by other terms for the part of the system that cannot be accommodated in the ground state because of interparticle collisions. Thus, following Penrose and Onsager, the criterion for Bose-Einstein condensation must be traced to the existence of one element of the form (9), namely, a product $\Phi^*(\mathbf{r})\Phi(\mathbf{r}')$ with a macroscopic size relative to other elements, so that the density matrix takes the form

$$\rho_1(\mathbf{r},\mathbf{r}') = \Phi^*(\mathbf{r})\Phi(\mathbf{r}') + \sum \quad \text{(other matrix elements)}. \tag{10}$$

The sum on the right-hand side of Eq. (10) is a mixed bag of terms describing the correlations between particles outside the condensate as well as terms involving both condensate and noncondensate particles. The function $\Phi(\mathbf{r})$ can be viewed as playing the role of a single-particle wave function of the interacting particles in the condensate, $n_0 = (1/V)\int|\Phi(\mathbf{r})|^2 d\mathbf{r}$ being the mean number density of those particles.[17] This number density n_0 can be orders of magnitude smaller than the total density n, but is assumed to still remain macroscopic.

As the ground state wave function for a boson system is nonzero everywhere, its absolute value for a homogeneous system $|\Phi(\mathbf{r})|$ is equal to $\sqrt{n_0}$ to the extent that n_0 is constant in space. This reasoning can be extended to situations that are slightly nonuniform in space. The term $\Phi^*(\mathbf{r})\Phi(\mathbf{r}')$ in Eq. (10) does not decay as the particle locations $\mathbf{r}$ and $\mathbf{r}'$ become far apart compared to interatomic distances: it describes the long-range correlations in the condensate, or ODLRO. The excited states with $\mathbf{k} \neq 0$ and distribution $n_\mathbf{k}$ are not macroscopically populated and have only short-range coherence. The summation over all these remaining contributions in Eq. (10) may also amount to a macroscopic term $\sum_\mathbf{k} n_\mathbf{k}$, of order N. Each of these terms decays as $|\mathbf{r}-\mathbf{r}'|$ becomes large but there are a large number of them: all of the excited states are also macroscopically populated.

Needless to say, the single-particle wave function $\Phi(\mathbf{r})$ in Eq. (10) bears no relationship to that for free particles in Eq. (9) for the ideal gas. Neither the $\Phi^*(\mathbf{r})\Phi(\mathbf{r}')$ term in Eq. (10) nor the incoherent terms have been expressed in full for the dense helium-4,[18] contrary to near-ideal BEC gases and to the BCS theory (for Cooper pairs and superfluid ^{3}He). But in superfluid ^{4}He as in these other situations, ODLRO is found to be present and to constitute a unifying feature sufficient to ensure flux quantization (BCS superconductors) or velocity circulation quantization (dense superfluid helium). That the simple factorization of the coherent part of the density matrix ensures superfluidity is a remarkable result. It has been established on general grounds by Yang (1962).

Penrose (1951) and Penrose and Onsager (1956) used various approximate forms for the ground state wave function of dense helium-4 at $T = 0$ to illustrate the splitting of the density matrix, Eq. (10), and to evaluate the depletion of the condensate, i.e., the value of n_0. They have used, in particular, Feynman's simple ansatz for the superfluid wave function (Feynman, 1953a, 1953b, 1954, 1955), which assumes strong hard-core repulsion and weak two-body attraction with a minor role in interparticle correlations. Only the former can be kept for an approximate evaluation of n_0.

Building on this remark, Penrose and Onsager noticed that the depletion under scrutiny can conveniently be derived from the known pair distribution for a classical gas of hard spheres such as the one pictured in Fig. 2. They found that collisions between hard spheres with diameters 2.6 and 3.6 Å apart leave only about 8% of the helium atoms in the zero-momentum state. This value of n_0/n in ^{4}He has been confirmed by more elaborate theories and by experiment.[19] While the depletion of the condensate is a small effect in low density atomic gases (Dalfovo *et al.*, 1999), it is considerable in liquid helium.

This large depletion raises the following question: how is it that the condensate fraction is only 8% at $T = 0$ while the superfluid fraction in the two-fluid model is 100%? The answer is simple: these are not the same quantities.[20] The superfluid density stands for the inertia of the superfluid fraction, as measured for instance by a gyroscopic device sensitive to trapped superfluid currents (Reppy and Lane, 1965) or, less directly, by the decoupling of the superfluid component in an oscillating disk experiment (Andronikashvili and Mamaladze, 1966). In these experiments, only the elementary quasiparticles couple to the transverse oscillations of the cell walls; the remaining the superfluid is not set into motion.

The superfluid fraction ρ_s/ρ is not directly related to the probability of finding bosons in the $\mathbf{k} = 0$ quantum state. The occupation of the condensate is seen experimentally as a hump at zero energy transfer in the dynamic structure factor measured by neutron inelastic scattering (Glyde, 2013), a quantity rather well hidden from experimentalists' view in helium. When the superfluid is set into motion, the condensate enforces long-range order and drags the excited states along through the short-range correlations; there is entrainment of the atoms in the fluid by the condensate. Microscopic theory is needed to describe this process in detail.

[17] Nozières and Pines (1990) give an account of ODLRO using the notation of field theory, in which the density matrix reads

$$\rho_1(\mathbf{r},\mathbf{r}') = \sum_n \langle\phi|\psi^\dagger(\mathbf{r})|\phi_n\rangle\langle\phi_n|\psi(\mathbf{r}')|\phi\rangle,$$

$\psi^\dagger(\mathbf{r})$ and $\psi(\mathbf{r}')$ being the boson creation and annihilation field operators, $|\phi_n\rangle$ a complete set of eigenstates of the system, and $|\phi\rangle$ the state in which the average is expressed, which is taken as the ground state $|\phi_0\rangle$. Among the intermediate states $|\phi_n\rangle$, those of special relevance to the kicking out and relocation processes discussed here connect the ground state with N bosons to the ground state with $N-1$ bosons. So attention must be focused on the following matrix element:

$$\Phi(\mathbf{r}) = \langle\phi_0(N-1)|\psi(\mathbf{r})|\phi_0(N)\rangle,$$

that is taken to represent the condensate wave function.

[18] As stated in Nozières and Pines (1990), Sec. 9.4.

[19] For a recent review, see Glyde (2013).

[20] This point was discussed by Griffin (1987, 1993).

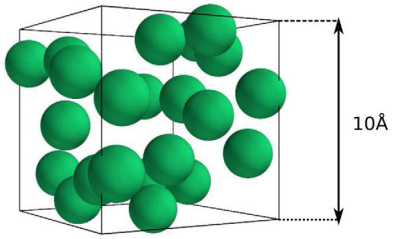

FIG. 2 (color online). A 3D view of 2.6 Å diameter hard spheres randomly distributed in a $10 \times 10 \times 10$ Å cube with a 3.6 Å mean spacing, as for liquid helium-4 at SVP. In helium, atoms are both strongly confined by hard-core repulsion and dynamically delocalized by the zero-point energy motion. Courtesy of Nelle Varoquaux.

Deferring to Sec. VIII.B, further discussion on the merits of, and differences between, the microscopic approach, the ODLRO concept of Penrose (1951), Penrose and Onsager (1956), and Yang (1962), and the macroscopic quantum field point of view, a discussion found in Appendix A1 of Anderson (1966b), the superfluid order parameter in ^{4}He will be taken in the following as the macroscopic wave function Eq. (7), namely, $\Psi(\mathbf{r}) = f(\mathbf{r})e^{i\varphi(\mathbf{r})}$ with $f = n_s^{1/2}$, n_s being the superfluid number density. This choice conforms to that of Sec. I.B and leads straightforwardly to the two-fluid model. The alternate choice to set $f = n_0^{1/2}$ would be less productive: the condensate density n_0 remains half buried in the formalism and is difficult to access experimentally. This situation differs markedly from that in cold atomic gases. There the condensate can be imaged directly in momentum space; it comprises most of the particles in the gas so that $n_0 \simeq n$. The corresponding order parameter emerges seamlessly from perturbation theory applied to the weakly interacting Bose gas following Bogolyubov's prescriptions.

For weakly interacting bosons, the macroscopic wave function dynamics is governed by the Gross-Pitaevskii equation.[21] The relevance of the Gross-Pitaevskii equation to the Bose-condensed systems has been put in a new perspective for ultracold atoms in a trap, for which it constitutes an excellent description (Dalfovo *et al.*, 1999; Cohen-Tannoudji and Robilliard, 2001). However, the approach based on this equation turns out to be less adequate for the dense superfluid, sometimes not even qualitatively correct, as found for instance by Pomeau and Rica (1993) in the context of the breakdown of superflow. It will not be pursued here, except to mention that it does provide an estimate of the distance over which the two-fluid hydrodynamics needs to be supplemented by quantum corrections, as discussed in Sec. VII.

In all cases, the phase, a variable of lesser relevance in the old days of quantum mechanics, is now assigned the role of governing superfluid dynamics. A fundamental result, established early by Beliaev (1958), relates the phase of the condensate particles to the chemical potential $\varphi = \mu t/\hbar$, where t is time. The deep significance of this relation only became apparent later, when the Josephson effects became apparent.

[21]In the context of superfluids, see Gross (1961), Pitaevskii (1961), Langer (1968), and Nozières and Pines (1990).

The role of the phase as a dynamical variable was extended to superfluid helium by Anderson (1964, 1965, 1966a, 1984) who noted that phase and particle number are canonically conjugate variables. This property is well known in quantum electrodynamics for photons in a cavity. The number of photons in a given mode and their phase, defined for coherent electromagnetic fields in the cavity, are noncommuting operators. As such, they obey an uncertainty relation (Heitler, 1954) that reads

$$\delta N \delta\varphi \sim 1. \tag{11}$$

As remarked by Heitler, "If the number of quanta of a wave are given it follows from Eq. (11) that the phase of this wave is entirely undetermined and vice versa. If for two waves the phase difference is given (but not the absolute phase) the total number of light quanta may be determined, but it is uncertain to which wave they belong." This remark will bear implications throughout this review.

Superfluidity is more than simply the absence of viscosity supplemented by the condition that vortices have quantized circulation. The urge to observe the role of the phase in a Josephson-type effect, and the failure to do so for a long period of time, became quite pressing to confirm the picture drawn by Anderson of helium as obeying quantum mechanics in a more profound way than simply as an ideal inviscid fluid with quantized velocity circulation.

E. Anderson's phase slippage

Anderson's famed "considerations" on the flow of superfluid ^{4}He (Anderson, 1966a) provided the conceptual basis for this experimental search for Josephson-type effects in neutral matter. Their underlying aim was to convey a physical, laboratory-oriented meaning to the order parameter Eq. (7) and, in particular, to its phase. These considerations provided the groundwork for phase-slippage experiments in ^{4}He; they were gradually fostered in a series of lectures notes (Anderson, 1964, 1965, 1984) and built upon the ideas of London (1954), Feynman (1953a, 1953b, 1954, 1955), Penrose (1951), and Penrose and Onsager (1956), and also on the quantum field theoretic approach of Beliaev (1958).

In the absence of a fully established microscopic theory of dense boson systems, these considerations rest on the following set of well-argumented conjectures:

(1) By extrapolation of the properties of the coherent photon fields in quantum electrodynamics, N and φ are taken in dense liquid helium as canonically conjugate dynamical (quantum) variables in the sense that $N \leftrightarrow i(\partial/\partial\varphi)$ and $\varphi \leftrightarrow -i(\partial/\partial N)$.

As such, they obey the uncertainty relation (11). For a closed system with a fixed number of particles, the phase is completely undetermined. For the phase to be determined within $\delta\varphi \ll 1$, N must be allowed to vary; that is, the condensate must be able to exchange particles with other parts of the complete physical system, which includes the noncondensate fraction of the bosons and the eventual measuring apparatus.

For the Josephson-effect experiments specifically considered by Anderson, the two weakly coupled

helium baths also exchange particles. For all these reasons, N is allowed to fluctuate locally so that δN takes a nonzero value. It can be shown (Beliaev, 1958) that δN is of the order of N rather than unity, so that $\delta\varphi \sim \mathcal{O}(1/N)$ and φ is well defined.

(2) A Hamiltonian $\mathcal{H}$ should therefore exist such that, N being free to vary,

$$\hbar\frac{\partial N}{\partial t} = \frac{\partial \mathcal{H}}{\partial \varphi}, \tag{12}$$

$$\hbar\frac{\partial \varphi}{\partial t} = -\frac{\partial \mathcal{H}}{\partial N}. \tag{13}$$

Upon coarse graining, the quantum operators become quasiclassical and their coarse-grained average obeys equations formerly identical to Eqs. (12) and (13). Equation (12) defines the particle current $J = \partial E/\hbar\partial\varphi$ since $\partial\mathcal{H}/\partial\varphi \Rightarrow \partial E/\partial\varphi$ upon averaging. Likewise with $\partial\mathcal{H}/\partial N \Rightarrow \partial E/\partial N = \mu + (1/2)m_4 v_s^2$, where μ is the chemical potential in the fluid at rest, namely, $\mu = m_4 P/\rho + m_4 g h + s_4 T$ with the usual notations, Eq. (13) becomes

$$\hbar\frac{\partial \varphi}{\partial t} = -[\mu + (1/2)m_4 v_s^2]. \tag{14}$$

Equation (14) states that, whenever there exists a chemical potential difference between points (1) and (2) in a superfluid (or a superconductor), the phase of the order parameter varies in time with a rate proportional to $\mu_1 - \mu_2$: this ac effect is quite detectable and has many applications. It was first discussed by Josephson (1962, 1964) for the tunneling current between superconductors coupled through a thin barrier. A full derivation for superfluid helium can be found in Nozières and Pines.[22]

Upon taking the gradient of both the left- and right-hand sides, Eq. (13) becomes, using the definition (6) of v_s,

$$\frac{\partial v_s}{\partial t} + \nabla\left(\frac{P}{\rho} + \frac{v_s^2}{2}\right) = 0, \tag{15}$$

which is the Euler equation for an inviscid fluid with no vorticity ($\boldsymbol{\omega} = \nabla \times \mathbf{v}_s = 0$). Equation (15) is precisely the same as that for the velocity of the superfluid component in Landau's two-fluid hydrodynamics.

(3) Anderson assumed that Eq. (14) for the time variation of the order parameter phase holds with no solution of continuity between the classical inviscid fluid case and the quantum-tunneling one and it has universal applicability. This unifying approach is internally consistent but details are missing of how the normal component interacts with the superfluid component, which brings dissipative terms into Eq. (15), and how the definition of v_s as $(\hbar/m)\nabla\varphi$ breaks down at small distances where coarse graining cannot be performed. These points have been raised in Anderson's communication at the Sussex Symposium on Quantum Fluids (Anderson, 1966b). His views are that the phase equation (14), being more fundamental than Eq. (15), always holds. This equation describes both simple superfluid acceleration, expressed by Eq. (15), the ideal tunneling situation envisioned by Josephson (see Sec. VII), and when the variation of the phase is caused by the motion of vorticity.

(4) The last conjecture asserts that the dissipation of the kinetic energy of a superflow is, when averaged over time, proportional to the rate at which vorticity crosses the superflow streamlines. In fact, a stronger statement was rigorously proved by Huggins (1970), which governs the detailed transfer of energy between the potential flow of the superfluid and moving vorticity. This process is pivotal to the understanding of superflow decay and, more generally, of vortex dynamics as discussed in Sec. II.

Anderson's ideas on phase slippage, linked to the motion of vortices, have provided the conceptual framework for the experiments on the onset of dissipation and the Josephson effects in superfluids, discussed in Secs. III and VII.B. All facets of these experiments in superfluid ^{4}He and ^{3}He can be well accounted for with the help of the macroscopic quantum phase φ. However, these ideas are still surrounded by an aura of mystery that lingers on in spite of the facts that (1) the formal theoretical groundwork has been put on a firmer basis.[23] (2) The implications of the uncertainty relation to laboratory observations, as well as of the other conjectures of Anderson, have been clarified by the developments of the experiments in the past 40 years since they were formulated.

This review will tackle some of these advances, in particular, by showing what the phase-slippage experiments really consist of, how phase slippage proceeds from a dissipative regime governed by vortex dynamics to a true dissipationless Josephson regime, and that this truly quantum behavior manifests itself in matter wave interferometric measurements.

II. QUANTIZED VORTEX DYNAMICS CLOSE TO $T = 0$

Vortex filaments are extended quasi-one-dimensional structures in the superfluid, line vortices. At the core of these

[22] See Nozières and Pines (1990), Sec. 5.7.

[23] Following, for instance, Lifshitz and Pitaevskii (1980), the density operator takes the form $\hat{\rho}(\mathbf{r}) = \sum_i m_4 \delta(\mathbf{r}_i - \mathbf{r})$ and the current density operator the form $\hat{\mathbf{j}}(\mathbf{r}) = \frac{1}{2}\sum_i \hat{\mathbf{p}}_i \delta(\mathbf{r}_i - \mathbf{r}) + \delta(\mathbf{r}_i - \mathbf{r})\hat{\mathbf{p}}_i$; cf. Eqs. (4) and (5). The liquid velocity operator $\hat{\mathbf{v}}$ is in turn defined by $\hat{\mathbf{j}}(\mathbf{r}) = \frac{1}{2}(\hat{\rho}\,\hat{\mathbf{v}} + \hat{\mathbf{v}}\,\hat{\rho})$. These operators obey the commutation rule $\hat{\Phi}(\mathbf{r})\hat{\rho}(\mathbf{r}') - \hat{\rho}(\mathbf{r}')\hat{\Phi}(\mathbf{r}) = -i\hbar\delta(\mathbf{r} - \mathbf{r}')$, $\hat{\Phi}$ being the potential for the velocity operator $\hat{\mathbf{v}} = \nabla\hat{\Phi}$. The quantities $\hat{\rho}$ and $\hat{\Phi}$ are thus canonically conjugate. Their fluctuations obey an uncertainty relation of the form $\delta\hat{\rho}\delta\hat{\Phi} \geq \hbar/2$. Using the phase of the macroscopic wave function, Eq. (6), instead of the velocity potential, the uncertainty relation (11) is obtained.

defects, the superfluid order parameter is either zero as in ^{4}He or heavily distorted as in ^{3}He. They form the prevalent topological defects in superfluids.[24]

At distances larger than the core size, superfluid vortices behave according to the laws of ideal fluid hydrodynamics, that is, as classical vortices with a given quantized vorticity. Classical vortices have been studied for many decades (Lamb, 1945; Saffman, 1992). Their properties have been the subject of detailed studies in recent years in order to clarify in a number of standing problems, their mass and impulse, the Magnus and Iordanski forces, the eigenmodes of isolated vortices (the Kelvin waves, the collective behavior of vortex arrays) the Tkachenko waves, the reconnection of two vortices, superfluid vortex tangles, and, last, the formation of vortices and their annihilation. This review is concerned mainly with the last topic but use will be made of other properties of vortices, either single or a few at a time, mostly without consideration to the normal fluid background. These properties bear a close resemblance to those of magnetic vortices in superconductors as discussed by Sonin and Krusius (1994).

At temperatures below 1 K, vortices in superfluid ^{4}He experience negligible friction from the normal fluid, the fraction of which becomes very small. If they deform only little and slowly, they constitute stable fluid eddies: their velocity circulation is conserved (and, furthermore, quantized) and they cannot vanish to nothing. Their core radius a_0 is of the order of the superfluid coherence length, a few angstrom in ^{4}He (Glaberson and Donnelly, 1986; Donnelly, 1991), 1 to 2 orders of magnitude larger in ^{3}He depending on pressure (Vollhardt and Wölfle, 1990). As the temperature increases, the scattering of phonons and rotons by the vortex cores causes dissipation. Mutual friction between the superfluid vortices and normal fluid sets in. Close to the superfluid transition temperature, the core size increases and eventually diverges.

Some of the properties of vortices that are relevant to phase slippage are summarized below. Extended coverage of this topic can be found in Donnelly (1991) and Sonin (2015). Here the dynamical properties of superfluid vortices are derived directly from the existence of a superfluid order parameter. Some approximations are made in order to get a simpler physical description of a vortex element, treated more in the manner of a quasiparticle with mass, energy, and impulse. The following discussion then rests on physical concepts such as energy conservation or the balance of forces. It largely follows the approach of Sonin (1987). It differs from the more traditional and rigorous fluid-mechanical approach as can be found for instance in Saffman (1992). It provides a more intuitive feel for the behavior of superfluid vortices that will prove useful in the description of phase slips.

A. Quantization of circulation

Superfluid vortices have quantized circulation. This property comes about because their core is nonsuperfluid: it disrupts the order parameter field and constitutes a topological defect in the superfluid. The circulation of the superfluid velocity $\mathbf{v}_s$ on any path around such a defect

$$\oint \mathbf{v}_s \cdot d\mathbf{l} = \frac{\hbar}{m_4} \oint \nabla\varphi \cdot d\mathbf{l} \tag{16}$$

amounts[25] to $\kappa_4 = 2\pi\hbar/m_4$ because the phase φ of the order parameter can change only by multiples of 2π along any closed contour entirely located in the superfluid. This property holds for the true condensate wave function as a basic requirement of quantum mechanics. It is not altered in the coarse-graining average.

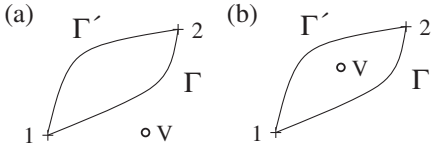

FIG. 3. Two different situations for the path of integration in Eq. (17): (a) Γ can be deformed continuously into Γ'; both paths give the same phase difference between point 1 and point 2. (b) Vortex V stands between the two paths; the phase differences along Γ and Γ' differ by 2π.

Consider the velocity circulation from point 1 to point 2 in Fig. 3 along a path Γ entirely located in the superfluid:

$$\kappa = \int_1^2 \mathbf{v}_s \cdot d\mathbf{l} = \frac{\hbar}{m_4} \int_1^2 \nabla\varphi \cdot d\mathbf{l} = \frac{\hbar}{m_4}(\varphi_2 - \varphi_1). \tag{17}$$

Along another path Γ' also going from 1 to 2, as shown in Fig. 3, the circulation is $(\hbar/m_4)(\varphi_2 - \varphi_1 + 2n\pi)$. If Γ' can be deformed into Γ continuously while remaining in the superfluid, then $n = 0$. If this cannot be done, n may be a nonzero integer, 1 in the case under consideration.

Thus, when path Γ crosses the core of a ^{4}He vortex, in which superfluidity is destroyed and the order parameter amplitude goes to zero, n changes by 1 because ^{4}He vortices carry a single quantum of circulation for reasons discussed next. Conversely, when a vortex crosses a superfluid path from 1 to 2, the circulation along that path changes by one quantum and the phase difference by 2π. This simple property forms the basis of the phase-slip phenomenon described in Sec. III.

Experiments have confirmed to a high accuracy the quantization of hydrodynamic circulation both in ^{4}He (Vinen, 1961; Whitmore and Zimmermann, 1968; Karn, Starks, and Zimmermann, 1980) and in ^{3}He (Davis *et al.*, 1991). This feature constitutes a cornerstone of superfluid physics and evidence for the reality of the superfluid quantum phase.

B. Vortex flow field and line energy

The flow velocity induced by a straight vortex filament, chosen along the unit vector $\hat{\mathbf{z}}$, at a distance $\mathbf{r}$ measured in the

[24]There are a number of different topological defects in superfluid ^{3}He owing to the large number of degrees of freedom of the order parameter as briefly discussed in Sec. VII.B.

[25]The quantum of circulation in ^{4}He takes the value 9.97×10^{-4} cm^2 s^{-1} and in ^{3}He where the boson mass is $2m_3$, $\kappa_3 = \pi\hbar/m_3 = 6.65 \times 10^{-4}$ cm^2 s^{-1}.

plane perpendicular to $\hat{\mathbf{z}}$ is easily expressed from the quantization of the velocity circulation and the symmetry around the vortex axis as

$$\oint \mathbf{v}\cdot d\mathbf{l} = \kappa_4 \Rightarrow \mathbf{v}_v = \frac{\kappa_4}{2\pi}\hat{\mathbf{z}}\times\frac{\hat{\mathbf{r}}}{r}, \tag{18}$$

provided that r is larger than a_0. For $r \lesssim a_0$, the detailed structure of the core becomes important.[26] The quantity $\mathbf{v}_v$ is the vortical flow due to the vortex element. The superfluid velocity $\mathbf{v}_s$ is the sum of an eventual potential flow $\mathbf{v}_p$ existing independently of the vortex, for instance, applied externally, and of $\mathbf{v}_v$. The contribution of $\mathbf{v}_p$ to the loop integral in Eq. (18) is nil and leaves the circulation unchanged. Straight vortex filaments are created by rotating the helium container; they have been the object of detailed studies.[27]

Equation (18) can be extended to *curved* vortices, provided that their radii of curvature are much larger than the core radius a_0. It bears a direct analogy with Ampère's law, $\mathbf{v}$ standing for the magnetic field and κ for the electric current carried by the conductor.[28] The velocity at point $\mathbf{r}$ induced by a *closed* vortex filament lying along the curve $\mathbf{s}$ is then given by the analog of the Biot-Savart law in electrodynamics[29]:

$$\mathbf{v}_v(\mathbf{r}) = \frac{\kappa_4}{4\pi}\oint d\mathbf{l}\times\frac{\mathbf{r}-\mathbf{s}(l)}{|\mathbf{r}-\mathbf{s}(l)|^3}. \tag{19}$$

The geometrical representation of the vortex loop by $\mathbf{s}$ is such that $d\mathbf{l} = d\mathbf{s}$ is a vector oriented along the tangent to the loop $\hat{\mathbf{t}}$ of infinitesimal length dl, l being the arc length of the loop (see the sketch in Fig. 4). The tangent $\hat{\mathbf{t}}$ is the unit vector $d\mathbf{s}/dl = d\mathbf{l}/dl$. Its derivative with respect to l defines the normal to the loop $\hat{\mathbf{n}}$ and the radius of curvature R: $d\hat{\mathbf{t}}/dl = d^2\mathbf{s}/dl^2 = \hat{\mathbf{n}}/R$. As noted above, the radius of curvature R should be large, and the change of orientation of the tangent $d\hat{\mathbf{t}}/dl$ small, with respect to the core radius for this representation of the vortex element as a one-dimensional line to be valid.

The integrand in Eq. (19) gives the contribution of the vortex element $d\mathbf{l}$ located at $\mathbf{s}$ on the loop to the full velocity field. An integration by parts yields

$$\mathbf{v}_v(\mathbf{r}) = \frac{\kappa_4}{4\pi}\nabla\times\oint\frac{d\mathbf{l}}{|\mathbf{r}-\mathbf{s}(l)|} = \nabla\times\mathbf{A}(\mathbf{r}), \tag{20}$$

which defines a vector potential for the vortex velocity field $\mathbf{v}_v = \nabla\times\mathbf{A}$.

Equation (20) fulfils the mantra of conventional mathematical physics according to which a vector field can be split into an irrotational part, which derives from a scalar potential, and a remainder, the solenoidal part, which is not curl free and which derives from a vector potential.

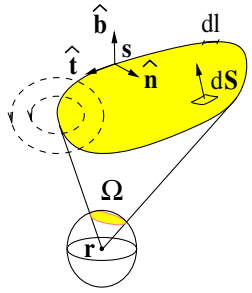

FIG. 4 (color online). The geometrical representation of a vortex loop, an arbitrary surface S spanning the loop, with element $d\mathbf{S}$, and the solid angle Ω subtended by the loop from point $\mathbf{r}$, the tangent $\hat{\mathbf{t}}$, normal $\hat{\mathbf{n}}$, and binormal $\hat{\mathbf{b}}$ at point $\mathbf{s}$. The flow lines of the vortex velocity field (dashed line) thread surface S where the phase changes determination by 2π. Solid angle Ω offers a geometrical representation of the integrand in Eq. (21).

While utterly correct in mathematical terms, this point of view may be slightly misleading for the superfluid velocity fields. The latter are a subset only of the more general vector fields in the sense that vorticity is localized in space to the vortex cores and that the vortex line can be treated as a line singularity. The Biot-Savart law (19) can then be put in the following form[30] :

$$\mathbf{v}_v(\mathbf{r}) = \frac{\kappa_4}{4\pi}\nabla_{\mathbf{r}}\left\{\int\!\!\int_S \frac{\mathbf{r}-\mathbf{R}}{|\mathbf{r}-\mathbf{R}|^3}\cdot d\mathbf{S}\right\} = \frac{\hbar}{m_4}\nabla\varphi_v, \tag{21}$$

the infinitesimal surface element $d\mathbf{S}$ being located at position $\mathbf{R}$. Thus the velocity fostered by the vortex derives from a scalar potential as well as a vector potential. Everywhere in the superfluid but at the precise location of the vortex cores, the superfluid velocity v_s is indeed irrotational and derives from a scalar potential, the quantum phase.[31]

The velocity induced by a vortex loop decreases at large distance from the loop as that of a dipole in the electromagnetic analogy, that is as $1/r^3$, much faster than the $1/r$ dependence for straight vortex filaments [see Eq. (18)]. The $1/r$ dependence can still be expected to hold at a distance away from the core smaller than the local radius of curvature of the vortex filament. At distances larger than the loop size, the velocity field rapidly dies away. This property is well known for magnetic fields generated by electric current loops. It means, for practical purposes, that vortex loops far apart interfere very weakly and that distant boundaries have negligible effect. These simplifying features will often be assumed in the following.

[26]See Fetter (1976), Sonin (1987), Salomaa and Volovik (1988), and Dalfovo (1992) for more extended discussions.

[27]See Hall (1960), Andronikashvili and Mamaladze (1966), Sonin (1987), Krusius *et al.* (1993), and Finne *et al.* (2006).

[28]See, for example, Lamb (1945), Sec. 147.

[29]See Saffman (1992), Sec. 2.3.

[30]Stokes's theorem can be invoked to transform the line integral in Eq. (19) into an integral over the surface spanned by the vortex loop

$$\oint dl\times\mathbf{a} = \iint[(\nabla\mathbf{a})\cdot d\mathbf{S} - \nabla\cdot\mathbf{a}d\mathbf{S}]$$

with $\mathbf{a} = (\mathbf{r}-\mathbf{R})/|\mathbf{r}-\mathbf{R}|^3$. Equation (21) then follows.

[31]The situation in superfluid ^{3}He-A is more complicated, as discussed in Sec. VII.E.

1. Vortex line energy

The flow around the core of a vortex element carries kinetic energy, obtained by integration of $\int(1/2)\rho_s v_v^2 d\tau$ over the volume V in which this flow extends. The quantity ρ_s is the superfluid density. This integral is evaluated by introducing the vector potential $\mathbf{A}$, Eq. (20), from which derives the vortical flow field, as follows:

$$E_v = \frac{\rho_s}{2}\int_V d\tau \mathbf{v}_v \cdot \mathbf{v}_v = \frac{\rho_s}{2}\int_V d\tau \mathbf{v}_v \cdot \nabla \times \mathbf{A}$$
$$= \frac{\rho_s}{2}\int_V d\tau \nabla \cdot (\mathbf{A} \times \mathbf{v}_v) + \frac{\rho_s}{2}\int_V d\tau \mathbf{A} \cdot (\nabla \times \mathbf{v}_v).$$

The last line is obtained with the help of vector identity $\nabla \cdot (\mathbf{a} \times \mathbf{b}) = \mathbf{b} \cdot (\nabla \times \mathbf{a}) - \mathbf{a} \cdot (\nabla \times \mathbf{b})$. It consists of the sum of two volume integrals. The first can be changed into a surface integral over $\mathbf{A} \times \mathbf{v}$ with the divergence theorem. By taking the volume boundary sufficiently far from the vortex element, supposedly isolated in a large volume, the surface integral can be made negligible. In the second integral, the curl of $\mathbf{v}_v$ is zero everywhere but on the vortex core, where it is singular: $\nabla \times \mathbf{v}_v = \kappa_4 \hat{\mathbf{t}} \delta_2(\mathbf{r} - \mathbf{s})$. Integration over the two-dimensional delta function $\delta_2(\mathbf{x})$, defined in the plane normal to the tangent $\hat{\mathbf{t}}$ to the loop, reduces this volume integral to a line integral over the vortex element:

$$E_v = \frac{\rho_s \kappa_4}{2}\oint d\mathbf{l} \cdot \mathbf{A}. \tag{22}$$

The vortex kinetic energy is the circulation of the vector potential along the vortex filament.

By substitution of Eq. (20) for the vector potential $\mathbf{A}$ into Eq. (22), the vortex energy can be expressed by a double contour integral over the vortex loop[32]:

$$E_v = \frac{\rho_s \kappa_4^2}{8\pi}\oint\oint \frac{d\mathbf{s}(l_1)}{dl_1} \cdot \frac{d\mathbf{s}(l_2)}{dl_2} \frac{dl_1 dl_2}{|\mathbf{s}(l_1) - \mathbf{s}(l_2)|}. \tag{23}$$

Because E_v in Eq. (23) varies as κ_4^2, loops carrying two quanta of circulation would have 4 times the line energy of single charge ones. Vortices with multiple quanta of circulation are thus strongly disfavored on energy grounds compared to separate singly charged vortices with the same total vorticity charge; they are energetically unstable and decay spontaneously into several singly charged entities. Only loops and filaments carrying one quantum of circulation are considered here.

For a circular ring of radius R the integral can be evaluated in terms of elliptic functions[33] and expanded in terms of the small parameter a_0/R. The kinetic energy associated with the ring velocity field is then given by

$$E_R = \frac{1}{2}\rho_s \kappa_4^2 R \ln\frac{8R}{a_0} + \mathcal{O}\left(\frac{a_0}{R}\right). \tag{24}$$

For a straight vortex filament, the integral for the kinetic energy in the volume comprised between two planes perpendicular to the filament stems out directly from Eq. (18). For a unit length of vortex the result reads

$$\epsilon_f = \frac{\rho_s \kappa_4^2}{4\pi}\ln\left(\frac{r_m}{a_0}\right). \tag{25}$$

The logarithmic divergence is cut at short distance to a_0, taken as the definition of the core radius. Its value, of the order of 1 Å at low pressure, is obtained from experiment (Rayfield and Reif, 1964). The far distance cutoff r_m is the minimum distance over which the vortex flow field is undisturbed: it is the smallest of (1) the size of the container, (2) the average radius of curvature of the vortex, and (3) the distance to neighboring vortices. For ångström-size vortices, taking $r_m/a_0 = 10$, $\epsilon_v \sim 2$ K/Å: vortices are high-energy excitations of the superfluid as compared to thermal excitations, phonons, or rotons. Changes in r_m along the vortex line are disregarded because they enter logarithmic terms and yield small corrections only for $r_m \gg a_0$: when the vortex deforms, its energy changes mostly as its length, and little with its shape.

The line energy of the core, usually taken as

$$\epsilon_{sb} = -\frac{7}{4}\frac{\rho_s \kappa_4^2}{4\pi},$$

for a core rotating as a solid body,[34] must be added to Eq. (25) to obtain the full vortex energy per unit length

$$\epsilon_v = \epsilon_f + \epsilon_{sb} = \frac{\rho_s \kappa_4^2}{4\pi}\left\{\ln\left(\frac{r_m}{a_0}\right) - \frac{7}{4}\right\}. \tag{26}$$

The full energy of a curved vortex line is thus approximated by ϵ_v times its total length. For instance, the energy of a vortex ring, Eq. (24), stems from Eq. (25) if r_m is taken to be $8R$.

Equation (26) holds for straight vortex lines, rings, curved filaments, or general loops provided than $r_m \gg a_0$. It can be viewed as a force developing along the vortex axis, a line tension that tends to shorten the vortex length. That is, the vortex line pulls on its ends: if an end becomes loose, it shrinks to zero. Stable vortices in finite-size containers are either closed on themselves in loops or connected to the container walls.

2. Stable vortices

It follows from the existence of a positive line tension that a vortex loop would tend to spontaneously reduce its length and minimize the line energy. However, the energy so released by the vortex loop in its motion can be disposed of into the surrounding fluid only in certain conditions of flow. The line tension is opposed by other forces that arise from the vortex motion in the fluid or from its interaction with the boundaries, namely, the Magnus force and pinning forces.

[32] See Lamb (1945), Sec. 153, or Saffman (1992), Sec. 3.11.

[33] See Lamb (1945), Sec. 163.

[34] Using the Gross-Pitaevskii equation, Roberts and Grant (1971) found that the prefactor 7/4 should be replaced by the not-so-different number 0.615.

As stand-alone loops or pinned filaments, their length is constant as long as they cannot exchange energy with the rest of the fluid (or the external world). In the presence of hard walls, their flow field must be such as to satisfy the condition that no fluid can penetrate into the wall. A convenient way of satisfying such a boundary condition is to continue the vortex filament into the wall, forming an imaginary image vortex. Such a continuation procedure can be shown to be possible and to yield a unique velocity field.[35] Vortices meeting with walls usually satisfy the condition of no flow through a solid boundary by standing perpendicular to it.[36] Thus, finite length vortices always close on themselves or end at walls. In this latter case, they also form closed loops if their image is taken into account. The opposite view, namely, that vortices are most of the time infinitely long as, for instance, vortices formed under rotation in a cylindrical helium bucket, is also held.[37] The process of nucleation of vortices considered next requires that their size be finite (otherwise, the energy involved would be infinite): the isolated vortex loops dealt with in the following have a finite size, usually small.

3. Vortex line impulse

If an external potential flow with velocity $\mathbf{v}_p = (\hbar/m_4)\nabla\varphi_p$ imposed by moving boundaries, a piston for instance, or by nearby vortices, the kinetic energy of the combined flow $\mathbf{v}_p + \mathbf{v}_v$ in a given volume V is the sum of the kinetic energy of the remotely applied superflow $\mathbf{v}_p$, that of the vortex loop, obtained from Eq. (23), and the volume integral of the cross term of the scalar product of $\mathbf{v}_p$ and $\mathbf{v}_v$. This last term reads

$$E_I = \rho_s \int_V \mathbf{v}_p \cdot \mathbf{v}_v d\tau = \rho_s \frac{\hbar^2}{m_4^2} \int_V \nabla\varphi_p \cdot \nabla\varphi_v d\tau, \tag{27}$$

and represents the energy of interaction between the vortex and the applied flow. Making use of Green's first identity,[38] the integral in Eq. (27) can be rewritten as

$$E_I = \rho_s \frac{\hbar}{m_4} \int_S \varphi_v \mathbf{v}_p \cdot d\mathbf{S}, \tag{28}$$

where φ_v is the phase change contributed by the vortex's own flow field.

The bounding surface S yields not one but two contributions to the integral in Eq. (28), the outer surface bounding V and, quite importantly, the cut spanning the vortex loop over which φ_v changes discontinuously by 2π (see Fig. 4). If V can be chosen large enough, the velocity induced by the vortex on its surface is negligible and φ_v is a constant: the contribution to Eq. (28) of the outer surface reduces to the net flux of $\mathbf{v}_p$, which is zero. The contribution of the cut is 2π times the flux of $\mathbf{v}_p$ through the vortex loop. Introducing the mass flux of the applied potential flow through the vortex loop J_p, the contribution of the cross term (27) takes the simple form

$$E_I = \rho_s \frac{2\pi\hbar}{m_4} \int_{\text{loop}} \mathbf{v}_p \cdot d\mathbf{S} = \kappa_4 J_p. \tag{29}$$

Thus, an applied flow contributes to the vortex loop energy by the additional mass flux J_p that it causes through the loop times the quantum of circulation. This result will be derived in Sec. II.C from the more general phase-slippage theorem governing the exchange of energy between potential and vortical flows.

In the event that $\mathbf{v}_p$ can be considered as constant over the surface spanned by the vortex loop, Eq. (29) becomes even simpler:

$$E_I = \rho_s \kappa_4 \mathbf{S} \cdot \mathbf{v}_p, \tag{30}$$

in which $\mathbf{S}$ is the vectorial area of the loop, $\int d\mathbf{S} = (1/2)\oint \mathbf{r} \times d\mathbf{l}$, $d\mathbf{l}$ being the line element at point $\mathbf{s}$ of the oriented loop.

The total energy of the vortex immersed in an applied flow field is the sum of its energy in the rest frame E_0, given by Eq. (23), and the energy of interaction with the potential flow E_I. For Eq. (30), this reads

$$E_v = E_0 + \mathbf{P} \cdot \mathbf{v}_p, \quad \text{with} \quad \mathbf{P} = \rho_s \kappa_4 \mathbf{S}, \tag{31}$$

where $\mathbf{P}$ is defined as the impulse of the vortex loop.

For a circular loop of radius R, a vortex ring, Eq. (31) gives the well-known result (Lamb, 1945)

$$P_R = \pi \rho_s \kappa_4 R^2. \tag{32}$$

It emerges from this derivation (and the various approximations made along the way) that, under a Galilean boost, vortex loops do behave as Landau quasiparticles, with an energy proportional to their length and an impulse proportional to their area. This approach puts some flesh on the bare bones of the conventional (and exact) fluid-mechanical vortex dynamics; it gives substance to the intuitive view that they can be treated as independent elementary entities. This physically meaningful manner of separating the vortical flow from the local value of the remotely potential superflow v_p will prove quite useful in the following.

4. Vortex self-velocity

The impulse is not simply a plain geometrical quantity as Eq. (30) or (31) would let one think. It is the resultant of the impulsive pressures that must be applied to the fluid at rest to create the vortex loop from rest.[39] It possesses some of the

[35] See Saffman (1992), Sec. 2.4.

[36] It is understood here that the boundary does not carry vorticity. A case to the contrary is discussed by Sonin (1994).

[37] Such a point of view is discussed by Saffman (1992), Sec. 1.4.

[38] As expressed by

$$\int_V \nabla\Psi \cdot \nabla\Phi d\tau = \int_S \Phi \nabla\Psi \cdot d\mathbf{S} - \int_V \Phi \nabla^2\Psi d\tau,$$

with S being the surface bounding volume V and $d\mathbf{S}$ being the outward pointing surface element, and taking into account mass conservation of the fluid in incompressible flow [$\nabla^2\Psi = 0$, $\Psi = (\hbar/m_4)\varphi_p$ being the velocity potential of $\mathbf{v}_p$].

[39] See Lamb (1945), Sec. 152.

properties of a true momentum. For instance, the propagation velocity of the vortex ring, Eq. (34), can be expressed as the group velocity associated with the energy (24) and impulse (32) (Langer and Reppy, 1970; Roberts and Donnelly, 1970):

$$v_{\mathrm{R}} = \frac{dE_{\mathrm{R}}}{dP_{\mathrm{R}}} = \frac{\kappa_4}{4\pi R}\left(\ln\frac{8R}{a_0} - \frac{3}{4}\right). \tag{33}$$

Equation (33) tends asymptotically to the actual velocity of a ring with a hollow core as computed directly from the Biot-Savart law,[40] which moves along its symmetry axis $\hat{\mathbf{n}}$ with velocity

$$\frac{d\mathbf{s}}{dt} = \mathbf{v}_{\mathrm{R}} = \frac{\kappa_4}{4\pi R}\left(\ln\frac{8R}{a_0} - \frac{1}{4}\right)\hat{\mathbf{n}}. \tag{34}$$

However, these simple properties do not imply that a vortex has actual linear momentum. The vortical impulse is more elusive. For instance, it can be shown that a vortex ring moving freely under its own force at velocity v_{R} and impinging on a wall exerts no force on it (Fetter, 1972). This somewhat counterintuitive result arises from the distribution of the flow around the vortex loop (Cross, 1974). The contribution of the flow that goes in the forward direction, and which causes the ring free motion, does impart a momentum impulse into the wall equal to P_{R}, but the returning fluid away from the ring, the backflow, yields an opposite contribution that leads to full cancellation of the momentum transfer recorded over an infinitely extended wall for the complete collision event. This push and pull action constitutes a reminder that actual momentum is carried by the individual fluid elements and that a vortex is a hydrodynamical object made up of many of those elements.

Isolated circular rings propagate undistorted under their own velocity field in the superfluid at rest for symmetry reasons. Only a few vortex shapes propagate undistorted in their own velocity field. Straight vortex pairs and helical vortices are other examples (Langer and Reppy, 1970).

For an arbitrarily curved vortex, the self-velocity of each curve element can be approximated by Eq. (34), R being replaced by the local radius of curvature $r_{\mathrm{m}} = |d^2\mathbf{s}/d\xi^2|^{-1}$, the parameter ξ being the line length of the curve represented by $\mathbf{s}(\xi)$. The validity of this "local induction" approximation, which requires that r_{m} be large with respect to the vortex core radius, has been discussed, in particular, by Schwarz (1978, 1985) who has used it in extensive numerical simulations of 3D vortex motion.

5. The vortex mass

The impulse of a vortex discussed earlier is in no way related to the vortex self-velocity as the product of this velocity by an inertial mass. The problem of the mass of a vortex has been a long lasting riddle, which has now been resolved in a satisfactory way in superfluid ^{4}He.[41]

This mass arises from several contributions. If it is assumed that the vortex has a hollow core of radius a_0 and that the compressibility of the surrounding superfluid in rapid rotation can be neglected, the vortex mass is simply the mass of the displaced fluid. For a cylindrical body, this amounts to $\pi\rho_{\mathrm{s}}a_0^2$ per unit length, a standard result of classical fluid dynamics (Lamb, 1945). The minuteness of a_0 in ^{4}He, $1-2$ Å, of the same order as the interparticle spacing, makes this contribution very small.

However, compressibility cannot be neglected in the vicinity of the vortex core because the peripheral velocity Eq. (18) becomes large. The corresponding pressure drop is given by the Bernoulli equation

$$\frac{\delta P}{\rho_{\mathrm{s}}} = -\frac{1}{2}\delta(v_{\mathrm{s}}^2) = 0. \tag{35}$$

The change in density at distance r from the core, where the velocity is $\kappa_4/2\pi r$, is then

$$\delta\rho_{\mathrm{s}} = \frac{\delta P}{c_1^2} = \frac{\kappa_4^2}{8\pi^2}\frac{\rho_s}{c_1^2}\frac{1}{r^2}, \tag{36}$$

using the relation between the (first) sound velocity and the compressibility $c_1 = (\partial P/\partial\rho)^{-1/2}$,[42] which is justified when the normal fluid fraction is small ($\rho_{\mathrm{s}} \simeq \rho$). The overall change of mass about a unit length of vortex filament arising from the fluid compressibility is obtained by integrating Eq. (36) over space:

$$\mu_{\mathrm{v}} = \int_{a_0}^{r_{\mathrm{m}}}\int_0^{2\pi}\int_0^1 \delta\rho_{\mathrm{s}} r dr d\theta dz = \frac{\kappa_4^2}{4\pi}\frac{\rho_s}{c_1^2}\ln\frac{r_{\mathrm{m}}}{a_0}. \tag{37}$$

The vortex mass per unit length μ_{v} diverges logarithmically with r_{m} and ranges from negligible for $r_{\mathrm{m}} \sim$ a few core radii to important for large vortices, $r_{\mathrm{m}}/a_0 \gtrsim 10^3$. However, in most cases, the mass of the vortex remains small and can be neglected except for high frequency phenomena (Baym and Chandler, 1983; Sonin, 1987) and, possibly, for quantum tunneling (Volovik, 1997).

The Bernoulli effect, Eq. (36), also causes ^{3}He impurities and ions to be trapped on the vortex cores because their chemical potential decreases with the ^{4}He density. They prefer to sit in low density regions of the fluid. Trapped impurities add their own inertial mass m_{I} to that of the core. In superfluid ^{3}He, the core is large and yields the dominant contribution to the vortex mass (Kopnin, 1978, 1995; Duan and Leggett, 1992; Volovik, 1997).

C. Energy exchange between potential and vortical flows

Following the insight of Anderson (1966b), the idea that phase slippage by moving vorticity causes dissipation in superfluids and superconductors has become conventional wisdom. If, referring for instance to the situation of Fig. 5, there is not just one vortex as in Fig. 3 but a constant stream of vortices crossing the path 1-2 at a rate of n per second, driven

[40] See Lamb (1945), Sec. 163.

[41] Notably from the work of Baym and Chandler (1983), Duan (1994), and Sonin *et al.* (1998).

[42] See Landau and Lifshitz (1959), Sec. 131.

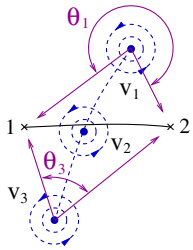

FIG. 5 (color online). Stream of vortices $v_1, v_2, v_3, \ldots$ crossing a path between points 1 and 2, moving from bottom to top. The vortices are represented by dots and are assumed perpendicular to the figure and nearly straight in the vicinity of 1-2. Each contributes angle θ_i to the phase difference recorded between 1 and 2. In its travel from far below to far above line 1-2, each vortex contributes 2π to the phase difference. According to the ac Josephson effect, a pressure difference develops in the superfluid due to the stream of vortices [see Eq. (38)].

by some external force, a pressure difference develops in the superfluid according to the Josephson ac relation (14). When the superfluid is free to move, it is accelerated by the cross stream of vortices: work is done onto the superfluid by the applied external force, for instance, an electric field acting on charges trapped in the vortex cores. This section focuses on the mechanism for this exchange of energy between the purely potential superflow and vorticity.

Anderson (1966b) noted in an appendix entitled "A 'new' corollary in classical hydrodynamics" that, whenever there exists a steady stream of vortices, for instance at the mouth of an orifice, the quantum phase in the superfluid would change there at a constant rate and, according to Eq. (14), the following chemical potential difference would build up:

$$\hbar \frac{dn_{\text{vortices}}}{dt}\bigg|_1^2 = \left\langle \hbar \frac{d(\varphi_2 - \varphi_1)}{dt} \right\rangle = \langle \mu_2 - \mu_1 \rangle. \tag{38}$$

In Eq. (38), the brackets represent time averaging and the quantity dn_{vortices}/dt for the rate of passage of vortices across a line joining points 1 and 2, as depicted in Fig. 5.

This result is of no special importance in classical hydrodynamics because the velocity circulation carried by each vortex, albeit constant, can take any value, while in the superfluid it is directly related to the phase of the macroscopic wave function and quantized. A formal proof of this conjecture based on the standard decomposition of any vector field into an irrotational contribution and a solenoidal one was given by Huggins (1970).[43] The following derivation is based on the more physical approach to vortex dynamics, which makes use of the concepts of force and energy.

1. The Magnus force

Consider the interaction energy between a vortex loop and a potential flow $\mathbf{v}_p$, Eq. (30). Under an infinitesimal displacement $\delta\mathbf{x}$ of a small line element $\Delta\mathbf{l}$, as shown in Fig. 6, the energy of the vortex loop changes according to

FIG. 6. Virtual displacement by δx of a small line element Δl.

$$\delta(\Delta E_I) = \kappa_4 \rho_s \delta\mathbf{x} \times \Delta\mathbf{l} \cdot \mathbf{v}_l = \kappa_4 \rho_s \Delta\mathbf{l} \times \mathbf{v}_l \cdot \delta\mathbf{x}, \tag{39}$$

where $\mathbf{v}_l$ is the local superflow velocity as seen by the vortex element standing still. The local flow velocity $\mathbf{v}_l$ is the sum of the applied superflow $\mathbf{v}_p$ and the flow induced by the other parts of the vortex loop $\mathbf{v}_v$. Equation (39) expresses the functional derivative $\delta(\Delta E_I)/\delta\mathbf{x}$ of the energy with respect to an infinitesimal deformation of the vortex line.

If the vortex loop moves along at velocity $\mathbf{v}_{\text{loop}}$ together with the element under consideration in the rest frame of the observer, $\mathbf{v}_l$ in Eq. (39) becomes $\mathbf{v}_l - \mathbf{v}_{\text{loop}}$ and this force takes the same form as the Magnus force for a line vortex in classical hydrodynamics[44] with a fluid density ρ_s:

$$\frac{\delta(\Delta E_I)}{\delta\mathbf{x}} = \Delta\mathbf{F}_M = \kappa_4 \rho_s (\mathbf{v}_{\text{loop}} - \mathbf{v}_l) \times \Delta\mathbf{l}. \tag{40}$$

The Magnus force, Eq. (40), has a simple physical origin. It is due to the Bernoulli effect that arises from the rotational flow around the vortex core. As shown in Fig. 7, this flow adds to the potential flow in the lower half plane and subtracts from it in the upper half plane. Integrating the resulting pressure difference obtained from the Bernoulli equation (35) over the cylinder yields a downward force expressed by Eq. (40). The Magnus force on each element of the vortex line arises ultimately from momentum conservation in the fluid and comes into play whenever the vortex trajectory differs from that of the local fluid particles. When no other force acts on the vortex core (such as an electric field on charges trapped in the core, or friction from the normal fluid component, etc.), $\mathbf{F}_M$ must be zero, hence $\mathbf{v}_{\text{loop}} = \mathbf{v}_l$: the vortex core moves with the local superfluid velocity. The velocity of the core at point $\mathbf{s}$ is the sum of the velocity of the local potential flow $\mathbf{v}_p$ at $\mathbf{s}$ when there is no vortex, and of the velocity $\mathbf{v}_v$ induced at $\mathbf{s}$ by the other parts of the vortex. If no flow is applied, $\mathbf{v}_p = 0$, then $\mathbf{v}_{\text{loop}} = \mathbf{v}_v$: the vortex loop moves under its own flow field in the superfluid at rest at large distance. The vortex thus appears to behave as a quasiparticle in its own right although it stands only for the vortical part of the total flow. The physical picture that emerges from this approach rings a familiar bell to condensed matter physicists.

2. Quantized vorticity and the Kelvin-Helmholtz theorem

The fact that free vortex loops move with the local fluid particles conforms to the Kelvin-Helmholtz theorem. This

[43] See also Zimmermann (1996) and Greiter (2005) for alternate derivations.

[44] See Sonin (1997) for a complete discussion of the Magnus force in classical fluids, neutral superfluids, and charged superfluids.

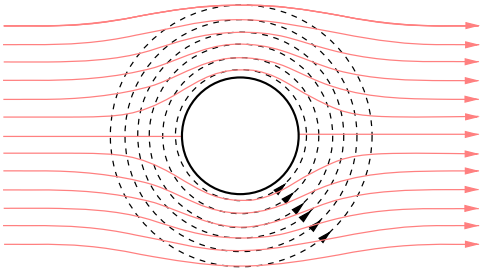

FIG. 7 (color online). Potential streamlines past the cylindrical vortex core flowing from left to right in thin plain lines. The flow from the vortex, in dashed lines, subtracts from the potential flow in the upper half and adds to it in the lower half, inducing a Bernoulli pressure difference between top and bottom.

result has been obtained as a consequence of the quantization of circulation, Eq. (18). The Kelvin-Helmholtz theorem is usually derived from the Euler equation and the implicit assumption that the motion of the fluid is isentropic (Landau and Lifshitz, 1959).[45] A further implicit assumption is that the velocity field and the loop deformation are well behaved analytically, that is, continuous in space and time.[46] The relevance of these remarks will become apparent in Sec. V.A on vortex nucleation, which deals with the spontaneous appearance of vorticity, in other words, the violation of the Kelvin-Helmholtz theorem. The derivation given above does not hide these fine points under the rug; it explicitly rests on the quantization of circulation, hence its conservation, and also implies isentropic and continuous superfluid motion. When this fails new phenomena occur: vortices may be nucleated.

As the effect of external forces and mutual friction has been set aside for simplicity, no work is done on the vortex itself except by the interaction with the local superflow. Thus any gain or loss of energy by the vortex balances that lost or gained by the potential flow. The way by which this conservation of energy proceeds is instructive; the detailed analysis is given in the following.

3. The phase-slippage theorem

If $\delta\mathbf{x}$, used in Eq. (39) as a virtual displacement to compute the forces acting on $\Delta\mathbf{l}$, becomes a real displacement $\mathbf{v}_{\rm loop}\Delta$t, actual work during the time Δt is done by the applied potential flow on the vortex loop. The energy balance is expressed by rewriting Eq. (39) as

$$\delta(\Delta E_{\rm I}) = \kappa_4\rho_{\rm s}\Delta\mathbf{l}\times(\mathbf{v}_{\rm p}+\mathbf{v}_{\rm v})\cdot\delta\mathbf{x} = \kappa_4\rho_{\rm s}\Delta\mathbf{l}\times\mathbf{v}_{\rm p}\cdot\mathbf{v}_{\rm loop}\Delta t+\kappa_4\rho_{\rm s}\Delta\mathbf{l}\times\mathbf{v}_{\rm v}\cdot\mathbf{v}_{\rm loop}\Delta t. \quad (41)$$

In free motion, disregarding friction of the core on the normal component and with no force applied externally, the vortex loop follows the fluid stream $\mathbf{v}_{\rm loop}=\mathbf{v}_{\rm l}=\mathbf{v}_{\rm p}+\mathbf{v}_{\rm v}$. The triple products are equal in magnitude and opposite in sign. The energy increment expressed by Eq. (41) is equal to zero. Total energy is conserved in the course of the vortex motion by the balance of the two terms in the last equality (41). The first, rewritten as

$$\delta(\Delta E_{\rm I})_1 = \kappa_4\rho_{\rm s}(\mathbf{v}_{\rm loop}\Delta t\times\Delta\mathbf{l})\cdot\mathbf{v}_{\rm p}, \quad (42)$$

is readily seen proportional to the rate at which the potential flow streamlines are crossed by the vortex element $\Delta\mathbf{l}$. It expresses the change of the potential flow kinetic energy when its streamlines are crossed by the vortex line, causing a change of the phase difference of 2π along them.

The second term requires a little more formal work to be recognized as a contribution to the vortex self-energy $E_{\rm v}$. What needs to be shown is that it corresponds to the energy variation for a small, local deformation of the vortex loop. This is established in the Appendix with the following result:

$$\delta(\Delta E_{\rm I})_2 = \kappa_4\rho_{\rm s}\Delta\mathbf{l}\times\mathbf{v}_{\rm v}\cdot\mathbf{v}_{\rm loop}\Delta t = \Delta E_{\rm v}(\delta\mathbf{x},\mathbf{v}_{\rm loop}), \quad (43)$$

for the displacement $\delta\mathbf{x}=\mathbf{v}_{\rm loop}\Delta t$ of the loop element $\Delta\mathbf{l}$.

The energy balance expressed by Eq. (41) between the potential flow kinetic energy and the vortex self-energy constitutes the fundamental relation governing phase slippage. In integral form, it yields Eq. (29). It shows the way by which a vortex loop of arbitrary shape can form by expanding from an infinitesimal loop.

The gist of Eq. (43) is that whenever a vortex cuts potential flow streamlines, it reversibly exchanges energy with the potential flow and it concurrently changes the velocity circulation along these streamlines by one quantum unit, causing slippage of the quantum phase. This process takes place in real time and locally, not only in a time-averaged fashion as in Anderson's conjecture, Eq. (38). If the potential flow is divergent (for instance outward from the mouth of a duct where the streamlines flare out), the vortex expands in length, collects energy from the flow, and slows it down. If the vortex runs away from that point to a far off distance and never comes back, this energy is irreversibly lost for the potential flow: dissipation of superflow energy has occurred. Reversing the flow direction, which then becomes convergent, results in the vortex shrinking and the potential flow picking up energy: a collapsing vortex dumps its energy into the potential flow and speeds it up.

These processes alter the quantum phase and will be discussed in Sec. V.E on the phase-slip mechanism. But before turning to the inner details of the phase slips, their experimental observations are briefly sketched in the next section.

III. PHASE-SLIPPAGE EXPERIMENTS

As the dc and ac effects predicted in the early 1960s by Josephson (1962, 1964, 1965) to take place between two suitably coupled superconductors were quickly observed (Anderson and Rowell, 1963; Shapiro, 1963), the search for analogous effects in superfluids also began, with the goal of observing unique quantum-mechanical effects in hydrodynamics. This search for a long time gave inconclusive

[45] See Sec. 8.

[46] For a discussion, see Saffman (1992), Sec. 1.6.

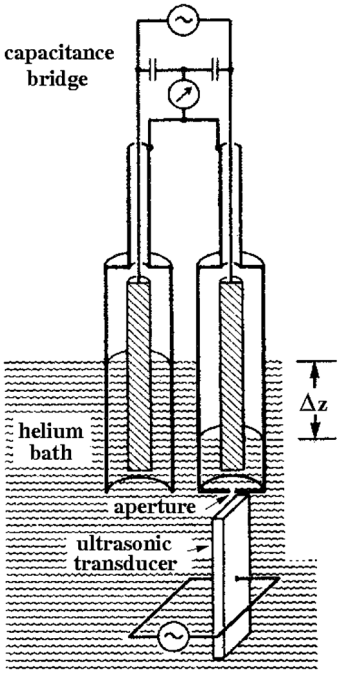

FIG. 8. The Richards-Anderson cell (1965).

results,[47] or led to blind alleys.[48] It was only in the mid-1980s that decisive steps forward were taken.[49]

A. The Richards-Anderson experiment

In order to observe the Josephson ac effect in superfluid helium, Richards and Anderson (1965) designed an experiment based on the beat note expected to form between the sound wave emitted by a quartz transducer immersed in the superfluid and the internal pressure fluctuation due to the ac effect. In this historical setup, shown in Fig. 8,[50] two identical coaxial capacitors are suspended over a liquid helium bath cooled at a temperature below the lambda point (of the order of 1.15 K). One of the capacitors is fully open ended, the other is partially closed at the bottom by nickel foil with a very small aperture. The foil is 25 μm thick, in which a 15 μm aperture had been punched with a sharp needle: the pinhole thus manufactured constitutes the "weak link" between the two superfluid pools.

If a helium level difference Δz between the two coaxial capacitors is created by lowering and raising the whole assembly over the liquid helium bath, the return to hydrostatic equilibrium is impeded by the pressure head of the steady stream of vortices corresponding to Eq. (38). The level difference can be precisely monitored by a capacitance bridge. When an ultrasound wave is shone by a quartz transducer facing the microaperture as shown in Fig. 8, it can couple to the stream of vortices and modulate the flow.

Steps in the return to equilibrium were indeed observed at level differences which were multiples and submultiples of the fundamental head difference frequency expected from the Josephson ac relation: $\Delta z = n\hbar\omega/n' m_4 g$, where n and n' are integers, and g is the acceleration of gravity. Richards and Anderson's results were reproduced by other researchers using similar setups, notably Khorana and Chandrasekhar (1967), Khorana (1969), and Hulin *et al.* (1971, 1972). Different setups, involving rotating or oscillating toroidal cells (Guernsey, 1971; Gregory, 1972), vortices accelerated by ions (Carey, Chandrasekhar, and Dahm, 1973), or a two-orifice flow arrangement (Gamota, 1974), were also tried but with mixed success at best, suffering from lack of reproducibility and poised with numerous unexpected features.

It eventually became clear that the early claims of observation of the Josephson ac effect by synchronization of the pressure head on the sound frequency did not meet universal acceptance. On the contrary, an alternate explanation in terms of acoustic standing waves in the cell was put forward on experimental grounds by Leiderer and Pobell (1973), as well as Musinski and Douglass (1972) (Musinski, 1973), and on theoretical grounds by Rudnick (1973). It was nonetheless argued by Anderson and Richards (1975) that, although acoustic resonances in the cell could be a concern, they could not account for all of the features observed in their experiments.

These efforts directed toward the demonstration of the hydrodynamic Josephson effects, together with direct studies of the critical velocity itself (Trela and Fairbank, 1967; Gamota, 1973), did bring experimental confirmation of the views of Feynman and Anderson that vortices were associated with the appearance of dissipation in superfluid flow. However, quantitative studies leading to a clear picture of how these vortices were created and how they interacted with the superflow were lacking. A consensus grew that somehow their formation and evolution had a chaotic character, presumably due to random preexisting vorticity in the superfluid and to a probable evolution toward some form of turbulent motion of the quantized vortices, a belief confirmed in part by the more recent studies described in Sec. VI. The flurry of activity stirred by the initial reports of observations related to the Josephson effects in helium receded almost completely.

With the hindsight gained from the experiments described later, it can now be concluded that the synchronization envisioned by Richards and Anderson (1965) would be nigh impossible to achieve. A particularly clear exposition of this synchronization experiment is given by Anderson, Beecken, and Zimmermann (1984) in terms of parametric effects due to the system nonlinearities, of the same kind as frequency pulling in radio frequency oscillators. These effects require that energy be stored reversibly in a nonlinear element, here the Josephson junction or, for rf devices, a nonlinear inductance. In ^{4}He far from the λ point the relation between the current and the phase difference across the weak link shows no nonlinearities. The energy that the vortices gather from the potential flow is carried swiftly away from the orifice and is irreversibly lost. It can be used to pull or push the flow in

[47]See Richards and Anderson (1965), Khorana and Chandrasekhar (1967), Khorana (1969), Richards (1970), Guernsey (1971), Gregory (1972), and Hulin *et al.* (1972).

[48]As mentioned by Schofield (1971), Musinski and Douglass (1972), Musinski (1973), and Gamota (1974).

[49]The work of Avenel and Varoquaux (1985, 1986b), Varoquaux, Avenel, and Meisel (1987), Amar *et al.* (1990, 1992), and Zimmermann (1993b, 1996) is described later.

[50]Later refined by Richards (1970).

synchronism with the sound excitation for a very brief lapse of time only, much shorter than the period of the audiofrequencies used in these experiments.[51] Furthermore, for the comparatively large orifices used then, vortices appear in a rather irregular fashion, not individually but in lumps with varying numbers, as discussed in Sec. VI.B. These peculiarities hamper the eventual synchronization to a regular pattern of steps.

B. The hydromechanical resonator

In the early 1980s, several groups went on striving to improve the detection techniques used in the search for the hydrodynamical Josephson effects. The use of a diaphragm-driven hydromechanical resonator fully immersed in the superfluid was pioneered by Zimmermann and his students.[52] A similar device with two chambers was built by Manninen and Pekola (1983) for critical velocity measurements in superfluid ^{3}He, and used by Lounasmaa *et al.* (1983) for the search of an ac Josephson effect in superfluid ^{3}He, a topic that will be covered in Sec. VII.B. The expertise developed at Cornell on torsional oscillators was put to use in superfluid ^{3}He by Reppy and his students (Crooker, 1984). Again, the hydrodynamic Josephson effects could not be observed in these various experiments for one or several of the following reasons:

- the apertures used as weak links were too large;
- the mass flow rate sensitivity was only marginally adequate;
- the superfluid motion was driven from current sources that were too stiff to let the response of the weak link be seen;
- and, last but not least, the cells were too bulky and too sensitive to external mechanical vibrations to allow for noninvasive measurements.

The first reason was clearly perceived as essential. Efforts shifted from superfluid ^{4}He to the newly discovered superfluid ^{3}He because the coherence length is 2 orders of magnitude larger, putting the fabrication of a genuinely weak superfluid link within reach of experimental low-temperature physicists. Work was carried out in that direction by Wirth and Zimmermann (1981), who were the first to use submicronic orifices in freestanding ultrathin foils, and others (Sudraud *et al.*, 1987; Amar *et al.*, 1990).

The detection of the minute mass currents that would flow in microapertures improved markedly in the early 1980s as reliable rf SQUIDs became available.[53] Ultrasensitive pressure and displacement gauges could then be developed (Avenel and Varoquaux, 1986a).

C. Early phase-slippage experiments

The phase-slippage experiments that were carried out starting from the mid-1980s using these refined techniques (Avenel and Varoquaux, 1985; Varoquaux, Avenel, and Meisel, 1987) confirmed Feynman and Anderson's views on dissipation in superflows and brought a large measure of clarification to the critical velocity problem (Varoquaux, Zimmermann, and Avenel, 1991) and to the formation of vortices in superfluid ^{4}He (Avenel, Ihas, and Varoquaux, 1993). These experimental results and their interpretation have since been largely confirmed by other workers.[54]

The design of the first weak link in which hydrodynamical Josephson effects were seen (Sudraud *et al.*, 1987) struck a compromise between two conflicting requirements that it be weak enough to effectively depress the wave function amplitude while preserving the macroscopic coherence of the superfluid and that it be large enough to let a measurable flow of liquid go through. A slit geometry was chosen for the microaperture, the smaller dimension of which was comparable with the coherence length in superfluid ^{3}He, ξ_0, which is in the submicron range (see Sec. VII.B). This orifice was micromachined by ion milling in a freestanding foil the thickness of which was also comparable to ξ_0. The third dimension of the slit was made large to provide a substantial cross-sectional area through which the superfluid would flow.

Phase slippage was studied with the help of a miniature hydromechanical device, represented schematically in Fig. 9, which is basically a flexible-wall Helmholtz resonator with two vents, immersed in the superfluid bath.[55] The flexible wall is constituted by a Kapton membrane coated with aluminum. In the version shown in Fig. 9, there are two openings connecting the resonator chamber to the main superfluid bath. One is a microaperture in which the critical velocity is reached. The critical event consists of a sudden change of the resonance amplitude corresponding to a departure from the expected classical hydrodynamics response of the flow velocity through the microaperture as discussed in the following. The other opening is an open duct and provides a parallel path to the superfluid, along which the quantum phase remains well determined in all circumstances. The velocity circulation along the superfluid closed loop threading the two openings shown in Fig. 9 changes by an integral number of quanta for each critical event.

The operation of these resonators is described in detail in the literature.[56] Flow is driven in and out of the resonator by an electrostatic ac drive applied to the aluminum-coated Kapton membrane. The membrane is mounted in such way as to be as flexible as possible; it provides the restoring elastic force in the resonator. The "common-mode" flow of liquid in and out

[51] As will become clear in the discussion of phase-slip mechanism in Sec. V.E.

[52] See Wirth and Zimmermann (1981), Anderson, Beecken, and Zimmermann (1984), and Beecken and Zimmermann (1987a).

[53] SQUID is an acronym for superconducting quantum interferometric device. The present sensitivity of dc-SQUID based displacement sensors used in the phase slippage described later on is $\sim 10^{-15}$ m/$\sqrt{\text{Hz}}$, or 1 F/$\sqrt{\text{Hz}}$.

[54] See Zimmermann (1996) and Packard (1998).

[55] Calling the device a "Helmholtz" resonator has been criticized as the compressibility of the fluid inside the chamber has a negligible effect at the low frequencies of the experiments, hence the little more convoluted appellation used here. The term "hydromechanical resonator" is also used in this paper.

[56] See Avenel and Varoquaux (1987), Beecken and Zimmermann (1987b), Varoquaux, Avenel, and Meisel (1987), Varoquaux and Avenel (1994), and Avenel *et al.* (1995).

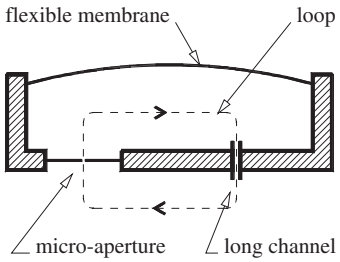

FIG. 9. Schematic of the flexible-diaphragm double-hole hydromechanical resonator. The dashed line shows a closed loop threading the two holes (microaperture and long channel) located entirely in the superfluid.

of the cell body through the two vents of the resonator provides a force of inertia to the hydromechanical device. These inertial and elastic terms determine the resonance frequency. The device is usually driven at or close to resonance in continuous mode. The raw data consist of peak amplitude charts as represented in Fig. 10. A strong impulsive force may also be applied to the membrane; the large transient response of the resonator reveals additional features when it becomes nonlinear.

In the absence of dissipation, the resonance motion under a small steady ac drive increases linearly in amplitude under the action of the drive as energy gradually gets stored in the resonator. This linear rise on the left of the trace in Fig. 10 proceeds until the flow velocity in the microaperture becomes critical. Sudden drops of the peak amplitude from one half cycle to the next then appear. These drops signal that a lump of

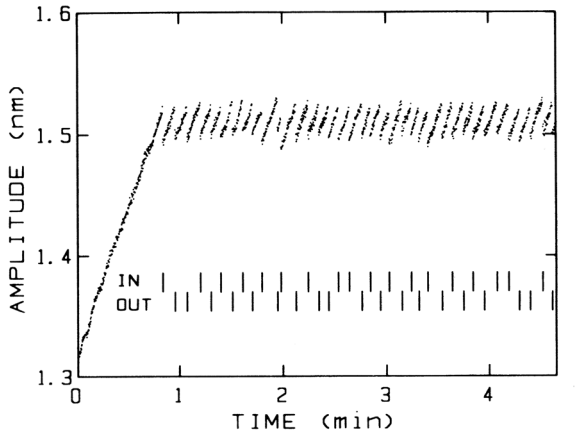

FIG. 10. Time chart of the peak resonance amplitude of the resonator membrane, in nm, for positive and for negative excursions. Each dot represents a measurement. The time interval between individual measurements is half a period, 177 ms here. The ticks labeled "in" and "out" indicate whether the jumps occur when the liquid flows in or out of the cell. The drive power applied to drive the resonance is very small (2.4×10^{-18} W). When the peak amplitude is subcritical, its value builds up linearly with time as seen at the left of the chart. The critical events are sharply defined and quite reproducible but occur at a threshold that varies slightly from event to event. The superfluid ^{4}He contained 100 to 300 ppb of ^{3}He and was cooled to about 10 mK under a very small hydrostatic pressure head. From Avenel and Varoquaux, 1985.

resonator energy has been lost between two successive recordings of the absolute peak amplitude. Quite importantly, these lumps are identical—to experimental uncertainty—from event to event.

These events are interpreted as the footprint left by vortices crossing the potential flow pattern in the vicinity of the microaperture. In their course, they cut all potential flow lines, pick up energy at the expense of the potential flow of the resonator, and change the phase difference along these flow lines by 2π. Hence the name "phase slips." These slips of the phase are sudden and take place at a fairly well-defined threshold, which defines the phase-slip critical velocity. It will become apparent in the following that this critical velocity, while signaling a breakdown of superfluidity, differs from other quantities also called "critical velocities." These features are discussed in detail in Secs. V and V.E.

D. Phase-slippage experimental results

The observation of phase slips in ^{4}He has led to a number of significant results. They brought a confirmation of Anderson's ideas, much welcome in view of the controversies about previous experiments. And quite importantly, they shed light on the previously indecipherable problems of the critical velocity and of vortex nucleation. Their most important qualitative features and some of their implications are summarized here.

(1) The critical velocity threshold, which can be seen on time charts such as that shown in Fig. 10, is markedly temperature dependent down to below 200 mK and reaches a well-defined plateau below 150 mK. These features are shown in Fig. 12 and are analyzed in Sec. V. As the thermodynamic properties of superfluid ^{4}He are very nearly independent of temperature below 1 K, this observation indicates that the critical process in action is not governed solely by hydrodynamics. Statistical mechanics may well play the leading role.

(2) Aperture size is not found to be a relevant factor, as long as it is "small enough," roughly below a few μm. This feature and the temperature dependence mentioned earlier are in sharp contrast with the Feynman critical velocity, which, as discussed in Sec. IV.B, exhibits a well-characterized dependence on size and none on temperature (except very close to the λ transition).

(3) The actual velocity threshold for phase slips shows significant scatter from one slip to the next in a given sequence, as can be seen in Fig. 23. This scatter lies much above the instrumental noise level of peak amplitude detection. It represents a genuine stochastic property of the physical process at work, which turns out to display a temperature dependence similar to that of the critical velocity itself, as shown in Fig. 13.

(4) The phase-slip pattern shows quite reproducible properties in the course of a given cooldown as long as the experimental cell is kept at a temperature below 10–15 K. If the temperature is cycled up to liquid nitrogen temperature and down again, small changes to the critical threshold and to the pattern itself can occur. These changes reveal the importance of minute

alterations in the surface state of the cell, e.g., contamination of the microaperture walls by solidified gases during thermal cycling.

(5) Quite importantly, phase slips are the signature that *quantized vortices* are created in aperture flow above a well-defined threshold of flow velocity. This statement is based on the measured value of the phase change, found to be 2π to the accuracy of the experiment (Avenel and Varoquaux, 1985). This amounts to a change of precisely one quantum of circulation in the superfluid loop threading the microaperture and the long parallel channel.[57] A detailed scenario for the occurrence and development of these phase slips has been described by Burkhart *et al.* (1994) and is discussed in Sec. V.E.

Critical velocities and phase slips in the superfluid phases of ^{3}He show different features that are discussed in Sec. VI.

IV. CRITICAL VELOCITIES IN SUPERFLUIDS

The critical velocity in a superfluid is defined as the threshold above which the flow of the superfluid component becomes dissipative, that is, the property of superfluidity is lost. This rather broad definition encompasses a number of different physical situations. This section begins with an overview of the different brands of critical velocities that comply with this definition. It concludes by focusing on that which involves the phase-slip phenomenon, namely, the nucleation of superfluid vortices.

Neither the problem of critical velocities in superfluids nor that of the nucleation of vortices are new. The former is as old as the discovery of superfluidity [see Wilks (1967)]. The latter, first discussed by Vinen (1963), has met an even more tortuous fate. It was first thought, still in some quarters not so long ago, to be highly impossible: such an extended hydrodynamical object as a vortex line with a finite circulation involving the collective motion of a large number of helium atoms would have a vanishingly small probability of occurring spontaneously. More recent experiments probing superflow on a finer scale of length have shown otherwise.[58]

A. The Landau criterion

As discussed previously in Sec. I.A, Landau (1941)[59] explained the absence of dissipation in the flow of helium-4 by the existence of a sharply defined dispersion curve for elementary excitations, the phonons and the rotons. This property is now associated with the phenomenon of Bose-Einstein condensation (Griffin, 1987, 1993), as has long been suspected (London, 1954). Elementary excitation energy levels $\epsilon(\mathbf{p})$ are well defined. They have a negligible spread in energy. States with very low energy are thus extremely rare. This scarcity of low-lying states is held responsible for the inviscid property of ^{4}He.

An impurity, or a solid obstacle, can exchange only an energy $\epsilon(\mathbf{p})$ at momentum $\mathbf{p}$ that exactly matches the energy of an elementary excitation of the fluid. If the superfluid moves at velocity $\mathbf{v}_s$, the energy of elementary excitations in the frame of reference at rest becomes $\epsilon - \mathbf{v}_s \cdot \mathbf{p}$ (Wilks, 1967; Baym, 1969). The same holds for a moving obstacle, by Galilean invariance. If this energy turns negative, elementary excitations proliferate and superfluidity is lost. The condition on the superfluid velocity for this to happen reads

$$v_s \geq v_L = \left.\frac{\epsilon(p)}{p}\right|_{\min} \simeq \left.\frac{\epsilon(p)}{p}\right|_{\text{roton}}. \tag{44}$$

Unless this condition is met, there is no dissipative interaction between the fluid and its surroundings: the flow is viscousless.

The minimum value of ϵ/p for helium lies very close to the roton minimum, as shown in Fig. 1. This means that rotons are created when the Landau critical velocity is reached in ^{4}He. At low pressure, the roton minimum parameters are such that $v_L \simeq 60$ m/s. The Landau critical velocity has been observed under certain conditions in the propagation of ions in which rotons are created in ^{4}He as reviewed by McClintock and Bowley (1995). The much less dense Bose-Einstein condensed gases sustain a phononlike energy spectrum at low momentum (Bogolyubov, 1947) and no rotonlike features; the Landau velocity is the sound velocity $c = \epsilon(p)/p|_{p=0}$ and phonons are emitted. The Landau critical velocity v_L in superfluid ^{4}He is smaller than the sound velocity ($c = 220$ m/s at low pressure) but is still much larger than the critical velocities observed in most experiments.

B. Feynman's approach

Feynman (1953a, 1953b, 1954, 1955), realized, following Onsager, that not only would vorticity be quantized in ^{4}He in units of the quantum of circulation $\kappa_4 = 2\pi\hbar/m_4$ but, preceding Anderson, that these vortices would be responsible for the onset of dissipation and for a critical velocity in the superfluid. In Feynman's views, vortices would be puffed out of the mouth of orifices much in the way of smoke rings—or von Karmann alleys past obstacles in classical (Navier-Stokes) fluids.

Such vortex rings can be treated as elementary excitations of the superfluid, which they rightfully are from the vantage point taken in Sec. II. Hence Landau's criterion applies. The limiting velocity associated with these vortex rings, assumed to be circular, can be evaluated from the expressions for the energy E_R and impulse P_R, Eqs. (24) and (32). The critical value set by Eq. (44) is reached for a radius R such that E_R/P_R is at a minimum, which occurs when R is as large as feasible, that is, of the order of the orifice size d. This minimum value sets the lowest velocity at which vortices can start to appear and defines the Feynman critical velocity:

$$v_F \simeq \frac{\kappa_4}{2\pi d}\ln\left(\frac{d}{a_0}\right). \tag{45}$$

As discussed next, v_F is much closer to experimental values than the Landau critical velocity for rotons. Although this

[57] See Fig. 9 or Fig. 34 for a more realistic cell.

[58] As reported by Muirhead, Vinen, and Donnelly (1984), Varoquaux, Avenel, and Meisel (1987), and Varoquaux and Avenel (2003).

[59] For complete accounts of Landau's work, see Khalatnikov (1965) and Wilks (1967).

agreement is heartening, it also raises questions: how do these vortices come about and how do they evolve?

C. Several kinds of critical velocities

The compilation of the critical velocity data in various apertures and channels from various sources available at the time of the Exeter Meeting in 1990 (Varoquaux, Zimmermann, and Avenel, 1991) is shown in Fig. 11 together with more recent data. Two different critical velocity regimes appear on this graph, a fast regime for small apertures, of the phase-slip type, which is temperature dependent, and a slower regime for larger channels, of the Feynman type, which is temperature independent. The data points from various sources for these two different types of critical velocity do not fall on well-defined lines but merely bunch into clusters of points. As stated, critical velocities in apertures and capillaries are not very reproducible from experiment to experiment indicating that, besides size, temperature, and pressure, some less-well-controlled parameters also exert an influence. In some occasions, switching between these two types of critical velocity has been observed in the course of the same cooldown (Hulin *et al.*, 1974; Zimmermann, 1993a).

The critical velocity that depends on channel size follows on average Eq. (45) for the Feynman mechanism. The higher critical velocities, bunched around 5 to 10 m/s, faster than the Feynman v_F even for the smallest apertures but still considerably slower than Landau's v_L relate to the phase-slip phenomenon and are discussed later.

As a basis for comparison, it is worthwhile to summarize the findings of the ion propagation studies in superfluid ^{4}He at various pressures, which have been reviewed by McClintock and Bowley (1991, 1995). Ions can be created in liquid helium and accelerated by electric field until they reach a limiting velocity. The resulting drift velocities are measured by time-of-flight techniques. For negative ions, hollow bubbles 30 Å in diameter with an electron inside, two different behaviors are observed:

- Below about 10 bars, vortex rings are created, on the core of which single electrons get trapped: the drift velocity suddenly drops from that of the negatively charged bubbles to that of the much slower vortex rings (Rayfield and Reif, 1964).
- Above 10 bars, the accelerated ion runs into the roton emission mechanism before vortex rings can be created. The Landau critical velocity is observed to be ≈ 46 m/s at 24 bars down from a calculated value of 60 m/s at SVP as the roton parameters change with pressure while the vortex creation velocity increases with pressure (Varoquaux and Avenel, 1996b).
- Around 10 bars, both critical velocities, the Landau critical velocity for the formation of rotons and that for the formation of vortex rings, can be observed to occur simultaneously because ions can be accelerated above the threshold for roton emission.

These ion propagation measurements provide a vivid illustration not only of the existence of a critical velocity obeying the Landau criterion but also that roton creation and vortex formation constitute different phenomena and can exist concurrently.[60] The vortex emission threshold displays other noteworthy features. It depends on temperature in a nontrivial way, comparable to that of the phase slip and also shows the marked dependence on ^{3}He impurity concentration observed for phase slips in microaperture flows but not in larger channels. In both ion propagation and aperture flow measurements, vortex formation displays similar features.

Altogether, a study of the experimental data in superfluid ^{4}He reveals three different, well-defined, types of critical velocities: one, the celebrated Landau critical velocity v_L observed in ^{4}He only for ion propagation; another, v_F, that appears to follow the Feynman criterion as shown in Fig. 11 with all the uncertainties on the hydrodynamical process of vortex creation in larger channels; and a third, v_c, for phase slips, in need of an explanation: how are the vortices of phase slips in aperture flow created, and how does the situation differ from that in larger channels?

The short answer, based on qualitative evidence, is that the temperature dependence of v_c and its stochastic properties clearly point toward a process of nucleation by thermal activation above ~150 mK or so and by quantum tunneling below. This conclusion contradicts the common-place daily observations of the formation of whirlpools and eddies, and also the widely held belief that large-scale topological defects with a quantum charge of circulation cannot appear out of nowhere in the superfluid. It will be seen to hold in ^{4}He only because the nucleated vortices have nanometric size, a fact that came to be appreciated because of the detailed analysis of phase-slippage observations related below.

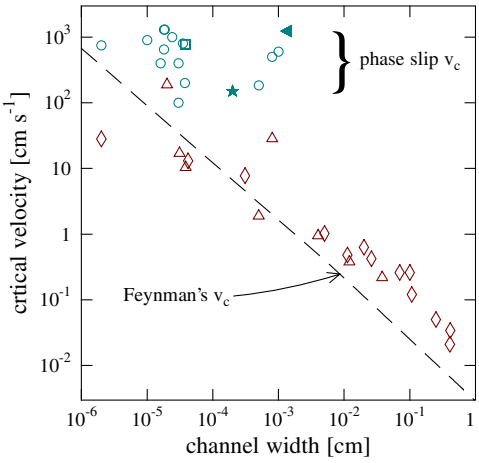

FIG. 11 (color online). Critical velocity data vs channel width (◇) Wilks (1967); (○) and (△) temperature-dependent and temperature-independent data as compiled by Varoquaux, Zimmermann, and Avenel (1991); (◀) Shifflett and Hess (1995); (★) Flaten, Lindensmith, and Zimmermann (2006); (□) Steinhauer *et al.* (1995) as reanalyzed by Varoquaux and Avenel (1996a). For the temperature-dependent data, the highest value, i.e., that at the lowest temperature, has been retained. The dashed line is obtained from Eq. (45) for the Feynman critical velocity.

[60] A noteworthy attempt to by-pass this experimental finding is that of Andreev and Melnikovsky (2004).

V. PHASE-SLIP CRITICAL VELOCITY: A STOCHASTIC PROCESS

A more firmly established answer to the question formulated comes from a quantitative analysis of the experimental data for phase slips. The clues given conclusively show that, in small apertures, vortices are nucleated by thermal activation above about 150 mK, and by quantum tunneling below.[61]

The first piece of evidence for the nucleation of vortices, that is their creation *ex nihilo*, rests on the temperature dependence of the phase-slip critical velocity shown in Fig. 12. This figure, as Fig. 11 (and Fig. 13 to be discussed later on), represents an attempt to compare data from different groups. The data points are scattered but a general trend emerges. The phase-slip critical velocity increases in a near-linear manner when the temperature decreases from 2 to ~0.2 K. That is, the functional dependence of v_c upon T goes as $v_c = v_0(1 - T/T_0)$. The data depart from this linear dependence below 200 mK, where they reach a plateau, and above 2 K because the critical velocity goes to zero at T_λ.

This temperature dependence first observed in 1985 at Orsay (Varoquaux, Avenel, and Meisel, 1987; Varoquaux *et al.*, 2001) and now a well-established experimental fact (Steinhauer *et al.*, 1995; Zimmermann, Lindensmith, and Flaten, 1998) is very telling. It came as a surprise at first because the critical velocities observed before were temperature independent below ~1 K. As the quantum fluid is nearly fully in its ground state below 1 K, the normal fluid fraction becomes less than 1%, one is led to suspect that a Arrhenius-type process must come into play. If such is the case, that is, if thermal fluctuations in the fluid with an energy of at most a few $k_B T$ can trigger the appearance of fully formed vortex out of nowhere, the energy of this vortex must also be of the order of a few $k_B T$: it must be a very small vortex. But very small vortices require rather large superfluid velocities to sustain themselves as seen in Eq. (34). That these requirements can be met emerges from a detailed quantitative analysis of the experimental data in the framework of the nucleation process.

The nucleation rate for a thermally activated process is expressed by Arrhenius's law:

$$\Gamma_K = \frac{\omega_0}{2\pi}[(1+\alpha^2)^{1/2} - \alpha] \exp\left\{-\frac{E_a}{k_B T}\right\}, \qquad (46)$$

where $\omega_0/2\pi$ is the attempt frequency and E_a is the activation energy of the process, which depends on the velocity v_p and, more weakly, on the pressure P and the temperature T. The correction for dissipation in the square brackets was introduced by Kramers (1940) to describe the escape of a particle trapped in a potential well and interacting with a thermal bath in its environment. The particle undergoes Brownian motion fluctuations and experiences dissipation. This dissipation is characterized by a dimensionless coefficient $\alpha = 1/(2\omega_0\tau)$, τ being the time of relaxation of the system toward equilibrium. In superfluid helium, dissipation is small. Although some dissipation is necessary for the system to reach equilibrium with its environment, its influence on the thermal activation rate is very small and will be neglected in the following. However, this will not be so anymore in the quantum regime, considered next, because dissipation causes decoherence.

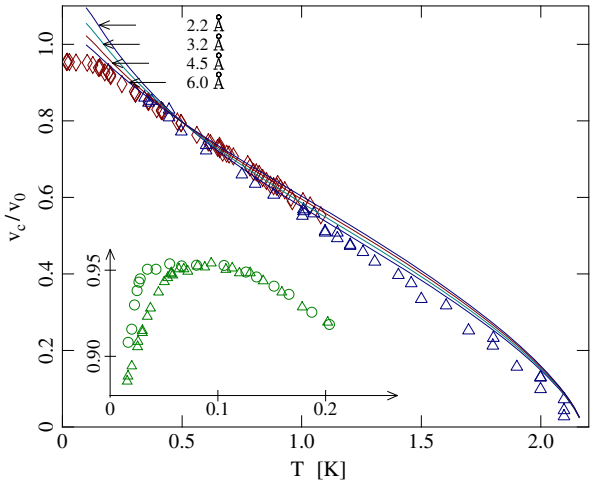

FIG. 12 (color online). Critical velocity, normalized to the zero-temperature linear extrapolation value v_0, vs T, in kelvin: (◇) Avenel, Ihas, and Varoquaux (1993), for ultrapure ^{4}He; (△) Zimmermann, Lindensmith, and Flaten (1998). The plain curves are computed from the half-ring model (see Sec. V.E) for $a_0 = 2.2$, 3.2, 4.5, and 6.0 Å and are normalized to match the experimental value at 0.5 K. The inset shows the influence of ^{3}He impurities on v_c: (∘) 3 ppb ^{3}He in ^{4}He; (△) 45 ppb, from Varoquaux *et al.* (1993). Adapted from Varoquaux *et al.*, 2001.

The expression for the critical velocity that stems from the Arrhenius rate, Eq. (46), is derived as follows. In experiments such as those shown in Fig. 10, the velocity varies periodically at the resonance frequency as $v_p \cos(\omega t)$, v_p being the peak velocity of the potential flow. The probability that a phase slip takes place during the half cycle $\omega t_i = -\pi/2$, $\omega t_f = \pi/2$ is

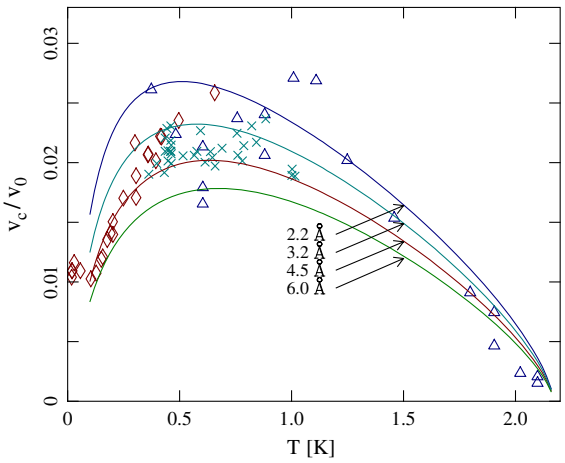

FIG. 13 (color online). Statistical width of the critical velocity transition, normalized to the linear extrapolation limit at $T = 0$, v_0, in terms of temperature: (◇) Avenel, Ihas, and Varoquaux (1993); (△) Zimmermann, Lindensmith, and Flaten (1998); (×) Steinhauer *et al.* (1995). The plain curves are computed as in Fig. 12 for four values for a_0. Adapted from Varoquaux *et al.*, 2001.

[61]This section is based on the work of Varoquaux *et al.* (2001), Varoquaux and Avenel (2003), and Varoquaux (2006).

$$p = 1 - \exp\left\{-\int_{t_i}^{t_f} \Gamma_K(P, T, v_p \cos(\omega t'))\right\} dt'$$
$$= 1 - \exp\left\{-\frac{\omega_0}{2\pi\omega}\sqrt{\frac{-2\pi k_B T}{v_p \partial E_a/\partial v|_{t=0}}}\exp\left(-\frac{E_a}{k_B T}\right)\right\}. \quad (47)$$

Equation (47) results from an asymptotic evaluation of the integral at the saddle point $t = 0$.

The critical velocity v_c is defined as the velocity for which $p = 1/2$. This definition is independent of the experimental setup, except for the occurrence in Eq. (47) of the natural frequency of the hydromechanical resonator ω. The implicit relation between v_c and E_a then reads

$$\frac{\omega_0}{2\pi\omega}\sqrt{\frac{-2\pi k_{BT}}{v_c \partial E_a/\partial v|_{v_c}}}\exp\left\{-\frac{E_a(P, T, v_c)}{k_B T}\right\} = \ln 2. \quad (48)$$

In Eq. (48), the attempt frequency is normalized by the resonator drive frequency: the Brownian particle attempts to escape from the potential well at rate $\omega_0/2\pi$ but an escape event is likely only in the time window in a given half cycle of the resonance during which the energy barrier stays close to its minimum value $E_a(v_c)$. This time interval is inversely proportional to ω, which explains why an instrumental parameter gets its way into Eqs. (47) and (48).

The velocity at which each individual critical event takes place is a stochastic quantity. Its statistical spread can be characterized by the "width" of the probability distribution defined (Zimmermann, Avenel, and Varoquaux, 1990; Avenel, Ihas, and Varoquaux, 1993) as the inverse of the slope of the distribution at v_c, $(\partial p/\partial v|_{v_c})^{-1}$. This critical width is found to be expressed by

$$\Delta v_c = -\frac{2}{\ln 2}\left[\frac{1}{2}\left\{\frac{1}{v_c} + \frac{\partial^2 E_a}{\partial v^2}\bigg|_{v_c}\bigg/\frac{\partial E_a}{\partial v}\bigg|_{v_c}\right\} + \frac{1}{k_B T}\frac{\partial E_a}{\partial v}\bigg|_{v_c}\right]^{-1}. \quad (49)$$

The quantities v_c and Δv_c are derived from p, itself obtained by integrating the histograms of the number of nucleation events ordered in velocity bins. The outcome of this procedure is illustrated in Fig. 14: p shows an asymmetric-S shape characteristic of the double exponential dependence of p on v, Eq. (47), a consequence of Arrhenius's law, Eq. (46), being plugged into a Poisson probability distribution. The observation of this asymmetric-S probability distribution constitutes an additional experimental clue for the existence of a nucleation process. The quantities v_c and Δv_c are easily extracted from the probability curves $p(v)$, but the inverse path from v_c and Δv_c back to $E_a(v)$ and ω_0 by numerical integration of the differential equation (48) leads to inaccurate results.

In view of these difficulties Varoquaux and Avenel (2003) improved the data analysis by obtaining the escape rate $\Gamma(v)$ directly from the phase-slip data. This rate is the ratio in any velocity bin of the number of slips that have occurred at that velocity to the total time spent by the system at that given velocity. The outcome of this procedure is illustrated in Fig. 15. The slope of $\ln\Gamma(v)$ directly yields $\partial E_a/\partial v|_{v_c}$; the value of $\ln\Gamma$ at v_c gives a combination of $\ln\omega_0$ and $E_a(v_c)$.

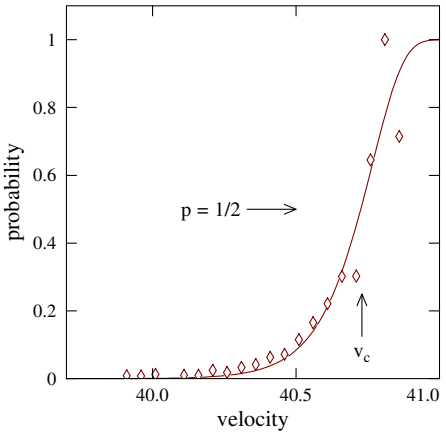

FIG. 14 (color online). Probability p vs phase-slip velocity in winding number. The plain curve is a nonlinear least squares fit to the analytic form Eq. (47), which contains two adjustable parameters v_c and Δv_c. The critical velocity resulting from this distribution of the measured values is defined as the fit value for $p = 1/2$. The critical velocity distribution width is given by the slope at $p = 1/2$. From Varoquaux and Avenel, 2003.

The need to solve Eq. (48) has been alleviated but to cleanly disentangle these two quantities and solve this inverse problem is still error prone. At this point experiment itself offers help as will shortly be shown.

A. Vortex nucleation: Thermal versus quantum

Below ~0.15 K, the phase-slip critical velocity v_c suddenly ceases to vary with T, as seen in Fig. 12 for ultrapure ^{4}He, and $v_c(T)$ remains flat down to the lowest temperatures (~12 mK). The effect of ^{3}He impurities, shown in the inset, could mimic the appearance of such a plateau but is ruled out because of the extreme purity of the ^{4}He sample, which contains less than 1 part in 10^9 of ^{3}He impurities. The

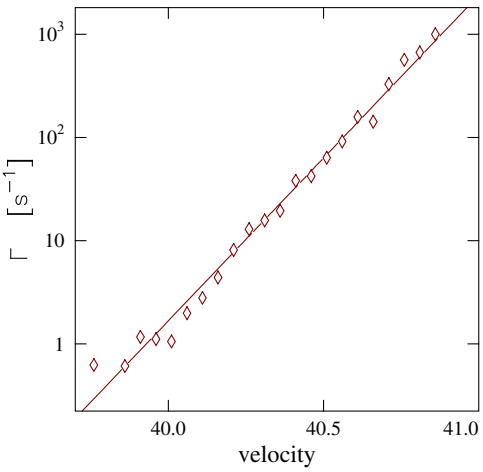

FIG. 15 (color online). Nucleation rate Γ expressed in s^{-1} on a semilogarithmic scale vs slip velocity in winding number in ultrapure ^{4}He at 17.70 mK and saturated vapor pressure. The line is a linear fit to the data. From Varoquaux and Avenel, 2003.

crossover between these two regimes is very sharp. At the same crossover temperature T_q, Δv_c also levels off sharply. It is believed on experimental grounds that this saturation is intrinsic and is not due to stray heating or parasitic mechanical vibrations (Avenel, Ihas, and Varoquaux, 1993).

If the nucleation barrier were undergoing an abrupt change at T_q, for instance because of a bifurcation toward a vortex instability of a different nature (Josserand and Pomeau, 1995), in all likelihood Δv_c would jump to a different value characteristic of the new process (presumably small since v_c reaches a plateau). Such a jump is not observed in Fig. 13. Furthermore, v_c levels off below T_q, which would imply through Eq. (48) that E_a becomes a very steep function of v, but Δv_c also levels off, which, through Eq. (49), would imply the contrary. This discussion leads one to investigate the possibility that, below T_q, thermally assisted escape over the barrier gives way to quantum tunneling under the barrier (Ihas *et al.*, 1992). This switch from thermal to quantum does induce plateaus below T_q for both v_c and Δv_c.

Independently of these phase-slippage studies, the group of Peter McClintock at Lancaster had also reached the conclusion from their ion propagation experiments of the existence of a crossover around 300 mK from a thermal to a quantum regime for the nucleation of vortices (Hendry *et al.*, 1988), as predicted by Muirhead, Vinen, and Donnelly (1984). There certainly are significant differences between the ion limiting drift velocity and aperture critical flow, in particular, the latter is nearly 1 order of magnitude smaller, but the qualitative similarities are strikingly telling. The two completely different types of experiments indicate that vortices would appear as a result of a nucleation process on a nanometric scale, both in a thermal regime above T_q and in a quantum one below.

B. The macroscopic quantum-tunneling rate

Taking this hint at face value, zero-point fluctuations are now assumed to overtake thermal fluctuations below T_q: the potential barrier is not surmounted with the assistance of a large thermal fluctuation, it is tunneled under quantum mechanically; the quantum-tunneling event is "assisted" by the zero-point fluctuations (Martinis and Grabert, 1988) in the same manner as the Arrhenius process is assisted by thermal fluctuations. What is remarkable here, and not so easy to admit at first, is that such a tunneling process affects a macroscopic number of atoms, those necessary to form a vortex of about 50 Å in length, as turns out to be the case.

These "macroscopic quantum-tunneling" (MQT) processes have been the object of numerous experimental and theoretical studies, mainly in superconducting Josephson devices (Caldeira and Leggett, 1983). The case for vortices in helium can be worked out in a similar manner.

The quantum-tunneling rate of escape of a particle out of a potential well $V(q)$ is a textbook problem.[62] The rate is proportional to $\exp(-S/\hbar)$, S being, in the Wentzel-Kramers-Brillouin (WKB) approximation, the action of the escaping particle along the saddle-point trajectory at the top of the potential barrier, the so-called "bounce" (Coleman, 1977). For a particle of mass m and energy E escaping from a one-dimensional barrier $V(q)$, this action reads

$$S = 2\int_{q_1}^{q_2} dq\sqrt{2m[V(q)-E]}. \tag{50}$$

The determination of the bounce yields the generalized coordinates q_1 and q_2 of the points at which the particle enters and leaves the barrier. A discussion of the quantum tunneling of vortices in terms of Eq. (50) thus requires a Lagrangian formulation of vortex dynamics. Such a formulation has been carried out, in particular, by Sonin (1995)[63] and Fischer (2000). However, analytic results can be obtained only at the cost of approximations that yield a less than fair comparison with experiments as discussed by Varoquaux *et al.* (2001).

A simplified and more productive approach can be borrowed from the literature for Josephson devices. Extending the work of Caldeira and Leggett (1983) and Larkin, Likharev, and Ovchinnikov (1984) to vortices in helium, Varoquaux (2006) used for $V(q)$ a simple analytic form reduced to a sum of two terms, respectively, parabolic and cubic in q:

$$V(q) = V_0 + \frac{1}{2}m\omega_0^2 q^2\left(1-\frac{2q}{3q_b}\right), \tag{51}$$

where ω_0 is the angular frequency of the lowest mode of the trapped particle (that will be found comparable to the attempt frequency) and q_b is the generalized coordinate of the barrier top location. The barrier height E_b is expressed in terms of these two parameters by $m\omega_0^2 q_b^2/6$.

Equation (51) expresses the vanishing potential barrier height when the applied velocity reaches the limiting velocity v_{c0} at which the system "runs away," the so-called "lability" point.[64] At this point where the system becomes labile, the critical velocity is reached even in the absence of thermal or quantum fluctuations. Such a hydrodynamic instability threshold at which vortices appear spontaneously has been shown to occur in numerical simulations of flows past an obstacle using the Gross-Pitaevskii equation by Frisch, Pomeau, and Rica (1992) and others.[65]

The zero-temperature WKB tunneling rate for the phenomenological cubic-plus-parabolic potential E_b, Eq. (51), is found to be (Caldeira and Leggett, 1983)

$$\Gamma_0 = \frac{\omega_0}{2\pi}\left(120\pi\frac{S_0}{\hbar}\right)^{1/2}\exp\left(-\frac{S_0}{\hbar}\right), \tag{52}$$

with the action S_0 being equal to $36E_b/5\omega_0$.

From this result, it can be anticipated that the crossover between the quantum and the thermal regime lies around a temperature close to that for which the exponents in Eqs. (46) and (52) are equal, namely, $T = 5\omega_0/36k_B$—assuming that

[62] See Landau and Lifshitz (1958), Sec. 50.

[63] See also Sonin (2015), Sec. 12.2.

[64] For an illustration, see Fig. 2 in Anderson (1966b) for the "tilted washboard" model.

[65] See Nore, Huepe, and Brachet (2000), Berloff and Roberts (2001), and Rica (2001).

the activation energy E_a in Eq. (46) reduces to the simple cubic-plus-parabolic form E_b. A more precise study of the mathematical properties of the quantum channel for escape leads to the following relation (Mel'nikov, 1991):

$$\hbar\omega_0 = 2\pi k_B T_q. \tag{53}$$

Thus, from the experimental knowledge of the temperature of the crossover from thermal to quantal, ω_0 is fixed to pinpoint accuracy by Eq. (53). Its value agrees with that (less precisely determined) obtained from the analysis of the Arrhenius regime outlined previously: some degree of self-consistency has been achieved. The values of the barrier height E_b at each given velocity then follow easily, using the full expressions for the rate in terms of E_b, ω_0, and, also, for the damping parameter α as discussed next.

C. Friction in MQT

Damping turns out to matter significantly for quantum tunneling of semimacroscopic objects, contrary to the thermal regime. The relevance and applicability of the concept of quantum tunneling to macroscopic quantities such as the electric current through a Josephson junction or the flow of superfluid through a microaperture, although still sometimes questioned, have been checked in detail for the electrodynamic Josephson effect (Martinis, Devoret, and Clarke, 1987). One of the conceptual problems is that, when a macroscopic quantum system is coupled to an environment that acts as a thermal bath, the coupling gives rise to a source of classical fluctuations and friction. The quantum process suffers decoherence and is profoundly affected.

This issue was tackled by Caldeira and Leggett (1983), and a number of others.[66] For weak frequency-independent damping ($\alpha \ll 1$) and the cubic-plus-parabolic potential, the tunneling rate takes the form[67]

$$\Gamma_{qt} = \frac{\omega_0}{2\pi}\left(864\pi\frac{E_b}{\hbar\omega_0}\right)^{1/2}\exp\left\{-\frac{36}{5}\frac{E_b}{\hbar\omega_0}\left[1+\frac{45\zeta(3)}{\pi^3}\alpha\right] + \frac{18}{\pi}\alpha\frac{T^2}{T_q^2} + \mathcal{O}\left(\alpha^2, \alpha\frac{T^4}{T_q^4}\right)\right\}. \tag{54}$$

According to Eq. (54), damping depresses the MQT escape rate at $T = 0$ (α being a positive quantity) and introduces a temperature dependence that increases the rate as T increases. These effects are large, even for weak damping, because they enter the exponent of the exponential factor in Eq. (54). Equation (53) between T_q and ω_0 is nearly unaffected by damping: ω_0 is simply changed into $\omega_0[(1+\alpha^2)^{1/2} - \alpha]$ according to Eq. (46), a minor modification for $\alpha \ll 1$.

Equation (54) is valid up to about $T_q/2$. From $T_q/2$ to $\sim T_q$, one has to resort to numerical calculations (Grabert, Olschowski, and Weiss, 1987). In the thermal activation regime $T \gtrsim T_q$ quantum corrections affect the Kramers escape rate up to about $3T_q$ and can be evaluated analytically. These high-temperature quantum corrections depend only weakly on friction. A complete solution of the problem of the influence of friction, weak, moderate, or strong, has first been worked out in the classical regime ($T \gg T_q$) by Grabert (1988) and extended to the temperature range $T \gtrsim T_q$ by Rips and Pollak (1990) who showed that the rate for arbitrary damping can be factorized in three terms,

$$\Gamma = f_q \Upsilon \Gamma_K, \tag{55}$$

each term having a well-defined physical meaning: Γ_K is the classical Kramers rate, f_q is the quantum correction factor, and Υ is the depopulation factor. The high-temperature limit of f_q is

$$f_q = \exp\left\{\frac{\hbar^2}{24}\frac{(\omega_0^2+\omega_b^2)}{(k_B T)^2} + \mathcal{O}(\alpha/T^3, 1/T^4)\right\}, \tag{56}$$

in which ω_0 and ω_b are the confining potential parameters depicted in Fig. 16. Analytic results for f_q are known to slightly below T_q (Grabert, Olschowski, and Weiss, 1987; Hänggi, Talkner, and Borkovec, 1990).

The depopulation factor Υ arises from the depletion of the occupancy of the energy levels inside the potential well in the course of the escape process. This depletion occurs when the intermediate levels, if they exist, are not replenished fast enough by the thermal fluctuations. For the nucleation of vortices, friction turns out to always be both sufficient and not too large so that depopulation corrections remain small and $\Upsilon \sim 1$.

The escape rate can be calculated over the full temperature range by piecing together Eqs. (46), (54), (55), and (56). The results for three values of the damping parameter α are shown in Fig. 17. A hand-sketched line pictures the escape rate for α varying from zero at $T = 0$ to 0.5 above T_q: it is seen to actually decrease when the temperature increases from

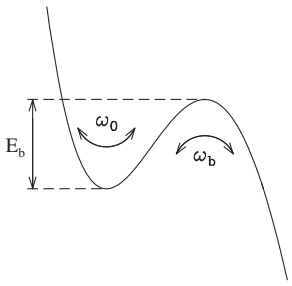

FIG. 16. Potential well trapping a particle in one dimension. The particle can escape to the continuum of states to the right. The lowest mode at the bottom of the well has angular frequency ω_0; ω_b would be the corresponding quantity if the potential was inverted bottom over top. For the simple case of Eq. (51), $\omega_0 = \omega_b$. There can exist intermediate energy levels within the well, which are populated according to the Boltzmann factor. Particle escape can take place by quantum tunneling "under" the barrier or by thermal activation "over" the barrier. The intermediate energy levels can be used as ladder rungs by the particle attempting to escape. These processes are embedded in Eq. (55).

[66] See, for instance, Mel'nikov (1991) and also Varoquaux and Avenel (2003) for more references and details on this section.

[67] As explained by Caldeira and Leggett (1983), Waxman and Leggett (1985), and Grabert, Olschowski, and Weiss (1987).

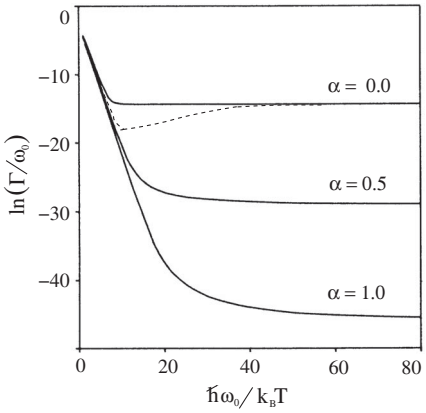

FIG. 17. Logarithm of the escape rate normalized to the attempt frequency in terms of inverse temperature, also normalized to ω_0 for various values of the damping parameter α (Grabert, Olschowski, and Weiss, 1987). The dotted line is a hand sketch of the situation where α increases with temperature, starting from zero at $T = 0$ (see Sec. V.C). From Varoquaux and Avenel, 2003.

absolute zero. This unique situation is found in the nucleation of vortices in ^{4}He as now described.

D. Experimental energy barrier and damping coefficient

Knowledge of the rate Γ makes it possible to extract from the measured nucleation rate and crossover temperature the values of the energy barrier in terms of v_c. The value of ω_0 given by Eq. (53) ($\omega_0/2\pi = 2 \times 10^{10}$ Hz for $T_q = 0.147$ K) is consistent with the attempt frequency appropriate to the thermally activated regime (Varoquaux, Meisel, and Avenel, 1986) and that found directly from the fits to the probability p as shown in Fig. 14. This agreement was mentioned previously.

This value of ω_0 is comparable to the highest Kelvin mode eigenfrequency that a vortex filament in ^{4}He can sustain. The Kelvin modes are helical waves with a dispersion relation expressed for a straight isolated vortex by

$$\omega^{\pm} = \frac{\kappa_4}{\pi a_0^2}\left[1 \pm \left\{1 + ka_0\left[\frac{K_0(ka_0)}{K_1(ka_0)}\right]\right\}^{1/2}\right], \tag{57}$$

where K_0 and K_1 are the modified Bessel functions of zeroth and first orders.[68] In the short wavelength limit, $k^{-1} \to 0$, the high frequency mode reduces to

$$\omega^{+} = \frac{\kappa_4}{\pi a_0^2}. \tag{58}$$

Equation (58) sets the shortest time scale on which vortices can be expected to respond.

By analogy with the 2D motion of point electric charges subjected to a rf magnetic field (Muirhead, Vinen, and Donnelly, 1985), this frequency is sometimes called the "cyclotron" frequency. This frequency is that of the cycloidal motion taken by a long hollow cylinder impulsively pulled sideways in an inviscid fluid (Donnelly, 1991). The cylinder stands for the vortex core, assumed to be hollow and with radius a_0. The displaced mass per unit length of such a cylinder is $\rho\pi a_0^2$. For high frequency motions, the vortex mass is modified as discussed in Sec. II.B.3, and Eq. (58) is renormalized to $\omega^{+} = \kappa_4/\pi a_0^2 \ln(r_m/a_0)$, r_m being defined below Eq. (25). With $a_0 = 2.5$ Å and $r_m/a_0 \sim 10$, $\omega^{+}/2\pi = 3.5 \times 10^{10}$ Hz, a value comparable to the attempt frequency given by Eq. (53). The fact that the attempt frequency be linked to the highest frequency that the nucleating vortex can sustain makes good physical sense.

With the known value of ω_0, the energy barrier E_b can be extracted from the measured rate with the help of Eqs. (54) and (55). These values of E_b for the experiments on ultrapure ^{4}He analyzed by Varoquaux and Avenel (2003) are shown in Fig. 18. The high T and low T analyses are seen to yield consistent results in the region where they overlap.

The quantitative analysis can be carried out one step further using the variation of the barrier energy E_b in terms of v to construct a Arrhenius plot—the logarithm of the escape rate Γ in terms of the inverse temperature for a fixed potential well—from the experimental data and directly comparing the outcome to the results from theory. Arrhenius plots are drawn at constant E_b and varying temperature but the experimental results are obtained at velocities that vary with temperature, hence at varying E_b. The correction can be computed from the experimentally determined E_b given in Fig. 18. The final outcome for the nucleation rate data of Varoquaux and Avenel (2003) in ultrapure ^{4}He is plotted in Fig. 19.

As can be noted in Fig. 19, the raw experimental, velocity-dependent rates exhibit little variation over the range of parameters: escape rates are observed only in a certain window determined by the measuring technique. At low temperatures $T < T_q$, the critical velocity is close to its zero-temperature limit v_q and the corrections to Γ are small. As T increases above T_q, v_c decreases and Γ has to be

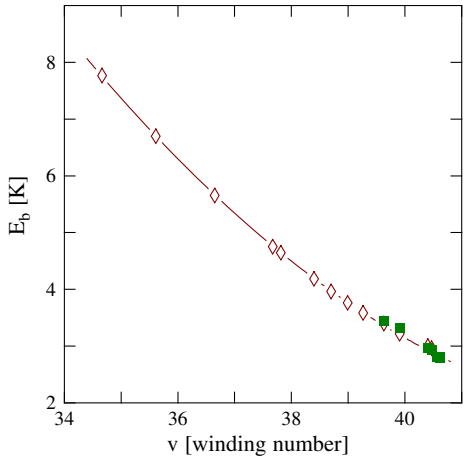

FIG. 18 (color online). The barrier energy E_b in kelvin vs v the mean velocity in the aperture expressed in phase winding numbers and obtained from the nucleation rate data of Varoquaux and Avenel (2003): (■) low-temperature data transformed using the numerical tables of Grabert, Olschowski, and Weiss (1987); (◇) high-temperature data. From Varoquaux and Avenel, 2003.

[68] See Fetter (1965), Glaberson and Donnelly (1986), Sonin (1987), and Donnelly (1991).

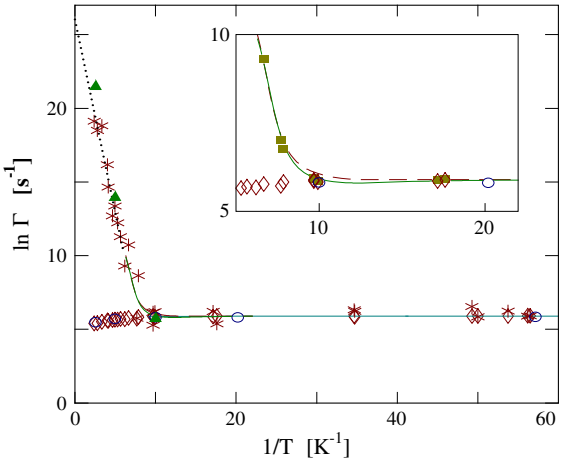

FIG. 19 (color online). Arrhenius plot $\ln\Gamma(v)$ vs $1/T$, Γ being expressed in s^{-1} and T in kelvin, as measured at varying T and v_c for two ultrapure ^{4}He samples (◇) and (△); (*) and (▲) after correction for the change of the velocity with T. The solid and the dotted curves are calculated from the experimental barrier energy E_b represented in Fig. 18. In the inset, $\ln\Gamma(v_q)$ (■) has been obtained with smoothed values of v_c. The curves represent the calculated values of $\ln\Gamma(v_q)$ with $\alpha = 0$ (dashed) or varying with T (solid). The latter gives a better representation of the data and illustrates the influence of damping depicted by the dotted line in Fig. 17. From Varoquaux and Avenel, 2003.

determined by piecewise integration of $d\ln\Gamma/dv$. The high-temperature extrapolation for Γ obtained in such a manner displays the usual $1/T$ dependence.

In the intermediate-temperature range, the corrected Γ shows, as can be seen in the inset of Fig. 19, a small but real drop below its zero-temperature limit as the temperature is raised. This drop reveals the influence of damping on the escape rate illustrated in Fig. 17. A damping coefficient α that increases from 0 at $T = 0$ to ~0.1 around T_q and more slowly above accounts for the observed drop (Varoquaux and Avenel, 2003). This T-dependent dissipation also makes the crossover between the thermal and quantum regimes even sharper than for $\alpha = 0$ and closer to observations. The nucleation of vortices in ^{4}He thus offers a rare observation of the effect of damping on MQT.

E. The vortex half-ring model

The case has been put so far for the nucleation of vortices, thermal or quantal. The nucleation barrier E_b is of the order of a few kelvins (see Fig. 18) and the attempt frequency $\sim 2\times 10^{10}$ Hz, close to that of the highest Kelvin wave mode.

A simple model accounts for these features. This model, the nucleation of vortex half rings at a prominent asperity on the walls, finds its roots in the work of Langer and Fisher (1967), Langer and Reppy (1970), and Volovik (1972). It was further developed and put on the firm experimental findings described above by Avenel, Ihas, and Varoquaux (1993).

The model premises are the following. Consider, as done by Langer and Reppy (1970), the homogeneous nucleation of a vortex ring in a homogeneous flow v_s extending over large distances. When the ring has grown to reach radius R in a plane perpendicular to the flow, its energy in the laboratory frame, where the observer is at rest and sees the superfluid moving at velocity v_s, is expressed by

$$E_v = E_R - P_R v_s. \tag{59}$$

The rest energy E_R and impulse P_R of the vortex ring are given by Eqs. (24) and (32). The minus sign on the right-hand side of Eq. (59) arises because the vortex opposes the flow, that is, its impulse P_R points straight against v_s: this configuration minimizes E_v.

The rest energy E_R increases with vortex size as $R\ln R$ and the impulse P_R as R^2: the impulse term becomes dominant at large radii and causes E_v to become negative. The variation of E_v in terms of R has the shape of a confining well potential, which becomes shallower and shallower with increasing v_s, as depicted in Fig. 20. The barrier height can easily be computed numerically and plugged into the expression for v_c, Eq. (48). An analytic approximation for v_c involving the neglect of logarithmic terms and valid for large vortices ($R \gg a_0$) has been given by Langer and Reppy (1970).

This critical process yields a mist of vortices in the bulk of the superfluid. This sort of vorticity condensation does not take place for two reasons. First, the velocity of potential flows, which follows from the Laplace equation, reaches its maximum value at the boundaries, not in the bulk. Second, the nucleation of a vortex half ring at the boundary itself involves, for the same radius hence the same self-induced velocity, one-half of the energy given by Eq. (59); for that reason alone, half-ring nucleation at walls is always much more probable at the same velocity v_s than full-ring nucleation in the bulk.

Halving the full-ring energy for the half ring holds for classical hydrodynamics, the other half being taken care of by the image in the plane boundary. For a superfluid vortex, the actual energy of a half ring is smaller than in the classical ideal

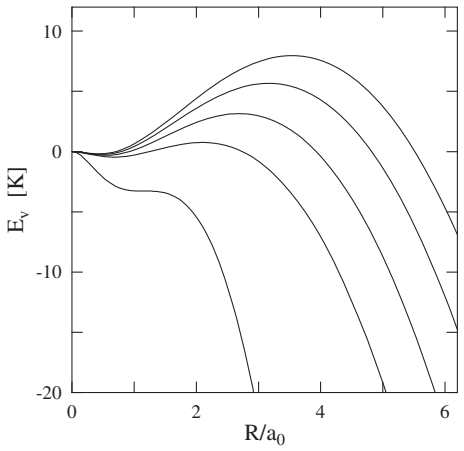

FIG. 20. Energy barrier E_v normalized by $\rho_s\kappa_4^2 a_0$ and expressed in kelvin vs the vortex radius R/a_0 for the vortex half-ring model. Illustration of various potential forms given by Eq. (59) at various superfluid flow velocities taken from the data in Fig. 12 at, from top down, $T \to T_\lambda$, 1 K, 0.5 K, and at the quantum crossover T_q. The lowest curve illustrates the situation in which the potential barrier vanishes and the trapped particle runs away, the so-called lability point. Adapted from Avenel, Ihas, and Varoquaux, 1993.

fluid because the superfluid density is depleted at the solid wall and the core radius increases.

The half-ring model for the nucleation of vortices has been proposed for ion critical velocity by Muirhead, Vinen, and Donnelly (1984) and for aperture flows by Burkhart *et al.* (1994).[69] A variant, based on a different accounting of the vortex core energy, has been studied by Zimmermann, Lindensmith, and Flaten (1998). Other mechanisms have been discussed (Josserand and Pomeau, 1995; Josserand, Pomeau, and Rica, 1995; Andreev and Melnikovsky, 2004) for which it is unclear that the end product of the nucleation process is actually a vortex.

The barrier height for the vortex half-ring nucleation can easily be computed and plugged into the expressions for v_c and Δv_c, Eqs. (48) and (49). Critical velocities v_c and statistical widths Δv_c computed in such a manner are shown as a function of temperature by the solid lines in Figs. 12 and 13 for several values of the vortex core parameter a_0. A value of 4.5 Å gives near-quantitative agreement with the experimental observations over the entire temperature range. This value exceeds that in the bulk ($a_0 \simeq 2.5$ Å). This is thought to reflect the proximity of the wall as discussed by Varoquaux *et al.* (2001). With this value, the nucleating half ring has a radius of approximately 15 Å at the top of the barrier and a self-velocity of $v_R = 13.5$ m/s from Eq. (33); this value compares well with the values shown by open circles in Fig. 11.

Once nucleated, the vortex half ring floats away, carried out by the superfluid stream at the local superfluid velocity and by its own velocity $v_R = \partial E_R/\partial P_R$. It can be noted that, at the top of the barrier, $\partial E_v/\partial R = 0$: the vortex self-velocity v_R exactly balances the applied v_s; the nucleating vortex is at a near standstill.

If the flow were uniform, with parallel streamlines, nothing much would happen. Downstream from the aperture, however, the flow is divergent, as pictured in Fig. 21. The vortex half ring tends to follow the local streamlines and grows under the combined action of the potential flow and its own self-velocity: it then gains energy at the expense of the potential flow as explained in Sec. II.C. In such a way, it expands from nanometric to micrometric sizes and above, and wanders away. Interaction with the normal fluid, encounters with other vortices, and friction on the solid boundaries cause a loss of vortex energy that eventually leads to its disappearance. The vortex in its motion away from the microaperture takes a given finite lump of energy to remote places of the cell and never returns.

This scenario for a phase slip produces a change of the phase difference between the two sides of the microaperture of exactly 2π because the vortex ends up crossing all the streamlines, as pictured in Fig. 21. This crossing causes the velocity circulation to change by exactly one quantum κ_4 on all the superfluid paths extending from one side of the aperture to the other. Such a dissipative event gives the signature of single phase slips that are seen in Fig. 10. Extensive numerical simulations by Schwarz (1993a, 1993b) and Flaten *et al.* (2006) fully confirm the above scenario for phase slips.

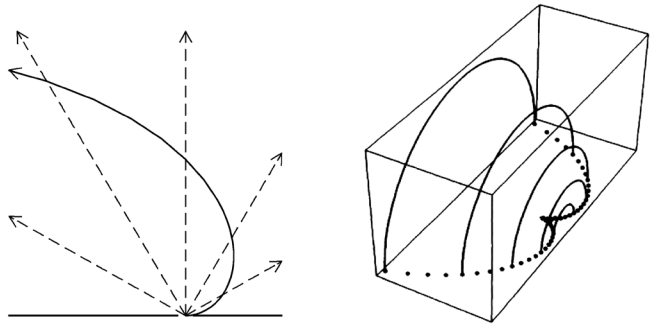

FIG. 21. Schematic views in 2D (left) and 3D (right) of the vortex half-ring trajectory over a pointlike pinhole punched in an infinite horizontal plane. The dashed lines on the 2D plot are the potential flow streamlines that emerge from the pinhole. The 3D view shows the vortex half ring being first pushed by the potential flow to the right and then flying back over the pinhole to finally drift away to the upper left. Adapted from Varoquaux, 2006.

The effect of ^{3}He impurities on the phase-slip critical velocity at low temperature is striking, as seen in the inset of Fig. 12. It is due to the condensation of these impurities on the vortex cores, which changes their line energy and the potential barrier for nucleation. This impurity dependence, studied by Varoquaux *et al.* (1993), was used as a local probe of the superfluid velocity at which vortices nucleate. This velocity was found to be 22 m/s, in reasonable agreement with the value derived from the vortex half-ring model.

In all, the model parameters give a physically consistent picture, showing that specific finer details are probably not very relevant and that the model simplifications are reasonably well founded. It nonetheless remains that the nature and geometry of a typical nucleation site are wholly unspecified and that the enhancement factor between the mean aperture velocity and the velocity at the nucleation site is not under control, as shown by Shifflett and Hess (1995).

VI. VORTEX PINNING, MILLS, AND FLOW COLLAPSE

Single phase slips are observed in experimental situations that may be loosely characterized as "clean," broadly speaking for uncontaminated apertures of relatively small sizes (a few micrometers at the most), with low background of mechanical and acoustical interferences, and with probing techniques that do not manhandle the superfluid, namely, with low frequency hydromechanical resonators.

When these conditions are not met, flow dissipation occurs in a more erratic manner in large bursts, multiple phase slips or "collapses" of the superflow. Such collapses of the superflow through an orifice were first observed by Sabo and Zimmermann[70] and Hess (1977).

Multiple phase slips and collapses constitute an apparent disruption of the vortex nucleation mechanism described in Sec. V. Their properties have been studied by Avenel *et al.*

[69]See Zimmermann (1994), Burkhart (1995), and Varoquaux and Avenel (1996a).

[70]As quoted by Hess (1977).

(1995) and are mentioned later, together with possible mechanisms for their formation. It is likely that these events provide a bridge between the clean single phase-slip case and the usual situation of the Feynman-type critical velocities that are temperature independent below 1 K and dependent on the channel size. Preexisting vorticity is widely suspected to come into play in these "extrinsic" critical velocities.

A. Pinned vorticity

Awschalom and Schwarz (1984) directly showed the existence of remanent vorticity in ^{4}He, which had long been assumed, and gave an estimate of its background level. They studied the propagation of ions in the presence of vortex lines. Ions get trapped in the vortex cores and completely change course, revealing the presence of these vortex lines. These vortices, presumably nucleated at the λ transition when the critical velocity is low and critical fluctuations large, remain stuck in various places of the superfluid sample container. This trapped vorticity, according to Adams, Cieplak, and Glaberson (1985), either is quite loosely bound to the substrate and disappears rapidly or is strongly pinned and dislodged only by strong perturbations.

To achieve a stable configuration, a pinned vortex has to take on a shape such that its local radius of curvature results in a self-velocity that exactly opposes at each of its points the local value of the superflow. This dynamic equilibrium is what is meant here by pinning. A vortex pinning exists in bulk ^{4}He as discussed here,[71] in films,[72] in ^{3}He,[73] in neutron stars, etc.[74]

To account for laboratory observations and with the outcome of extensive numerical simulations of vortex dynamics, Schwarz proposed the following formula for the velocity at which such strongly pinned vortices unpin (Schwarz, 1981, 1985),[75]:

$$v_u \lesssim \frac{\kappa_4}{2\pi D}\ln\left(\frac{b}{a_0}\right), \tag{60}$$

with D being the size of the pinned vortex and b being a characteristic size of the pinning asperity. Equation (60) bears a strong resemblance to that for the Feynman critical velocity, Eq. (45).

As a rule of thumb, the pinning energy of the vortex line on such an asperity with radius b is approximately equal to b times the line tension of the vortex given by Eq. (26). Long vortices unpin at very low velocities unless they are perched on a tall pedestal, but very small vortices pinned on microscopic defects can survive a wide range of superflow velocities; according to Eq. (60), a straight vortex filament pinned at both ends on 20 Å asperities 200 nm apart resists transverse flows of velocities up to 20 cm/s.

Such pinned vorticity has long been thought to play a role in critical velocities. The long-standing suggestion by Glaberson and Donnelly (1966) of vortex mills had its time of fame (Amar *et al.*, 1992). In their views, imposing a flow on a vortex pinned between the opposite lips of an aperture would induce deformations such that the vortex would twist on itself, self-reconnect, and mill out fresh vortex loops. Upon scrutiny, however, vortex mills are not so easy to set up.

The first thing to realize is that such a mill must involve a pinned vortex of submicrometric size so that it is not washed away by any flow velocity above a few cm/s. Pinned vorticity in large channels cannot withstand the Feynman-type critical velocities shown in Fig. 11.

Less obvious, vortices are not prone to twist on themselves and foster loops. As shown by numerical simulations of 3D flows involving few vortices only,[76] vortex loops and filaments are found to be stable against large deformations: it takes the complex flow fields associated with fully developed vortex tangles to produce small rings (Svistunov, 1995; Tsubota, Araki, and Nemirovskii, 2000).[77] And it takes some quite special vortex pinning geometry to set up a mill that actually works.

Schwarz (1990) demonstrated the existence of such a mill by numerical simulations. Imagine a vortex filament pinned at one end in a region close to the aperture mouth or the channel entrance where it bends sharply to withstand the local superflow. This end of the vortex is at a near-stagnation point. Its other end is being carried away by the flow along the streamlines; it moves freely with its end sliding perpendicular to the wall. The filament develops a helical instability as depicted in Fig. 22, a sort of driven Kelvin wave, and reconnects sporadically to the wall when the amplitude of the helix grows large enough. The freed bit immediately stands against the flow and forms a vortex half ring: such a helical vortex mill, which has to be of submicrometric size to withstand the near-by flow, churns out fresh vortices.

The occurrence of multiple slips such as those shown in Fig. 23 is probably caused by such a form of vortex mill on a microscopic size. Before coming to this topic, a description of multiple slips in greater detail must be provided.

B. The two types of large slips

Examples of multiple slips are shown on the peak amplitude charts in Figs. 23 and 24 for two different runs in the same experimental cell. They display rather different patterns. In Fig. 23, multiples slips are fairly frequent and their winding number multiplicity remains moderate. As the probability for a one-slip event per half cycle is not large, that for a double slip is small, and it becomes negligible for higher multiples. A separate mechanism for their formation must be found. The event shown in Fig. 24 is quite spectacular as it leads to near extinction of the resonance.

[71] See Varoquaux *et al.* (1998), Donev, Hough, and Zieve (2001), and Neumann and Zieve (2014) for more references.

[72] See Ellis and Li (1993).

[73] See, among others, Hakonen *et al.* (1987) and Zieve *et al.* (1992), or Krusius *et al.* (1993).

[74] See Packard (1972), Alpar, Nandkumar, and Pines (1985), and Langlois (2000).

[75] See Tsubota and Maekawa (1994) and Neumann and Zieve (2014).

[76] K. W. Schwarz, private communication to the author (1989).

[77] See Tsubota and Kobayashi (2009).

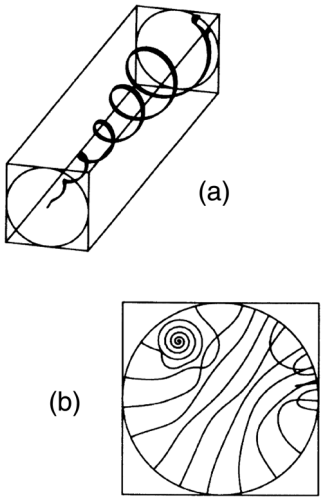

FIG. 22. Operation of a helical vortex mill: (a) Spiral-helix configuration of a streamwise vortex filament pinned at the center of the bottom left section of the channel. The helical vortex self-velocity opposes the superflow while the vortex filament grows in size and spirals on itself. (b) End-on view of subsequent reconnections. The vortex is pinned near the upper left of the channel cut view. The outwardly growing spiral sporadically reconnects to the wall and releases a new line segment, which then moves to the lower right. These numerical simulations are carried out in the presence of a sizable mutual friction with the normal component in order to stabilize the numerical algorithms, which is why the generated half rings rapidly decrease in size. From Schwarz, 1990.

In Figs. 23 and 24 aperture velocities are expressed by the number of turns $\delta\varphi/2\pi$ by which the quantum-mechanical phase winds across the aperture. Phase winding numbers are related to mean flow velocities in cm/s by multiplication by ℓ_h/κ_4, the "hydraulic" length ℓ_h characterizing the extension of the aperture along the flow. For a phase slip by 2π, the phase winding number changes by one unit and the trapped circulation in the resonator loop by one quantum. The hydraulic length is defined by lumping the (classical) kinetic energy of the fluid moving with velocity $\mathbf{v}$ inside the aperture of cross section s_h and in its vicinity according to

$$\ell_h = s_h \int_V \mathbf{v}(\mathbf{r})^2 d^3\mathbf{r} \Big/ \left(\int_S \mathbf{v}(\mathbf{r}) \cdot d^2\mathbf{r} \right)^2. \tag{61}$$

The actual flow velocity averaged over the cross section of the microaperture is proportional to $\delta\varphi$, the multiplying factor being $\hbar/m_4\ell_h$. The hydraulic length ℓ_h of the microaperture is of the order of 1 μm in the experiments shown in Fig. 10.

Some degree of understanding of the formation of multiple slips can be gained by plotting the mean value of the phase-slip multiplicity, expressed in number of quanta, against the flow velocity at which the slips take place (Varoquaux *et al.*, 1995). This flow velocity is close to the critical velocity for single phase slips, i.e., the vortex nucleation velocity; it varies with temperature, pressure, and resonator drive level. A plot summarizing these variations is shown in Fig. 25 for $\langle n_+ \rangle$, i.e., in the flow direction conventionally chosen as the (+) direction. Slips in the opposite (−) direction behave qualitatively in the same manner but the phenomenon displays a clear quantitative asymmetry.

As can be seen in Fig. 25, the mean slip multiplicity decreases, as does the nucleation velocity, on either side of the quantum plateau—a ^{3}He impurity effect on the low-T side—a thermal effect on the high-T side. At 16 bars, $\langle n_+ \rangle$ increases from ≈1 at 12 mK where the velocity is 43.2 in winding number to 15–20 on the plateau of v with a winding number of 48; $\langle n_+ \rangle$ drops back to 1 at 225 mK and the velocity to ∼46.2. The same trend is observed at 24 bars, with a lower velocity on the plateau of 46.4 and a higher mean multiplicity of ∼23. Rather oddly, the slip multiplicity $\langle n_+ \rangle$ increases with pressure while the mean velocity at which these multiples occurs decreases. One would have expected that more slips would be ushered into faster streams. The opposite may show

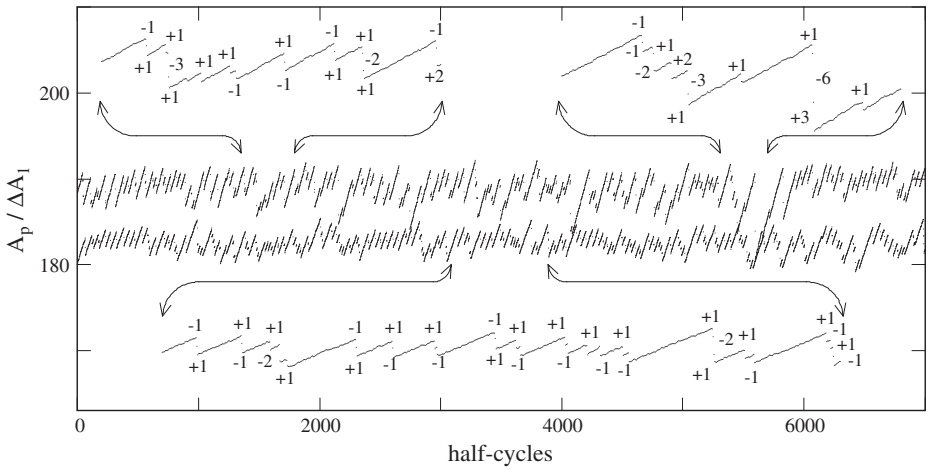

FIG. 23. Absolute peak amplitude A_p normalized to the amplitude jump of a single slip ΔA_1 during successive half cycles of the resonance plotted as a function of half-cycle index (time runs from left to right) at 100.7 mK (top) and 201.5 mK (bottom) in nominal purity helium at SVP. The expanded traces at the very top and bottom of the graph show the slip sizes in signed winding numbers (according to flow direction, in and out of the resonator chamber). The numerous multiple slips seen on these charts occur at or close to the critical velocity for single slips. From Varoquaux and Avenel, 2003.

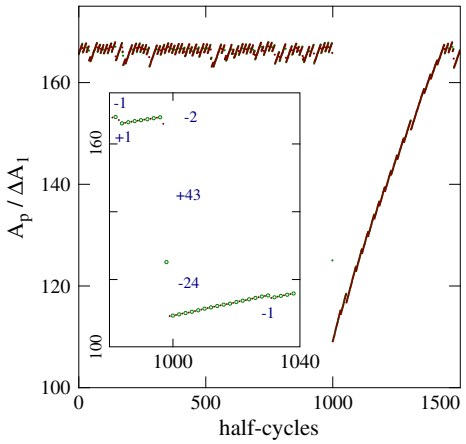

FIG. 24 (color online). Absolute peak amplitudes at successive half cycles of the resonator motion, normalized as in Fig. 23, vs half-cycle index in a ^{4}He sample containing 100 ppb of ^{3}He impurity, at 24.0 bars and 12.5 mK. The resonance half period is 31.8 ms. The top trace shows a succession of amplitude drops which correspond, for its main part, to phase slips by 2π of opposite sign, with occasional larger slips—the multiple slips of Fig. 23. The large feature around the 1000th half cycle is a "singular" collapse, as defined in the text. The inset shows the details of this collapse, (•) being for positive peaks, (◦) for negative peaks. It is preceded by a slip by -2 $(\times 2\pi)$ and followed by a slow recovery of the peak amplitude caused by the applied drive, punctuated by single and double slips. The time-resolved evolution of this collapse has actually been tracked. From Avenel *et al.*, 1995.

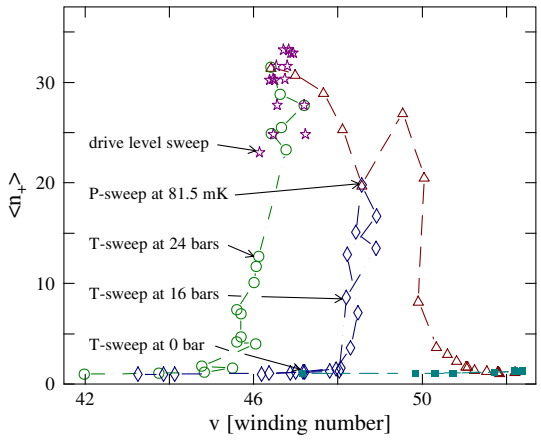

FIG. 25 (color online). Mean size of (positive) multiple slips vs velocity in phase winding number in nominal purity ^{4}He (100 ppb ^{3}He): (△) pressure sweep from 0.4 to 24 bars at 81.5 mK (for all even values of the pressure P, and 0.4, 1, 3, 5, and 7 bars); (◇) temperature sweep at 16 bars; (◦) temperature sweep at 24 bars; (*) drive level sweep at 24 bars, 81.5 mK; (■) temperature sweep at 0 bar. Lines connect successive data points in the temperature and pressure sweeps. For the temperature sweeps, from 14 to 200 mK approximately, v first increases when the ^{3}He impurities evaporate from the vortex core, reaches the quantum plateau, and then decreases, following the same pattern as shown in the inset of Fig. 12 for v_c. Adapted from Varoquaux *et al.*, 2001.

that the phenomenon under study is not purely ruled by hydrodynamics in the fluid bulk.

Another important feature of the data shown in Fig. 25 concerns the dependence of the velocity threshold for the appearance of multiple slips on hydrostatic pressure. The P dependence of the upturn of $\langle n_+ \rangle$ in terms of v exactly tracks that of v_c, the critical velocity for single phase-slip nucleation: multiple slips occur when single slips occur. Would multiple slips appear because of an alteration, or as a consequence, of single slip nucleation?

The very large drops in the resonance amplitude of the resonator such as the event shown in Fig. 24 and in the inset sometimes result in a complete collapse of the resonance. Under the conditions of this particular experiment (Avenel *et al.*, 1995), these events were rare (1 in 10^4 to 10^5 slips). A striking feature is that they may occur at velocities much below the vortex nucleation threshold, down to less than one-third of v_c, the critical velocity for phase slips. These intriguing singular collapses, first studied by Hess (1977), differ from the multiple slips of Fig. 25. The underlying mechanisms responsible for each are bound to be different, as discussed later (Varoquaux *et al.*, 2001).

The pattern of formation of multiple slips and collapses changes on cycling the cell from room temperature and back but remains stable during each given cooldown. It depends on the degree of contamination of the cell, degree which cannot easily be controlled experimentally. The detailed microscopic configuration of the aperture wall where nucleation takes place has a strong influence on multiple slip formation.

C. Extrinsic critical velocities

To try and clarify these matters, a series of experiments was conducted by Hakonen, Avenel, and Varoquaux (1998) and Varoquaux *et al.* (1998), in which the experimental cell was deliberately heavily contaminated by atomic clusters of air and of H_2 in order to favor the pinning of vortices. Numerous multiple slips and collapses of the singular type occurred. The peak amplitude charts of the resonator became very difficult to interpret except in a few instances. In one of these, two apparent critical velocities for single phase slips were observed. The higher critical velocity corresponded to the one observed in the absence of contamination. The lower critical velocity was thought to reveal the influence of a vortex pinned in the immediate vicinity of the prevailing nucleation site.

Following this interpretation, the pinned vortex induces a local velocity which adds to that of the applied flow and causes an apparent decrease in the critical velocity for phase slips. Because of this change, the presence of the pinned vortex can be monitored. The lifetime in the pinned state and the unpinning velocity can be measured, yielding information on the pinning process, reported by Hakonen, Avenel, and Varoquaux (1998).[78] This observation also brings evidence that pinned vorticity can alter the vortex nucleation process responsible for phase slips.

[78]This topic is also covered by Varoquaux *et al.* (1998, 2000, 2001) and Varoquaux (2000).

With such pinned vortices hanging around, multiple slips could form according to the following scheme (Varoquaux *et al.*, 2001). First, a vortex half ring is nucleated at a prominent nucleation site. It pins shortly after nucleation when its velocity relative to the boundary is still small and the capture by a pinning site is easy. A micromill is thus formed, which remains active as long as the flow is sufficient to maintain the helical instability. As it is set up to withstand one flow direction, it is destroyed when the flow velocity reverses itself in the resonance motion. It eventually reestablishes itself during a subsequent resonance cycle, causing a new multiple slip. This process depends on the precise details of the pinning site configuration and of the primordial vortex trajectory, factors which allow for the variableness of multiple slips on contamination and pressure.

In the same experiments by Hakonen, Avenel, and Varoquaux (1998), a large number of unpinning events were also observed to take place at an "anomalously low" unpinning velocity. A parallel can be made (Varoquaux *et al.*, 1998) with the singular collapses that also occur at "subcritical" velocities and that were also quite frequent in the same experiments, suggesting that the two effects might have a common cause. Noting furthermore that pinning and unpinning processes were also quite frequent, releasing a fair amount of vagrant vorticity, it appears quite plausible that both singular collapses and low velocity unpinning events are caused by vagrant vortices hopping from pinning sites to pinning sites, eventually hovering over a pinned vortex or a vortex nucleation site. The transient boost to the local velocity may push the pinned vortex off its perch, or may cause a burst of vortices to be shed.

These observations have important consequences for the critical velocity problem: existing vortices, either pinned or free moving, can contribute to the nucleation of new vortices at the walls of the experimental cell at apparent velocities much lower than the critical velocity for phase slips. A mechanism is thus provided by which superflow dissipation sets in at large scale for mean velocities much smaller than the velocity for vortex nucleation on the microscopic scale, possibly bridging the gap between phase slip and Feynman-type critical velocities.

To conclude this section, the critical velocities in superfluids that are true and proven include the Landau critical velocity for roton creation in ion propagation (McClintock and Bowley, 1995), the formation of vortices by a hydrodynamical instability in BEC gases (Madison *et al.*, 2001) and in ^{3}He (Eltsov, Krusius, and Volovik, 2005), the nucleation of vortices by thermal activation and quantum tunneling in ^{4}He, for both ion propagation and aperture flow.

There is also rather compelling experimental evidence for the interplay on a microscopic scale between vortex nucleation and pinned vorticity; this evidence points toward the existence of helical vortex micromills that can generate bursts of vortices, even, in some cases, at fairly low flow velocities. Finally, vagrant vortices interacting with these mills or with the vortex nucleation sites are found to generate enough vorticity to completely kill the superflow and explain singular collapses.

How these different events occur is illustrated in detail by the numerical simulations of the onset and decay of vortex tangles in large channels (Schwarz, 1983; Schwarz and Rozen, 1991), of the influence of surface roughness on the critical velocity for a self-sustaining vortex tangle (Schwarz, 1992), and of the evolution of phase-slip cascades from a single remnant vortex as a function of channel size (Schwarz, 1993b). These processes depend on the cell geometry but not on temperature.

A fair degree of understanding of the possible mechanisms behind the Feynman critical velocity has thus been achieved by the study of phase-slippage signatures of these various large slips.

VII. JOSEPHSON-TYPE EFFECTS IN SUPERFLUIDS

Anderson's conjectures, seen in the previous sections to be fully confirmed in the hydrodynamic (macroscopic) limit of quantized vortex dynamics, have also been carried over to the microscopic limit of quantum tunneling, as described next.

The reasoning goes that Eqs. (12) and (13) are *fundamental*[79] enough to carry the day at both large and short distances, namely, when the coherence length is either small or large with respect to characteristic dimensions of the hydrodynamic weak link. The former case has been covered in the previous sections. In the latter case, weak quantum coupling between two superfluid baths, the contention is that effects analogous to the famed Josephson effects between two weakly coupled bits of superconducting material must also exist between two loosely connected pools of superfluid provided that superfluid coherence is not entirely lost through the connection. These Josephson-type effects in superfluids are dealt with next.

A. A simple model

The Hamilton equations (12) and (13) express in a quite general way the time evolution of φ and N, as discussed in Sec. I.B. These equations hold in fact for the operators $\hat{N}$ and $\hat{\varphi}$ but their coarse-grained averages can be treated as c numbers to a very good approximation because their relative quantum uncertainties are very small. Averaging over a volume of superfluid small compared to the size of the sample but still containing a large number of atoms leads to Eq. (14):

$$\hbar \frac{\partial \varphi}{\partial t} = -[\mu + (1/2) m_4 v_s^2].$$

Equation (14) describes the Josephson ac effect.[80] When applied to the gradient of the phase, it can be cast, using Eq. (6), into the Euler equation (15):

$$\frac{\partial \mathbf{v}}{\partial t} + \nabla \left(v_a P + \frac{1}{2} m_a v^2 \right) = 0,$$

with m_a being the atomic mass of the effective boson.

[79]See the discussion following Anderson's talk at the Sussex University Symposium in 1965 (Anderson, 1966b).

[80]The contribution of the entropy to the chemical potential ST should also be taken into account in Eq. (14) if the temperature is not very low.

Equations (14) and (15) look plainly classical enough. Quantum mechanics hides in the possible multiple determinations of the overall phase $\varphi(t,\mathbf{r})$ of the order parameter, yielding a quantized circulation of the fluid velocity, and when $\hat{N}$ cannot be coarse-grained averaged because the amplitude of the order parameter vanishes or varies too rapidly over short distances. A quantum mechanism is then provided for φ to vary discontinuously from one determination to another, violating the Kelvin-Helmholtz theorem.

The second Heisenberg equation of motion, that for $\dot{N}$, expresses particle number conservation:

$$\hbar\frac{\partial N}{\partial t}=\frac{\partial E}{\partial\varphi}. \tag{62}$$

As stressed by Anderson (1966a), the range of validity of Eqs. (14) and (62) is quite wide. They will still hold when hydrodynamics breaks down as for tunneling supercurrents. In this kind of situation, the internal energy E depends in a nontrivial way on φ, as may be expected from Eq. (62).

When applied between two regions of the superfluid, Eqs. (14) and (62) describe the supercurrent flowing from one region to the other. This situation becomes interesting when the two regions, the two superfluid baths, are sufficiently well separated so that they only *weakly couple*: a well-defined phase difference between them $\delta\varphi$ can then be sustained.

Such a situation can be modeled by a potential barrier, as in Fig. 26. The thin partition separating the two baths presents a thin elongated slit through which a trickle flow only of superfluid can leak. If the two smaller dimensions of the slit are comparable to the superfluid coherence length—the distance over which its wave function can heal—the amplitude of the wave function is reduced in the narrow passage, as pictured in the bottom panel of Fig. 26. In superconductivity, such weak links, or microbridges, are known to lead to the same kind of effects as tunnel junctions (Likharev, 1979; Golubov, Kupriyanov, and Il'ichev, 2004).

For superflows through such a microaperture, the problem can be restricted to one dimension along z and, to simplify further, the barrier (the weak link) can be taken as a square potential wall of height U over length l_b.[81]

In the bulk of the fluid, the wave function corresponding to a state with energy E is taken as a plane wave with identical amplitude $|\Phi|=(\rho_s/m_a)^{1/2}$ on both sides of the barrier ($m_a=2m_3$ for superfluid ^{3}He), but with phases that differ by $\delta\varphi$: these are the boundary conditions at the weak link walls at $z=0$ and $z=l_b$.

Inside the barrier $|\Phi(z)|$ is assumed to be severely depressed: the interactions within the fluid can be neglected.[82] With this approximation of weak coupling, the tenuous fluid inside the weak link behaves as a simple noninteracting gas and the equation of motion reduces to a one-particle Schrödinger equation:

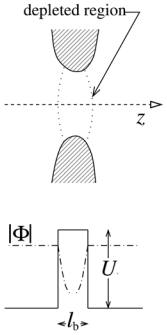

FIG. 26. Schematic representation of a two-dimensional weak link: (top) cut view of the elongated slit in the partitioning wall; (bottom) amplitude of the macroscopic wave function Φ in the region in which it is depleted by the energy barrier of height U and extent l_b due to the constricting walls.

$$i\hbar\frac{\partial\Phi}{\partial t}=-\frac{\hbar^2}{2m_a}\nabla^2\Phi+U\Phi,\quad U>E,$$

and also has a plane wave solution $\exp\{-i(Et/\hbar-kz)\}$. The momentum takes two values corresponding to the two possible directions of (damped) propagation:

$$k_\pm=\pm(i/\hbar)\sqrt{2m_a(U-E)}.$$

Let $b_b=\hbar/\sqrt{2m_a(U-E)}$: the barrier height is characterized by a penetration length. The wave function inside the barrier is found by standard methods:

$$\Phi(z)=\frac{|\Phi|}{\sinh(l_b/b_b)}\left\{\sinh\left(\frac{z}{b_b}\right)e^{i\delta\varphi}-\sinh\left(\frac{z-l_b}{b_b}\right)\right\}.$$

The modulus of Φ midway in the barrier is expressed by

$$\Phi^*(l_b/2)\Phi(l_b/2)=\frac{\rho_s/m_a}{2\cosh^2(l_b/2b_b)}[1+\cos\delta\varphi], \tag{63}$$

and is a 2π-periodic function that vanishes for $\delta\varphi=\pi\pm2n\pi$. The weak coupling condition is satisfied in superfluid helium for $l_b\gtrsim b_b$.

Knowing the wave function, the current density, Eq. (5), can be straightforwardly computed. The total current through a microaperture of effective cross section s_b is found to be

$$\begin{aligned}J&=\frac{\hbar s_b}{2ib_b}\frac{\rho_s/m_a}{\sinh^2(l_b/b_b)}\left\{\left[\sinh\left(\frac{z}{b_b}\right)e^{-i\delta\varphi}-\sinh\left(\frac{z-l_b}{b_b}\right)\right]\right.\\&\left.\times\left[\cosh\left(\frac{z}{b_b}\right)e^{i\delta\varphi}-\cosh\left(\frac{z-l_b}{b_b}\right)\right]-\text{complex conjugate}\right\}\\&=J_c\sin(\delta\varphi),\quad\text{with}\quad J_c=\frac{\hbar}{m_a}\frac{s_b}{b_b}\frac{\rho_s}{\sinh(l_b/b_b)}.\end{aligned} \tag{64}$$

Equation (64) describes the Josephson dc effect. Although this equation has been obtained in a drastically simplified manner, it is nearly identical to the result of more involved theories, each with its own set of approximations—the Ginzburg-Landau model (Monien and Tewordt, 1986,

[81] See Vinen (1968) and also Varoquaux *et al.* (1992).

[82] In the framework of the Gross-Pitaevskii equation, the interaction term $V_0(\Phi^*\Phi)\Phi$ becomes small in the depleted region and can be neglected; see Sec. VII.C for superfluid ^{3}He.

1987), an ideal tunnel junction (Rainer and Lee, 1987), or a strictly pointlike orifice (Kurkijärvi, 1988).

The supercurrent J is periodic by 2π in $\delta\varphi$ as it must be since changing the phase by 2π on one side of the barrier must leave the overall physical situation unchanged. It vanishes for $\delta\varphi = \pm\pi$ not because the velocity, proportional to $\delta\varphi$, goes to zero but because the superfluid density which is proportional to $|\Phi|^2 \sin(\delta\varphi)/\delta\varphi$ inside the barrier does; the modulus of the wave function at midpoint in the barrier, Eq. (63), vanishes: superfluidity is actually destroyed at that point, which is why the supercurrent goes to zero and the phase can slip by 2π (or lumps of 2π).

If the coupling is not weak, a more elaborate calculation is necessary: the sine function is replaced by a general 2π-periodic function $f_{2\pi}(\delta\varphi)$, the current-phase relation (CPR), for a "nonideal" weak link. Often this relation is not even single valued and, when the phase is varied, the current may jump discontinuously from one determination to another: the weak link is then said to be hysteretic. This behavior is due to the nucleation of topological defects such as vortices as seen Sec. VI. It is accompanied by dissipation while the ideal Josephson case [when $f_{2\pi}(\delta\varphi)$ is a sine function] is dissipationless (Likharev, 1979; Thuneberg, 2005; Viljas, 2005).

In the transition between the "ideal," nonhysteretic, purely sinusoidal CPR's and the mostly linear CPR seen, for example, in Fig. 10, a slanted sine function is often observed. Part of this distortion arises from purely classical fluid flow in the vicinity of the microaperture. The full phase difference across the weak link φ_w includes, besides the phase difference across the barrier φ_b, the rather trivial velocity potential drop in the vicinity of the weak link where the superfluid velocity v_s, and the corresponding phase gradient, behave in accord with classical ideal fluid dynamics.

In order to account in a simple manner for this classical contribution, it is convenient to introduce the equivalent hydraulic length and cross-sectional area of these regions ℓ_h and s_h in such a way that the flow is described in a "rodlike" manner.[83] The superfluid velocity is then expressed simply by $v_s = (\hbar/m_a)\delta\varphi_h/\ell_h$ and the current by $J = \rho_s s_h v_s$.

The total phase difference $\delta\varphi$ is the sum of the phase drop through this hydraulic region and through the barrier acting as the weak link, assumed ideal, such that

$$\delta\varphi = \delta\varphi_h + \delta\varphi_b = \frac{m_a \ell_h}{\rho_s \hbar s_h} J. \tag{65}$$

The same mass current also flows through the depletion region and varies, following Eq. (64), as a sine function of the phase difference $\delta\varphi_b$ as long as the coupling is weak.

Combining Eqs. (64) and (65), and renaming the hydraulic part $\delta\varphi_h$ of the phase difference ζ to stress its ancillary role yields the relation between the current and the phase of a (slightly more) realistic microaperture:

$$\varphi = \zeta + \alpha \sin\zeta, \qquad J = J_c \sin\zeta, \tag{66}$$

with $\alpha = (m_a \ell_h/\rho_s s_h \hbar) J_c$ and J_c expressed from Eq. (64).[84] The nonideality parameter α and the critical current through the junction J_c are given a meaning in terms the geometrical details of the microaperture. They can be derived from experiments and compared with the expected values.[85]

Since the healing length is of atomic dimensions for ^{4}He, a near-ideal Josephson effect cannot be expected to be found in the microapertures that can be manufactured at present, except very close to the λ transition when this length diverges. Experiments close to T_λ have been conducted successfully by Sukhatme *et al.* (2001) and Hoskinson *et al.* (2006) and are described in Sec. VII.F. The experiments that have first shown the existence of the Josephson dc effect in superfluids have been carried out in ^{3}He (Avenel and Varoquaux, 1988).

B. Current and phase in superfluid ^{3}He

The helium-3 nucleus is made up of two protons and one neutron: ^{3}He is a fermion. As for the abundant and heavier isotope ^{4}He, its zero-point energy in the condensed phase is large and it remains in the liquid phase down to absolute zero at pressures below about 35 bars. It thus forms a Fermi liquid with a Fermi sphere over which Landau quasiparticles float. Because the interatomic potential is attractive at large distance, these quasiparticles can form Cooper pairs and ^{3}He was long suspected to become a BCS superfluid below some hard-to-predict temperature. The discovery by Osheroff, Richardson, and Lee of the transition to not one but two superfluid phases (Osheroff *et al.*, 1972) fixed the transition temperature to 2.49 mK on the melting curve, at a pressure of 34.34 bars and opened an exciting new chapter of low-temperature physics.

As the experimental properties of these new superfluid phases were quickly unraveled (Wheatley, 1975a, 1975b; Lee and Richardson, 1978), they were identified from their nuclear susceptibility properties observed by nuclear magnetic resonance (NMR) as resulting from the formation of Cooper pairs in a *spin-triplet* state (Leggett, 1975). A new breed of superfluid was born. The overall antisymmetry of the wave function under the exchange of two fermions then requires an odd angular momentum state $l = 1, 3, \ldots$. The available experimental data, mainly the phase diagram, the specific heat, and the nuclear susceptibility, led to the identification of the A and B phases as p-wave Cooper-pair superfluids with total spin $S = 1$ and total angular momentum $L = 1$.

The formalism describing the properties of these anisotropic superfluid phases was quickly developed.[86] It extended the Bardeen-Cooper-Schrieffer theory of s-wave superconductivity to the neutral triplet-spin-state superfluid. The most general pair wave function with three possible substates for the spin and the orbital parts is an arbitrary superposition of these 3×3 substates, involving nine complex parameters. Assuming weak coupling between the pairs, a surprisingly

[83]The hydraulic length ℓ_h is defined by Eq. (61). The thickness of the tunnel barrier is neglected.

[84]Equations (66) were proposed by Deaver and Pierce (1972) for superconducting junctions; see also Likharev (1979).

[85]See Avenel and Varoquaux (1988) for an example of this procedure and Varoquaux *et al.* (1992) for a more complete analysis.

[86]As related by Anderson and Brinkman (1975) and Leggett (1975); see Vollhardt and Wölfle (1990).

good assumption at low pressure, this extension of the BCS theory (Leggett, 1975) leads to a 3×3 order parameter for the B phase of the form

$$A_{\mu i} = \Delta(\hat{\mathbf{k}}) e^{i\varphi} R_{\mu i}(\hat{\mathbf{n}}, \theta). \tag{67}$$

The gap parameter $\Delta(\hat{\mathbf{k}})$ and the phase factor $e^{i\varphi}$ have the same interpretation as for s-wave superconductors. The B phase contains the $S_z = 0$, $+1$, and -1 pairs ($|\uparrow\downarrow + \downarrow\uparrow\rangle$, $|\uparrow\uparrow\rangle$, and $|\downarrow\downarrow\rangle$) in equal amounts in zero applied magnetic field; $\Delta(\hat{\mathbf{k}})$ is isotropic and independent of $\hat{\mathbf{k}}$, the direction on the Fermi sphere.

The matrix $R_{\mu i}(\hat{\mathbf{n}}, \theta)$ describes the rotation bringing the spin quantization axis along the orbital quantization axis. This rotation is characterized by a unit vector $\hat{\mathbf{n}}$ and an angle θ. Both the gap parameter $\Delta(\hat{\mathbf{k}})$ and the rotation are real quantities independent of the overall phase φ. Therefore, the B-phase order parameter (67) takes the same form as that for ^{4}He, namely, the product of a phase factor $\exp(i\varphi)$ with a well-defined phase φ and a phase independent modulus. The same reasoning as for the ^{4}He case applies when performing a Galilean transformation: mass transport in the pseudoisotropic B phase is related to the gradient of φ.

The modulus of the order parameter (67), or the gap parameter Δ, can be thought of as the binding energy of a Cooper pair at $T = 0$; it is of the order of $k_B T_c$,[87] with T_c being the superfluid transition temperature. The smallest time lapse over which this energy can be defined is limited by the uncertainty relation for time energy: $\delta t \simeq \hbar/\Delta$. During that time, the pair spreads over a length $\xi_0 = \hbar v_F/\Delta$, where v_F is the velocity of the ^{3}He quasiparticles over the Fermi surface.[88] It can be seen from this heuristic argument (Lounasmaa *et al.*, 1983; Davis and Packard, 2002) that properties of the superfluid are well defined only over distances larger than the coherence length ξ_0 of the order of 600 Å at $T = 0$ and low pressure −120 Å at melting pressure. The prospect of observing quantum departures from classical hydrodynamics in ^{3}He appears much more favorable than in the case[89] of ^{4}He: the coherence length is no longer very small compared to the size of apertures that can be micromachined; genuine hydrodynamic Josephson effects can be expected to take place in the B phase in submicron size apertures, or pinholes.

C. Weak links in *p*-wave superfluids

Weak links for superfluids come in two breeds, single microapertures in thin wall partitions and larger scale arrays of such apertures geometrically arranged a few microns apart, actual pinholes for the former, a mock-up for tunnel junctions for the latter. The flow patterns in the vicinity of each kind lead to different weak link behaviors.

The first successful Josephson-type experiments were carried out by Avenel and Varoquaux (1988), using the same microresonator and single aperture as for their experiments on phase slippage in ^{4}He.[90] Their observations spurred intense theoretical interest in the description of phase slippage in ^{3}He.

Analytic calculations of the current through a pinhole orifice with all dimensions smaller than ξ_0 and with specular reflection of the quasiparticles on the walls by Kurkijärvi (1988) in the framework of quasiclassical theory, following earlier work by Kopnin (1986) and Monien and Tewordt (1986, 1987), led to the following current-phase relation:

$$J = \mathsf{a} s_h v_F N(E_F) \Delta(T) \sin\left(\frac{\varphi}{2}\right) \tanh\left[\mathsf{b} \frac{\Delta(T)}{k_B T} \cos\left(\frac{\varphi}{2}\right)\right], \tag{68}$$

where $N(E_F)$ is the density of states at the Fermi surface, v_F is the Fermi velocity, $\mathsf{a} = \pi/2$, and $\mathsf{b} = 1/2$ for the B phase. Equation (68) takes the same form as for a s-wave supercurrent through a superconducting microbridge.[91] A similar form also holds approximately for the A phase with $\mathsf{a} = \pi/\sqrt{6}$ and $\mathsf{b} = (3/8)\sqrt{3/2}$, and for the planar phase, a phase which may possibly be stabilized within the microaperture by the walls.

Equation (68) reduces in the limit $\Delta(T)/k_B T \ll 1$ to the sinusoidal dependence of Eq. (64) for the current in terms of the phase difference across the barrier φ_b. This result has been obtained using a variety of techniques.[92] It is no surprise that the details of the structure of the order parameter disappear when the dimensions of the orifice are small with respect to the coherence length and that s-wave-like results are found for both the A and B phases. Superfluid coherence is effectively weakened by the microorifice because the length over which it heals becomes larger than the physical size of the connecting duct; however, if the length of that duct is short enough, a sizable supercurrent can still exist, sustained by the quantum tunneling of quasiparticle pairs through the weak link.[93]

At temperatures such that $\Delta(T)/k_B T$ is no longer a small quantity, Eq. (68) becomes increasingly slanted with an abrupt slope close to $\varphi = \pi$ when $\cos\varphi/2$ changes sign while retaining the periodicity by 2π in the phase difference. It displays a discontinuity for $\varphi = \pi$ at $T = 0$. This behavior of

[87] For ^{3}He-B in weak coupling theory, $\Delta(0) = a k_B T_c$ with $a \leq 1.75$ (Leggett, 1975).

[88] The zero-temperature coherence length of the B phase is given by $\xi_0 = [7\zeta(3)/48\pi^2]^{1/2} \hbar v_F/k_B T_c$ (Vollhardt and Wölfle, 1990, Sec. 3.4). The temperature-dependent coherent length diverges as $\xi(T) = \xi_0 (1 - T/T_c)^{-1/2}$ in the Ginzburg-Landau regime.

[89] The state of the art in aperture manufacturing evolved over time from submicronic slits (Sudraud *et al.*, 1987) to nanometric holes (Pereverzev and Eska, 2001).

[90] See Sudraud *et al.* (1987) for an account of earlier attempts and Sato and Packard (2012) for later developments.

[91] As obtained by Kulik and Omel'yanchuk in 1977, see, for instance, Likharev (1979) or Golubov, Kupriyanov, and Il'ichev (2004).

[92] See Monien and Tewordt (1986, 1987), Hook (1987), Ullah and Fetter (1989), Kopnin and Salomaa (1990), Thuneberg, Kurkijärvi, and Sauls (1990), Kopnin, Soininen, and Salomaa (1991), and Soininen, Kopnin, and Salomaa (1991).

[93] A different situation was examined by Rainer and Lee (1987), that of tunneling through a very thin ^{3}He-^{4}He film spanning a microhole, much like a soap bubble. The barrier parameters l_b and $\xi_b(T)$ can e also be evaluated explicitly in this idealized case as well as the critical current through the weak link.

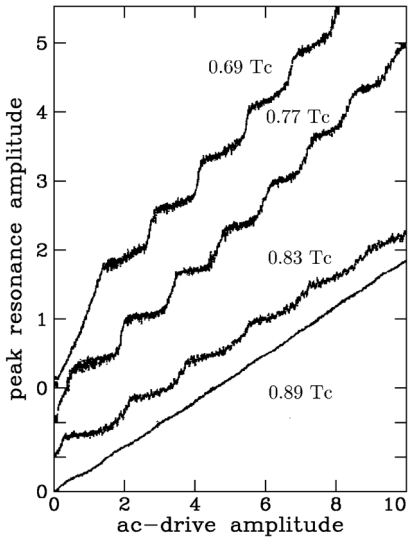

FIG. 27. Staircase patterns (peak resonance amplitude vs applied drive level, both in arbitrary units) in ^{3}He-B at a pressure of about 0.2 bar. The curves at various temperatures are shifted vertically for readability. Drive frequencies at the various temperatures are shifted from resonance so as to set comparable resonance conditions. From Avenel and Varoquaux, 1988.

the weak link comes on top of the effect of the hydraulic inductance of the Deaver-Pierce model: the CPR is bound to become hysteretic and multivalued even for an extremely small pinhole in the limit $T \to 0$.

This simple theoretical description accounts well for the experiments of Avenel and Varoquaux (1988), whose results are reproduced in Fig. 27. Similar findings have been reached by Backhaus *et al.* (1997) in an array of pinholes. Close to the superfluid transition, weakly coupled reservoirs of superfluid ^{3}He-B exhibit a behavior that involves the direct analogs of both Josephson ac and dc effects in superconductors. The relation between the superfluid current and phase, or CPR, is well represented by a slanted sine function. In the range of applicability of Eq. (68), single microapertures and arrays behave alike. The existence in superfluids of the analogs of the Josephson effects in superconductors was thus established in 1988 on firm grounds, both experimentally and theoretically, but more features were soon revealed by further studies.

D. Multivalued CPR's, π states, and π defects

While near-ideal Josephson behavior prevails in ^{3}He-B at low pressure close to T_c, departures from a sinusoidal current-phase relation were observed by Avenel and Varoquaux (1988, 1989) in a single orifice and later by Backhaus *et al.* (1997) and Marchenkov *et al.* (1999) in an array of 0.1 μm diameter apertures, evolving to a near-straight line relation below $0.6T_c$. The latter case is reminiscent of the situation in ^{4}He, in which vortices are nucleated.

As the temperature is lowered further below T_c, the superfluid coherence length becomes smaller than the aperture size used in present-day experiments. This trend is even more pronounced at higher pressure, where T_c is higher (and ξ_0 smaller). Room is thus left for a wall dominated order parameter texture within the weak link or its immediate proximity: the p-wave nature of superfluid ^{3}He can then reveal itself.

Detailed numerical simulations based on the time-dependent Ginzburg-Landau equations have been carried out by Soininen, Kopnin, and Salomaa (1992a, 1992b)[94] for a finite-size aperture quite similar to the one used by Avenel and Varoquaux (1988). These simulations show the time evolution, when the ^{3}He superfluid is set to flow through the microslit, of the components of the superfluid density tensor parallel to the two short dimensions of the slit. Both the mass and spin degrees of freedom of the spin-triplet p-wave order parameter take part in the phase-slippage process. The various components of the order parameter evolve separately in space and time and do not go to zero simultaneously at the same location in the microaperture. The regions of space, in which the order parameter is depressed and about which the phase slips, peel off from the walls and traverse the slit at right angle with the flow direction. Thus, phase slips in the p-wave superfluid exhibit a fairly complex spatial and temporal evolution both in the pseudoisotropic B phase and in the anisotropic A phase. In addition, the A phase may sustain coreless phase slippage as suggested by Anderson and Toulouse (1977) and as discussed later. These simulations also illustrate the details of operation of a vortex mill (Soininen, Kopnin, and Salomaa, 1992a, 1992b) in which phase-slip avalanches and multiple vortex creation take place. The state of sophistication of the microscopic description of superfluid ^{3}He makes it possible to obtain such detailed information.

The phase-slippage observations in superfluid ^{3}He reflect this wealth of riches. While near-ideal Josephson behavior prevails in ^{3}He-B at low pressure close to T_c, more complicated staircase patterns than those shown in Fig. 27 develop below $0.7T_c$ (Avenel and Varoquaux, 1989), which cannot be described by the Deaver-Pierce model. These patterns are not even reproducible from one cooldown through T_c, or through the A to B transition, to the next. It is likely that different order parameter textures and topological defects are coming into play.

Among those features, two notable ones were reported by Backhaus *et al.* (1998) and Marchenkov *et al.* (1999) and are shown in Fig. 28 in ^{3}He-B at saturated vapor pressure. They used a two-hole microresonator with a weak link made of a 65×65 array of 100 nm round holes micromachined in a 50 nm thick silicon nitride freestanding membrane. The 4225 holes in parallel offer a large enough flow path for the mass flow rate under an applied pressure head to be closely monitored. They operated the resonator in free ringing mode and recorded the transient response following a large impulsive drive excitation. The phase is derived from the measurement of the pressure head between the two sides of the weak link by integration of Eq. (14). The current-phase

[94]See Kopnin and Salomaa (1990) and Kopnin, Soininen, and Salomaa (1992).

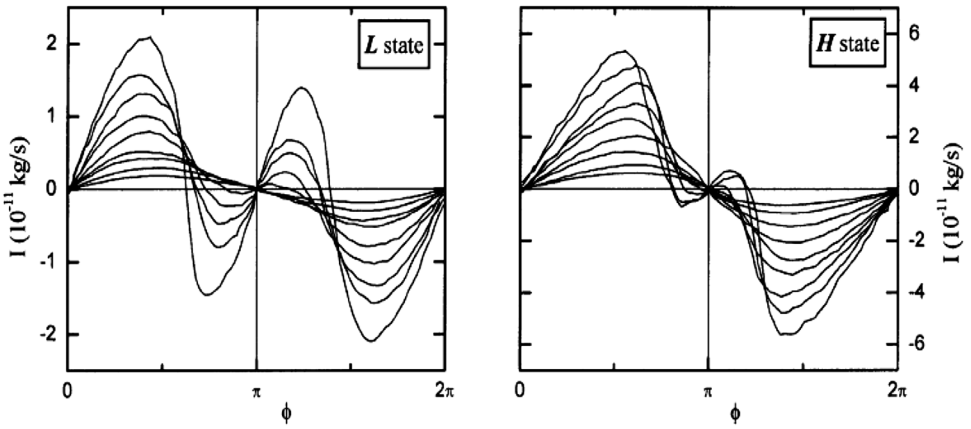

FIG. 28. Current-phase relations in ^{3}He-B observed in an array weak link. CPR's for the low current state (left panel) and the high current state (right panel) for temperatures ranging from $0.850T/T_c$ down to $0.450T/T_c$ in steps of approximately $0.05T/T_c$. The mass current through the weak link increases as the temperature is lowered. At temperatures close to T_c, the current-phase relations can be fitted well with the Deaver-Pierce model. As the temperature decreases (and the critical current increases), this model becomes inadequate as a π-periodic component gradually sets in. From Marchenkov *et al.*, 1999.

relations displayed in Fig. 28 are obtained with this direct technique.[95]

The first feature shown in Fig. 28 is the existence of two possible CPR's at the same temperature, one with a larger critical current than the other, the second, the appearance in the 2π-periodic CPR of an increasingly strong π-periodic admixture as the temperature is lowered. Avenel, Mukharsky, and Varoquaux (1999) pointed out that this admixture could simply arise from the unavoidable dispersion between the sizes of the microholes in the array.[96] This rather trivial explanation holds in part under all circumstances but is not the end of the story, as was soon shown by Avenel, Mukharsky, and Varoquaux (2000) observations using a single microaperture for which there is no scatter in critical currents or transit times.

Avenel, Mukharsky, and Varoquaux (2000) and Mukharsky, Avenel, and Varoquaux (2004) took advantage of the Sagnac effect (see Sec. VIII.A) to ramp up and down in a precise manner the macroscopic phase difference $\delta\varphi$ applied across the weak link. They reported the observation of several different CPR branches, usually more than two, most with π components and with different critical velocities at the same temperature but in different cooldowns through the superfluid transition temperature. Each of these several $J(\varphi)$'s was usually robustly fixed in each run and the general trend was to go from 2π periodicity to π periodicity as the temperature is lowered, although, occasionally, no π periodicity was observed even at the lowest temperature. At higher pressure (10 bars), hysteretic behavior in the single microaperture was prevalent and up to three simultaneous branches for the CPR were observed. Switching between these different branches could be triggered by applying strong transient drive voltage to the resonator, indicating that textural effects were most likely at play.

Some of these features were actually predicted long before their observation by Thuneberg (1988) who worked out a numerical solution for the Ginzburg-Landau equations of the state of ^{3}He-B confined inside a microaperture. Thuneberg found two different CPR's according to whether the $\hat{\mathbf{n}}$ vector of the B-phase order parameter, assumed to lie perpendicular to solid walls, is in a parallel or antiparallel configuration on both sides of the membrane carrying the microaperture. In the antiparallel configuration, the spin and mass currents are out of phase, resulting in a lower critical current. Eventually, the decoupling between mass and spin currents leads to the admixture of a π-periodic component to the 2π-periodic CPR.

The experimental discovery of these effects by Backhaus *et al.* (1998) and Marchenkov *et al.* (1999) spurred theoretical interest. Thuneberg's numerical findings were soon confirmed and sharpened by the analytic investigations of Viljas and Thuneberg (1999, 2002b) and Yip (1999) and extended numerical simulations for two-dimensional geometries by Viljas and Thuneberg (2002a). The upshots of these studies are the following[97]:

- Following Viljas and Thuneberg (1999) and Yip (1999),[98] the π states in ^{3}He-B are due to the interference of currents carried by quasiparticles with different spins that acquire different excess phases from the internal spin structure of the order parameter while traveling through the weak link. More specifically, the $|\uparrow\uparrow\rangle$ and $|\downarrow\downarrow\rangle$ Cooper-pair populations may be viewed as independent superfluids, the phases of which may be slightly shifted with respect to one another because of a differing

[95]More experimental details and further references can be found in the reviews by Davis and Packard (2002) and Sato and Packard (2012).

[96]An alternate explanation for the existence of π states is offered by Eska, Gladchenko, and Pereverzev (2010) and is based on the built-in nonlinearities of the single-hole resonator used in the experiments of Backhaus *et al.* (1998) and Marchenkov *et al.* (1999).

[97]See Janne Viljas's Thesis (Espoo 2004) available at http://lib.hut.fi/Diss/, Smerzi *et al.* (2001), Zhang and Wang (2001), and Nishida, Hatakenaka, and Kurihara (2002) and Viljas and Thuneberg (2004b). A related situation, that of "π junctions," has been much studied in electrodynamic junctions (Golubov, Kupriyanov, and Il'ichev, 2004).

[98]See Zhang and Wang (2001).

spin-orbit coupling. Summing the corresponding mass currents, given by Eq. (68), represented by slanted sine CPR's shifted in phase by $\pm\delta\varphi$ leads, if the shift is large enough, to a positive-slope branch in the CPR at π: this π-state mechanism relies on different spin-orbit orientations on both sides of the weak link and operates at the single pinhole level (Viljas and Thuneberg, 2002a).

- The Josephson coupling between two baths of ^{3}He-B mixes the phase difference to the spin-orbit texture of the order parameter: the equilibrium configuration of the texture then depends on the phase bias applied to (hence on the current carried by) the weak link. The texture is assumed fixed in the simpler calculations: this is the *isotextural* case, which offers only a coarse agreement with observations. If the texture is allowed to adjust to the local mass and spin currents by expressing the balance between its stiffness and its interactions with the walls and with the mass current, a π state can also arise: this *anisotextural* effect requires a self-adjusting string of calculations and provides quantitative agreement with pinhole array experiments (Viljas and Thuneberg, 2002b).
- These refined calculations led to the realization that multiple Andreev reflections and subgap structures also played a role in the transmission of the supercurrent through the weak link (Asano, 2001),[99] and that a A-like phase inside the superfluid junction could also result in the existence of a π state (Nishida, Hatakenaka, and Kurihara, 2002).
- Dissipation in pressure-driven dc supercurrents (Simmonds *et al.*, 2000) could also be explained by multiple Andreev reflections (Mukharsky, 2004; Viljas, 2005) or by time-dependent anisotextural effects and spin-wave emission (Viljas and Thuneberg, 2004a; Viljas, 2005): if a pressure difference is applied across the weak link, an ac oscillation (at the ac-Josephson frequency) of the texture ensues, causing dissipation by spin-wave radiation. The two dissipation mechanisms, subgap processes and textural losses, can come on top of one another.[100]

Observations related to these topics are those of Mukharsky, Avenel, and Varoquaux (2004) who, in the course of high-precision CPR measurements using the Sagnac effect described in Sec. VIII.A, found the signature of a stable textural defect that sustains a change of the phase by π away from the weak link. This differs from the π state discussed previously. "Cosmiclike" solitons, proposed by Salomaa and Volovik (1988), could constitute such a defect but they are thought to be unstable in the bulk of the superfluid.

A comprehensive study of the possible planar interfaces between two domains of superfluid ^{3}He-B has been conducted by Silveri, Turunen, and Thuneberg (2014). Of all the possible planar structures allowed by the symmetries of the B-phase order parameter, only one is found to be energetically stable in the presence of walls. This particular interface is characterized by the vanishing of one of the components of the interfacial order parameter along a *gap-node direction* contained in the plane of the domain wall. It sustains a phase change by π and can appear as a remnant of the A to B interface during cooldown through the transition.

In the perspective of this article [see also Davis and Packard (2002)], these complex features of the Josephson supercurrents illustrate the nature of the superfluid order parameter and of the phase coherence it entails. But their detailed studies are complicated because they are entangled with order parameter textures, as mentioned and also because the state of the superfluid inside the microjunction may not be precisely accounted for, as discussed in the next section.

E. The peculiarities of the A phase

The A phase takes over from the B phase at the superfluid transition temperature above a pressure of 21.2 bars. Strong coupling effects resulting from atomic localization increase with density. Part of these enhanced interactions is mediated by spin-spin exchange, the so-called paramagnons. Because of these effects, the A-phase condensate consists only of $S_z = +1$ and -1 pairs, ($|\uparrow\uparrow\rangle$ and $|\downarrow\downarrow\rangle$), and the energy gap above the Fermi surface $|\Delta(\hat{\boldsymbol{k}})|$ is strongly anisotropic while retaining the $L = 1$ symmetry: it vanishes at a node in the direction of $\hat{\mathbf{l}}$, the orbital quantization axis. As for its spin part, the A phase behaves in some respect as an antiferromagnet with a spin quantization axis $\hat{\mathbf{d}}$. Its stability with respect to the B phase is enhanced by an external magnetic field.

The A-phase order parameter in zero magnetic field is expressed in terms of three unit vectors, the spin quantization axis $\hat{\mathbf{d}}$, and the orthonormal vectors $\hat{\mathbf{m}}$ and $\hat{\mathbf{n}}$ forming a triad with $\hat{\mathbf{l}}$, the direction of the orbital angular momentum of the pairs. It is written in tensorial notation as

$$A_{\mu i} = \Delta_{\mathrm{A}} \hat{d}_\mu (\hat{m}_i + i\hat{n}_i). \tag{69}$$

In ^{4}He, the Bose order parameter is a simple complex number and the phase comes in quite naturally as it does for the BCS order parameter in s-wave superconductors, for ultracold atoms, and for the B-phase order parameter, Eq. (67), as discussed.

No single phase factor appears spontaneously in Eq. (69) for the A-phase order parameter. However, the single-particle wave function in the condensate still possesses an overall phase among other components. This phase goes over to the macroscopic Bose order parameter, which inherits of a global $U(1)$ phase rotation broken symmetry.

But this is not the entire story: a rotation of the triad $\hat{\mathbf{l}}, \hat{\mathbf{m}}, \hat{\mathbf{n}}$ about the angular momentum directrix $\hat{\mathbf{l}}$ by angle γ also contributes an overall phase factor to the A-phase order parameter. This property can be readily seen by considering the complex plane perpendicular to $\hat{\mathbf{l}}$ containing the complex vector $\hat{\mathbf{m}} + i\hat{\mathbf{n}}$ that appears in Eq. (69): a rotation by angle γ in the complex plane transforms $\hat{\mathbf{m}} + i\hat{\mathbf{n}}$ into $\exp(-i\gamma)(\hat{\mathbf{m}} + i\hat{\mathbf{n}})$.

[99] See Smerzi *et al.* (2001), Thuneberg (2005), and Viljas (2005).

[100] A related mechanism governing the vortex dynamics in Fermi superfluids at temperatures well below T_c, reported by Silaev (2012), arises from the kinetics of localized excitations bound to the vortex cores and driven out of equilibrium by vortex motion. The local heating of the vortex cores results in an energy flux carried by nonequilibrium quasiparticles and in a dissipation mechanism that can operate even at zero temperature.

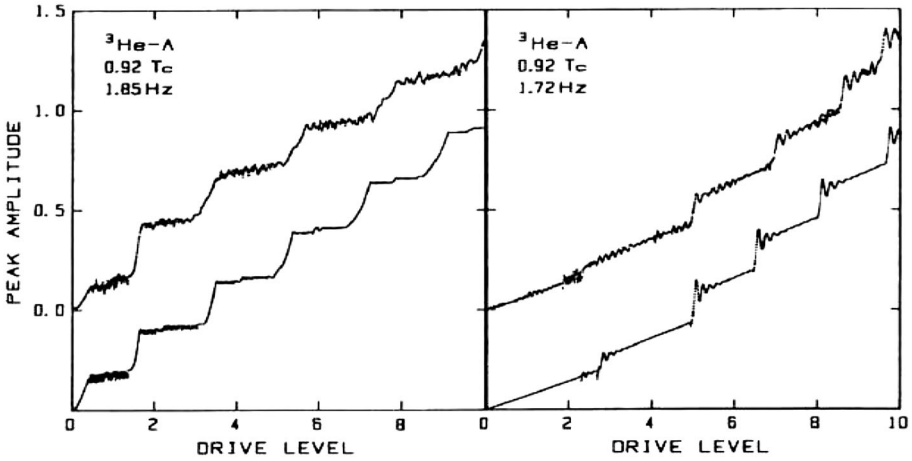

FIG. 29. Staircase patterns in the A phase at 28.4 bars and $T = 0.92T_c$ ($T_c = 2.417$ mK). The left and right panels show the patterns slightly above and below the resonator resonance at $\omega_m = 1.783$ Hz, as observed (upper curves) and as computed (lower curve) with the Deaver-Pierce model. From Avenel and Varoquaux, 1989.

The Galilean invariance argument as used to derive the two-fluid model for ^{4}He leads to the following expression for the velocity of superfluid mass transport[101]:

$$\boldsymbol{v}_s = -\frac{\hbar}{2m_3}(\nabla\gamma + \cos\beta\nabla\alpha). \tag{70}$$

The Euler angles α, β, γ fix the orientation of the orbital triad $\hat{\mathbf{l}}, \hat{\mathbf{n}}, \hat{\mathbf{m}}$ in the chosen reference frame, γ expressing a rotation about $\hat{\mathbf{l}}$ as mentioned. Two independent phase gradients appear in Eq. (70). In one, $-\nabla\gamma$, the angle plays the role of the usual phase φ. This feature arises because of the $U(1)$ phase rotation broken symmetry as mentioned. The other stems from the bending of the $\hat{\mathbf{l}}$ texture. Superflow is not simply governed by the gradient of the global phase alone. The velocity field $\boldsymbol{v}_s$ is no longer irrotational in general, hence the circulation of $\boldsymbol{v}_s$ over a closed loop is no longer necessarily quantized.

In the presence of nonuniform $\hat{\mathbf{l}}$ textures, the change of orientation of $\hat{\mathbf{l}}$ in space may also contribute to the supercurrent. The contour integral of Eq. (70) along a closed loop Γ can be put under the form

$$\oint_\Gamma \boldsymbol{v}_s \cdot d\boldsymbol{r} = \frac{\hbar}{2m_3}[2\pi n + \sigma(\mathcal{D})]. \tag{71}$$

The first contribution to the right-hand side of Eq. (71) is recognized as the quantized velocity circulation around line singularities, as found in superfluid ^{4}He, and the second is expressed (Ho, 1978) as the area circumscribed on the unit sphere by unit vector $\hat{\mathbf{l}}$ when carrying the loop integral along contour Γ. This last contribution is nil in the trivial case where $\hat{\mathbf{l}}$ keeps pointing in a fixed direction. There exist other less-trivial cases with $\sigma(\mathcal{D}) = 0$ as discussed by Ho (1978), but, in general, this contribution is nonzero and the velocity circulation is nonquantized.

The interplay between superflow, vortices, and textures of the order parameter becomes quite complex.[102] In particular, the A-phase persistent superflow can be relaxed by textural motion alone without the creation of topological singularities of the order parameter such as vortices. However, if large-scale motion of the texture is suppressed, dissipation can be quenched and persistent currents stabilized, as shown by the experiments of Gammel, Ho, and Reppy (1985). They demonstrated the existence of such currents in the annular space of a torsional oscillator packed with 25 μm silicon carbide powder. The effect of the powder was to immobilize $\hat{\mathbf{l}}$. The small supercurrent was detected indirectly through its effect on the damping of the small amplitude of the torsional oscillator. This crafty experiment showed that the A-phase possesses, if to a less convincing extent than the B-phase, the distinctive attribute of dissipationless flow.

The phase-slippage concept can also be extended to the A phase, as proposed by Anderson and Toulouse (1977). Josephson-type experiments can be contemplated with some uncertainty as to their outcome because of the lack of quantization of the velocity circulation, and also because of the large dissipation associated with the motion of the order parameter gap in the direction of $\hat{\mathbf{l}}$, where its nodes lie.

These experiments were attempted by Avenel and Varoquaux (1989) with the same resonator as for their B-phase experiments. They did observe staircase patterns in the A phase both close to the superfluid transition temperature with a rather nonideal current-phase relation and farther down in temperature where new features occurred. The patterns shown in Fig. 29 obtained in the A phase at $T = 0.92T_c$ at frequencies slightly above and below the resonance frequency of the flexible-wall resonator are quite well defined but differ markedly: they exhibit large dispersive effects, a sharply peaked resonance, and low dissipation. The outcome of numerical simulations of the resonator response using the

[101] See Vollhardt and Wölfle (1990), Sec. 7.1.

[102] For a pointed but still gentle introduction to the intricacies of the A-phase hydrodynamics, see Cross (1983) and Hall and Hook (1986) who also covered the effect of magnetic fields not considered here.

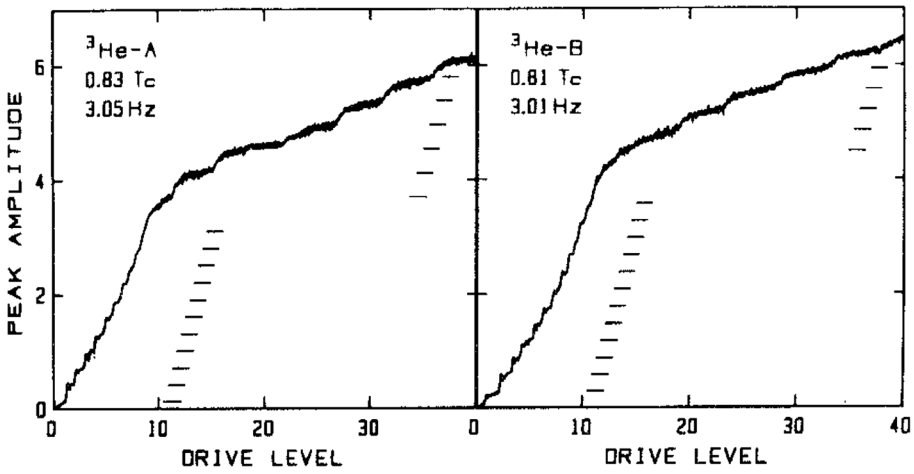

FIG. 30. Staircase patterns in the A and B phases at nearly identical frequencies and temperature. The horizontal ticks mark the periodicity of the staircase pattern (top) and of the low-level structure (bottom). This low-level structure has been attributed to solid friction of unknown origin somewhere in the resonator (but may also arise from subgap energy levels). From Avenel and Varoquaux, 1989.

Deaver-Pierce model, Eq. (66), are shown below the experimental data curves. The resonance quality factor is high, $Q = 80$. The nonideality parameter α is equal to 5: the phase slips are hysteretic and weakly dissipative.

Given this observation that the A-phase phase-slip pattern seems to follow the ubiquitous Deaver-Pierce model at 0.92 T_c, it could be expected to become more and more ideal when raising the temperature closer to T_c. This trend could unfortunately not be ascertained in these experiments because the operating frequencies, which decrease as ρ_s/ρ, become too low and the useful signal gets lost in the background $1/f$ mechanical noise of the detection device.

Farther down in temperature, an instructive direct comparison between the A-phase response and that of the B-phase at high pressure can be carried out by taking advantage of the following circumstance: at 28.4 bars, the A to B transition occurs at about 0.81 T_c; it is signaled by a sudden drop in resonance frequency caused by the drop in superfluid density accompanying the first order transition. As the A phase can be supercooled into the domain of stability of the B phase, both phases can be studies at comparable frequencies.

The outcome of this comparison is shown in Fig. 30 and reveals a remarkable similarity between the two phases. The response of the superfluid in the weak link depends little on whether the bulk of the liquid is in the A or the B phase. As discussed by Avenel and Varoquaux (1989), the observed behavior inside the microslit corresponds well to the situation described by Kurkijärvi (1988) who found that the current-phase relations for the A and B phases differ only little [see Eq. (68)]. It may also happen that the state of the superfluid in the weak link remains the same irrespective of the state in the bulk. It was predicted by Fetter and Ullah (1988) and Li and Ho (1988) that the A-polar phase would be favored by the depletion of some of the components of the A-phase order parameter close to the aperture walls.

The subgap structure, shown in Fig. 30, which develops for resonance amplitudes below the critical threshold at which dissipative phase slips start to occur, is quite intriguing. It was interpreted by Avenel and Varoquaux (1989) as arising from possible (aniso)-textural effects inducing solid friction. It could also possibly be revealing the existence of subgap resonant levels.

These experiments establish the fact that phase slippage takes place in the A phase, that persistent currents can be trapped in the loop threading the double-hole resonator, and that the velocity circulation along these trapped currents changes by multiples of the quantum of circulation in the same manner as in the B phase: it so turns out, as was the case in the persistent current experiments by Gammel, Ho, and Reppy (1985), that the $\hat{\mathbf{l}}$ texture is sufficiently well pinned in the regions where $\boldsymbol{v}_s$ picks up significant speed.

Topological defects, seen to play an important role in phase-slippage experiments, offer a vast and fascinating domain of study, in both the A and B phases. The vortex core develops complex structures, as reviewed by Salomaa and Volovik (1987). Vortex sheets can form in rotating ^{3}He-A, as observed by Parts *et al.* (1994) using very sensitive NMR techniques, which have brought about a wealth of information on vortices in superfluids under rotation. This work was reviewed by Finne *et al.* (2006). Analogies can be drawn between the formation of defects in superfluid ^{3}He and that of cosmic strings in the early Universe because the order parameter symmetries that can be broken are the same. These prospects for experimental cosmology were reviewed by Bäuerle, Fisher, and Godfrin (2000), Eltsov *et al.* (2000), Volovik (2003), and Bunkov (2010). Phase slippage is relevant in these situations and will be used to study this vast new field.

F. ^{4}He close to the λ point

The existence of Josephson-like effects was established in superfluid ^{3}He for the dc effect and in both ^{3}He and ^{4}He superfluids for the ac effect by 2000. The remaining problem was the possible observation of a quasisinusoidal current-phase relation in ^{4}He. The minuteness of the coherence length in ^{4}He makes the fabrication of a suitable weak link a tall order except in the immediate vicinity of the λ point, where it diverges as $\xi = \xi_0(1 - T/T_\lambda)^{-2/3}$ with $\xi_0 \sim 1$ to 2 Å (Langer

and Reppy, 1970). At the λ point, however, superfluidity is suppressed by thermal fluctuations. Would the hydrodynamic Josephson effects not be even more readily washed out by the same token?[103]

This concern was formalized by Zimmermann (1987) whose argument runs approximately as follows. The Josephson coupling energy is obtained from the Josephson current, Eq. (64), by integration with respect to $(\hbar/m_4)\delta\varphi$. Its maximum value is therefore $(\hbar/m_4)J_c$ and reads

$$E_J = \left(\frac{\hbar}{m_4}\right)^2 \frac{s_b}{b_b}\frac{\rho_s}{\sinh(l_b/b_b)}. \tag{72}$$

In the weak coupling limit for which Eq. (64) holds, the wave function is strongly depleted within the barrier and the penetration length is smaller than the length of the barrier $b_b \lesssim l_b$. Making use of the scaling relation between $\rho_s(T)$ and $\xi(T)$ (Josephson, 1966),[104]

$$\rho_s\xi = (m_4/\hbar)^2 k_B T, \tag{73}$$

and since $\sinh(l_b/b_b) > l_b/b_b$ it stems from Eq. (72) that

$$E_J \lesssim \frac{s_b}{l_b}\frac{k_B T}{\xi(T)}. \tag{74}$$

For the round pinhole with diameter d considered by Zimmermann, $s_b = \pi d^2/4$ and $l_b > \ell_h$, the hydraulic length ℓ_h being $\pi d/4$ for a circular orifice,[105] so that $E_J < k_B T d/\xi(T)$. Zimmermann concluded from this upper bound for the Josephson energy that, as $\xi(T)$ diverges upon approaching T_λ from below, the Josephson coupling energy will end up being less than the thermal energy and that the Josephson dc effect will be washed out by thermal fluctuations.

Similar concerns were spelled out by Ullah and Fetter (1989) for their calculations of weak link properties in ^{3}He-B in the Ginzburg-Landau regime: "We do not address the important problem of thermal fluctuations destroying the superfluidity in the very small volume of the weak link. To our knowledge, there is no reliable, quantitative theory of the stability of the superfluid phase is severely confined geometries. We believe that this question can be convincingly answered only by experiment." This remark is even more relevant to superfluid ^{4}He close to T_λ.

The first hint of a successful experimental observation was reported by Sukhatme *et al.* (2001). They used an array weak link of 24 microslits 3×0.17 μm^2 about 10 μm apart in a 0.15 μm thick membrane. Their findings are summarized in Fig. 31. At 3.72 mK below T_λ—the bottom curve in the figure, the scale of which is shrunk—the critical velocity is well marked, as well as the staircase steps, indicating a dissipative phase-slippage process. A phase-slip regime has been reached. This was hoped for since the temperature-dependent coherent length 3.72 mK below T_λ, $\xi(T) = 24$ nm,[106] is smaller than the microslit width, but by less than 1 order of magnitude.

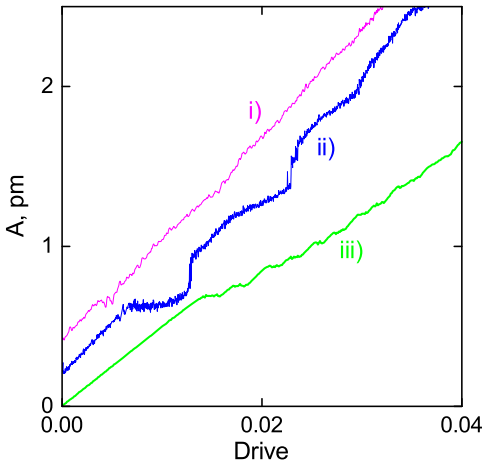

FIG. 31 (color online). Staircase patterns in ^{4}He close to T_λ (amplitude in picometers vs drive, in arbitrary units for (i) $T_\lambda - T = 61$ μK, (ii) 154 μK, and (iii) 3.72 mK. The plots are shifted vertically by 2 pm with respect to one another for clarity. The data for (iii) has been divided by 20 along the x axis and by 10 along the y -axis. As in the case of ^{3}He-B, shown in Fig. 27, the height of the first step corresponds to the critical current J_c. Each subsequent step corresponds to an additional phase difference of 2π. From Sukhatme *et al.*, 2001.

Getting closer to T_λ from below, successively at $T_\lambda - T =$ 154, and 61 μK, the expected trend toward a smoother, less dissipative staircase pattern is observed, much like in Fig. 27 for ^{3}He, supporting the conclusion that the same hydrodynamic ideal Josephson effect can be observed in superfluid ^{4}He close to the superfluid transition temperature $T_\lambda = 2.17$ K.

This conclusion raises the following questions:

- Would, for some reason, Zimmermann's argument be invalid?
- Why is it that dissipative phase slippage, the mechanism for which seems to rely on the nucleation of a single vortex and its crossing of all streamlines of the superfluid flow through a single microslit, also operates for an extended array of them?

Zimmermann's original argument, outlined previously, was applied to a single round hole. Sukhatme *et al.* (2001)'s 24 parallel slits yield an estimated enhancement factor of 500 in the superflow passage area s_b that appears in Eq. (74), provided that the supercurrents in the apertures effectively sum up. The overall Josephson energy is increased by the same factor and the disruptive effect of thermal fluctuations is pushed back much closer to T_λ. This line of reasoning was

[103] As already mentioned by Anderson (1964), p. 120.

[104] See Halperin, Hohenberg, and Siggia (1976) and Hohenberg and Halperin (1977) for details.

[105] As derived by Anderson (1966b), p. 305.

[106] Approaching T_λ from below, ρ_s is known to vanish as (Langer and Reppy, 1970)

$$\rho_s \simeq 2.4\rho_\lambda(1 - T/T_\lambda)^{2/3},$$

where ρ_λ is the density at the λ transition, 0.1459 g/cm^3. From Eq. (73), the temperature-dependent coherence length becomes $\xi(T) = 0.338/(1 - T/T_\lambda)^{2/3}$ in nm.

pursued by Chui, Holmes, and Penanen (2003), but its soundness depends on the answer to the second question, which turns out to be trickier.

The Berkeley group carried out a number of studies[107] with aperture arrays similar to those used for ^{3}He-B by Marchenkov *et al.* (1999). The size of the round pinholes in these arrays, 90 nm in diameter, is comparable to the coherence length 1 mK away from the λ point but the distance separating the pinholes, located on a 3 μm square lattice, is much larger. Two phase-slippage regimes are identified when the temperature is lowered below T_λ as reported by Sukhatme *et al.* (2001). At ~50 to 100 μK below T_λ [and slightly farther down in temperature in the experiments by Sato, Hoskinson, and Packard (2006)], a reversible (nondissipative) Josephson regime is observed. In this regime, the phase slips occur in a fully *synchronous* manner. Between approximately 0.3 to 15 mK below T_λ, a transition toward a dissipative phase-slip regime sets in as the synchronization between the apertures gets lost. Farther below T_λ, the phase-slip regime becomes *asynchronous*. The amplitude of the resultant phase-slippage signal from the array does not sum up to what it should be. It also exhibits large slips and collapses somewhat similar to those described in Sec. VI.B for a single orifice (but of a different sort).

It is clear that inhomogeneities in aperture size and surface properties, the edge effects at the periphery of the array, and local critical fluctuations introduce a spread in the values of the critical current in the different apertures. Phase slips occur at different times during resonator motion. The summation of the currents through the various apertures, as attempted in the numerical simulations of arrays of superfluid Josephson junctions by Avenel, Mukharsky, and Varoquaux (1999), Pekker, Barankov, and Goldbart (2007), and Sato, Hoskinson, and Packard (2007), has to be exercised with care.

It can be argued (Chui, Holmes, and Penanen, 2003) that the Josephson currents in the microapertures are small and perturb little the quantum phases in the bulk on both sides of the membrane supporting the weak link array. Phases are well defined below T_λ (for instance, the quantization of circulation is enforced) and so should their difference. This reasoning would appear to leave only 1 degree of freedom to undergo fluctuations, with a thermal energy of $k_B T/2$ to be shared among the N apertures of the array: the effect of fluctuations in each individual aperture would effectively be quenched on taking the average over the whole array.

This argument has to be stretched to explain the large span in $T_\lambda - T$ over which the synchronous phase-slippage regime subsides both very close to the λ point when quantum coherence should end up being killed by thermal fluctuations and quite a way below it where it should be randomized by array imperfections. In other words, the robustness of the coherence effect mentioned against dephasing by environmental effects appears quite remarkable. Perron *et al.* (2013) pointed out that the superfluid onset in the microslits used by Sukhatme *et al.* (2001) is expected to be depressed by size effects to $T_\lambda - T_c \simeq 430$ μK, whereas the Josephson effect could be tracked to as close as 28 μK below T_λ. Similarly, for the pinholes used by Sato, Hoskinson, and Packard (2006), $T_\lambda - T_c \simeq 2.3$ mK while the Josephson effect survived up to possibly 0.5 mK from T_λ. As concluded by Perron *et al.* (2013), "In both experiments one obtains superflow in a temperature region where the helium in the isolated weak links should be normal. Both of these experiments are thus relying on proximity effects, due to the surrounding bulk liquid, to maintain a nonzero order parameter in the weak links."

They draw their conclusion from studies of the interconnection of an array of 2×2 μm^2 micropools linked through the film of superfluid ^{4}He. They found from measurements of the specific heat and the superfluid fraction in the vicinity of T_λ that correlation effects are still effective at distances up to 100 times $\xi(T, L)$, the finite-size correlation length suitably renormalized for confinement over the distance L, the size of the micropool boxes. The unexpectedly large extent of the correlation observed between micropools can be likened to the robustness of the coherent behavior of Josephson junction arrays close to T_λ.

Pekker, Barankov, and Goldbart (2007), besides their numerical studies referred to previously, also treated the problem of aperture current summation in an irregular array as an order-disorder transition in a mean-field approximation approach. They introduced a distribution of aperture critical currents and an effective interaperture coupling parameter. They reported qualitative agreement with the experiments of Sato, Hoskinson, and Packard (2006) including "system-wide avalanches," both in the numerical simulations of the array behavior and in the ordering transition approach.

The observed long range of cross-aperture coupling may arise from a simple classical hydrodynamics scheme, which is an extension to arrays of the putative mechanism for single-aperture large slips discussed in Sec. VI.B. Suppose that, during the surge of the superflow through the array, a quantum phase slip occurs early in one of the apertures, releasing a vortex half ring that starts drifting classically sideways along the membrane supporting the array. Soon, this vortex half ring runs into the flow lines emerging from a nearby aperture, gaining energy from it to proceed in its course and, possibly, triggering the nucleation of another vortex half ring, and so on. This multiplication process may die by itself at the ebb of the flow. Or, if it overcomes the friction on the normal component, it may trigger 2π slips over all the microholes of the array, or, possibly, swell to the system-wide avalanches (Pekker, Barankov, and Goldbart, 2007) observed by Sato, Hoskinson, and Packard (2006). These mechanisms for avalanches are thus intrinsic to aperture array dynamics and distinct from flow collapses in single apertures discussed in Sec. VI.B.

Even more so than in single apertures, "macroscopic quantum coherence" manifests itself in the aperture array in a dual manner. First, the condensate acts as an ideal Euler fluid, maintaining orderly streamlines throughout the superflow in accordance to the Kelvin-Helmholtz theorem. Then, when a nonadiabatic process takes place, violating velocity circulation conservation, it does so in a quantum manner, allowing the phase to change by multiples of 2π, for instance by the nucleation of a quantized vortex or by the current source or sink provided by Josephson tunneling through a thin barrier of normal fluid.

[107] See Hoskinson, Sato, and Packard (2006), Sato, Hoskinson, and Packard (2006), Sato, Joshi, and Packard (2008), and Narayana and Sato (2010, 2011).

VIII. CONCLUDING COMMENTS

A. Matter waves and superfluid interferometry

The single-hole or two-hole hydromechanical resonators used in the phase-slippage experiments described above have been presented so far as the analogs of rf or dc superconducting quantum devices (SQUIDs), a useful analogy to help understand the way they operate. Another analogy is used in this section to illustrate the concept of coherent matter fields, or *matter waves*, introduced for superfluid helium by Anderson in 1965. These devices are now considered as the likes of optical Sagnac interferometers; as the latter, they can be used to measure absolute rotations with very high sensitivity.

Consider a pool of superfluid in the shape of a conduit bending on itself as shown in Figs. 32 or 34. The circulation of the velocity is quantized in the inertial frame, the reference frame fixed with respect to the distant stars, along any closed contour Γ located entirely in the superfluid:

$$\oint_\Gamma \mathbf{v}_s \cdot d\mathbf{l} = \frac{\hbar}{m_a} \oint_\Gamma \nabla\varphi \cdot d\mathbf{l} = n\kappa_a,$$

where $\kappa_a = 2\pi\hbar/2m_3$ for ^{3}He, 3/2 times that quantity for ^{4}He, and n is an integer.

If the cryostat housing the pool is set into rotation with rotation vector Ω, the velocity transforms in the new frame according to $\mathbf{v}_s' = \mathbf{v}_s - \Omega \times \mathbf{r}$ and the quantization of the circulation condition now reads

$$\oint_\Gamma \mathbf{v}_s' \cdot d\mathbf{l} = n\kappa_a - \oint_\Gamma \Omega \times \mathbf{r} \cdot d\mathbf{l} = n\kappa_a - 2\Omega \cdot \mathbf{S}_\Gamma, \qquad (75)$$

with $\mathbf{S}_\Gamma$ being the geometrical (oriented) area of the closed superfluid contour.

For an actual conduit with finite cross section such as the one pictured in Figs. 32 and 34, there is a variety of choices for the contour Γ. The mean circulation of the velocity results from a suitable average over the various distinct superfluid contours threading the conduit. Taking the average of Eq. (75) over all the streamlines threading the conduit amidst stray thermal currents, pinned vortices, and textures, weighed according to the (infinitesimal) mass current that they carry, leads to (Avenel, Hakonen, and Varoquaux, 1997)

$$\left\langle \oint_\Gamma \mathbf{v}_s' \cdot d\mathbf{l} \right\rangle = n\kappa_a + \kappa_b - 2\Omega \cdot \langle \mathbf{S} \rangle, \qquad (76)$$

where $\langle \mathbf{S} \rangle$ is the average of the contour areas over the conduit. The average of the quanta of circulation carried by the various streamlines, $\langle n \rangle \kappa_a$ has been written as $n\kappa_a + \kappa_b$ to explicitly separate the nonquantized phase bias $\delta\varphi_b = 2\pi\kappa_b/\kappa_a$ arising from pinned vorticity from the strictly quantized contribution $2\pi n$.

The last term on the right of Eq. (76) also amounts to a nonquantized contribution to the phase bias, which varies with the flux of the rotation vector Ω through $\langle \mathbf{S} \rangle$: the measurement of the corresponding phase difference with the interferometers depicted in Fig. 32 or 34, $\delta\varphi_S = (m_a/\hbar)2\Omega \cdot \langle S \rangle$, gives access to the rotation velocity. Alternatively, changing the orientation with respect to the north axis of the superfluid loop picks up more or less of the rotation flux due to the Earth rotation $\Omega_\oplus$. A known phase difference can be coupled to the weak link. The experimenter is provided with a "gauge wheel" to steer the phase.[108]

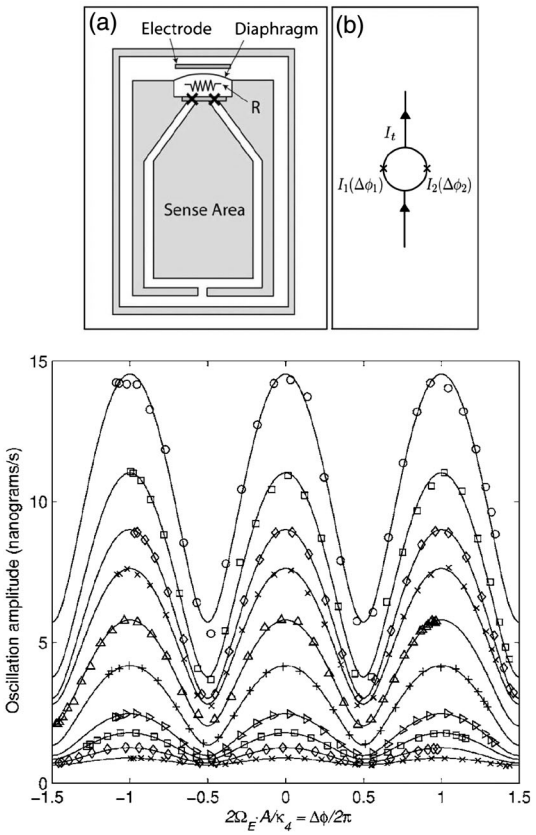

FIG. 32. Superfluid interferences in a two-aperture resonator. (a) The hydromechanical resonator. The unshaded regions are filled with superfluid ^{4}He. The flexible metallized diaphragm at the top of the upper chamber serves both as a microphone to detect the resonant oscillations and as a pressure pump to drive the flow across the two aperture arrays indicated by crosses. These arrays interrupt the superfluid channel enclosing the sense area. (b) The resonator equivalent circuit showing the analogy with the electrodynamic dc SQUID. There are two superposed currents flowing through the weak links, one corresponding to the rotation flux picked up by the sensing loop, Eq. (76), the other being the common-mode readout current from the flexible diaphragm. Bottom panel: Peak amplitude of the diaphragm displacement on resonance as a function of the rotation flux $2\Omega \cdot \mathbf{A}$ picked up by the superfluid loop enclosing the sense area; see Sec. VIII.A for a description of these interferometer operations based on the Sagnac effect. The measured data are shown by the symbols; the solid lines are fits to the data of the equation modeling the resonator motion as described by Hoskinson, Sato, and Packard (2006). The modulation curves were taken at temperatures $T_\lambda - T = 12$, 7.0, 4.0, 3.0, 2.0, 1.5, 0.9, 0.6, 0.4, and 0.3 mK from top to bottom. This temperature span covers the coherent Josephson regime in the array discussed in Sec. VII F. From Hoskinson, Sato, and Packard, 2006.

[108]The original gauge wheel proposal due to Liu was discussed by Ho and Mermin (1980b).

Exploiting the properties of superfluids to detect very slow rotations has been proposed even before the discovery of the Josephson effects in superfluids, understandably with some lack of accuracy as to how the experiment could be conducted. Cerdonio and Vitale clarified in 1984 the way in which inertial and gravitational fields could be detected with superfluid ^{4}He analogs of the rf SQUID (Cerdonio and Vitale, 1984; Bonaldi, Vitale, and Cerdonio, 1990). A number followed suit afterward for superfluid ^{3}He and ^{4}He (Hess, 1992; Packard and Vitale, 1992; Varoquaux *et al.*, 1992), and for the Bose-Einstein condensed gases (Stringari, 2001).

Detailed schemes for the actual implementation of superfluid ^{4}He gyros have been worked out with the help of numerical simulations (Avenel *et al.*, 1994) and from the analysis of the operation of existing double-hole hydromechanical resonators.[109] The first measurement of $\Omega_\oplus$ with a superfluid device was performed using a resonator operating in hysteretic mode in superfluid ^{4}He with a rotation-sensing loop of 4.0 cm^2 by Avenel and Varoquaux (1996). Soon after, the Berkeley group reported the observation of the effect of the rotation of the Earth with a similar device operated in the staircase mode, in much the same way as conventional rf-SQUID magnetometers.

We mention for the record that early attempts to measure $\Omega_\oplus$ led to disappointing results to the dismay of experimenters (Schwab, Davis, and Packard, 1996; Schwab *et al.*, 1996; Avenel, Hakonen, and Varoquaux, 1998). It was however quickly realized that the currents in the bulk of the cell outside the resonator (Avenel, Hakonen, and Varoquaux, 1998; Schwab, Bruckner, and Packard, 1998), simply caused by the reorientation of the cryostat, were interfering with the relatively weak $\Omega_\oplus$-induced Sagnac current in the pickup loop. The influence of these stray currents can be made negligible by a proper design of the cell. A sheath on the port connecting the resonator to the main body of the cell was used to that effect by Avenel and Varoquaux (1996) and Avenel, Hakonen, and Varoquaux (1997). The absence of such a decoupling device between the Sagnac current in the pickup loop and the stray currents around the cell could cause uncontrolled inaccuracies of several tens of % (Schwab, Davis, and Packard, 1996; Schwab, Bruckner, and Packard, 1997, 1998).

The potentialities of superfluid gyros as extremely sensitive and stable rotation sensors, able to track general relativity effects, have been considered by Avenel, Hakonen, and Varoquaux (1998), Chui and Penanen (2005), Sato and Packard (2012), and Sato (2014). It appears that these gyros can compete with the most advanced rotation sensors, in particular, because they are inherently driftless at very low temperatures.

These gyrometric devices are the direct superfluid analogs of the well-known Sagnac optical interferometers, as can be seen by inspection of Fig. 33 and of the superfluid device in Fig. 34: the light source provides the incident light beam, the flexible membrane, the supercurrent; counterrotating waves travel along the square optical path, and along the coiled capillary, for the corotating part; the waves interfere in the beam splitter in the optical case, in the Josephson weak link in the superfluid case. The interferometer shown in Fig. 32 is closer to a Mach-Zehnder interferometer than to a Sagnac one but the analogy goes along in the same way.

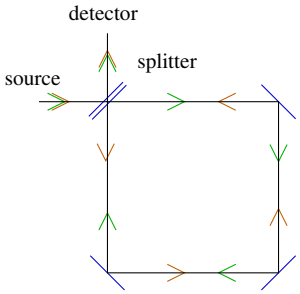

FIG. 33 (color online). Schematics of the optical Sagnac interferometer. A collimated beam from the source enters the interferometer through a beam splitter and is separated into two beams traveling along the optical path defined by the three mirrors in opposite directions, as indicated by the arrows. Reentering the beam splitter, they recombine and produce a fringe pattern on the detector plate.

But is this reasoning by analogy, or the display of clear fringe patterns such as those shown in Fig. 32, sufficient proof that the Sagnac effect is involved in the operation of these superfluid interferometers? Apparently not; superfluid gyros are still sometimes mistaken for purely inertial devices such as spinning tops, as discussed by Varoquaux and Varoquaux (2008). Clearly, the superfluid in a rotating bucket experiment is a dense medium. It can be weighed on a scale. For large enough rotation velocities, when enough vortex lines have been created, the fluid free surface eventually becomes concave, as in Newton's rotating water bucket experiment. For small velocities, however, things are different: the superfluid does not even start spinning because of the absence of viscosity. Hence the common sense reluctance to admit that the far-fetched analogy between the behavior of this condensed matter system and that of massless photons traveling at the velocity of light, or elementary particles like electrons or neutrons, or even confined ultracold atomic gases, holds.

A more formal approach is the following. As mentioned, the Sagnac effect has been observed in a number of different physical systems, ranging from photon, electron, neutron, and cold atomic gas interferometers to atomic clocks and the global positioning system.[110] The unifying concept behind these different situations is provided by the transportation of Einstein clocks from location A to location B on a rotating platform (Langevin, 1921, 1935, 1937; Rizzi and Ruggiero, 2003a, 2003b, 2004).

Consider how these clocks can be synchronized, first when they are infinitely close to one another. The space-time metric is characterized in the conventional notation by $-ds^2 = g_{00}d(x^0)^2 + 2g_{0i}dx^0dx^i + g_{ii}d(x^i)^2$. The infinitesimal time interval dt between two nearly simultaneous events

[109]See Aarts *et al.* (1994), Schwab, Davis, and Packard (1996), Schwab *et al.* (1996), and Sato and Packard (2012).

[110]The literature on the Sagnac effect is extremely vast. See Hasselbach and Niklaus (1993), Stedman (1997), and Neutze and Hasselbach (1998) for recent reviews on the effect with matter waves.

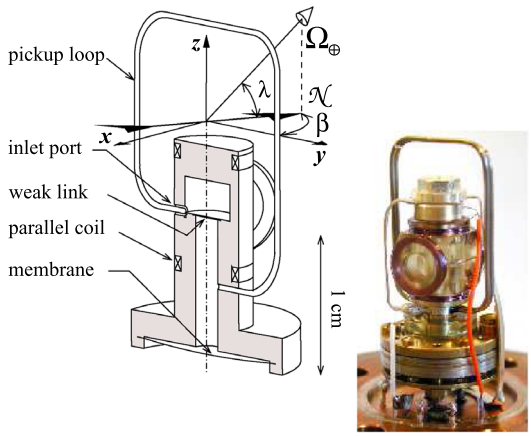

FIG. 34 (color online). Photograph and schematic view of the cell of Avenel, Mukharsky, and Varoquaux (2004), approximately to scale for the inner parts, except for the loop, which is made of two turns of 0.4 mm internal diameter capillary (only one turn is shown) with total area 5.90 ± 0.10 cm^2. The lower chamber of the resonator is a cylindrical duct, 1 mm in diameter, and connects the weak link to the flexible diaphragm (at the bottom) and to one end of the pickup loop (on the side); the upper chamber, a squat cylinder, is connected to the other end of the loop and to an inlet toward the main superfluid bath in which the resonator is immersed. Two pairs of coils produce fields parallel and perpendicular to the flow through the weak link to locally control the order parameter texture in ^{3}He. The cryostat is rotated about the vertical axis z by angle β from the north, shown by a compass needle; λ is the latitude, 48°43′ at Saclay. This cell has been used to detect the rotation of the Earth from a "blind" laboratory with a sensitivity of $5 \times 10^{-3}\Omega_\oplus$ Hz$^{-1/2}$.

taking place at this given location in space is such that $ds^2 = g_{00}d(x^0)^2 = -c^2dt^2$, with c being the velocity of light.

If the clocks are now separated in space by an infinitesimal amount dx^i and the two events taken, say at location A, as the ticking of clock A for one and as the signal transmitted by clock B of its ticking a small distance away for the second, the two ticks occur with a time lag given by $cdt = -g_{0i}dx^i/g_{00}$, the repeated summation being on the space coordinates.

If clock B is now transported over a finite path Γ closing on itself in a frame rotating with velocity Ω, the total time shift results from an integration along path Γ[111]:

$$\Delta t = \frac{1}{c}\oint_\Gamma \frac{g_{0i}dx^i}{-g_{00}} = \oint_\Gamma \frac{\Omega \times \mathbf{r} \cdot d\mathbf{r}}{c^2 - (\Omega \times \mathbf{r})^2} \simeq \frac{2}{c^2}\Omega \cdot \mathbf{S}, \tag{77}$$

with $\mathbf{S}$ being the vector area subtended by the loop Γ.

Time delay (77) between the reading of the clock standing still on the rotating platform and that of the transported clock lies at the root of the Sagnac effect. As it depends on the rotation velocity and the actual path Γ, absolute clock synchronization cannot be achieved. Sagnac corrections, Eq. (77), must be performed as done routinely for global positioning systems (Ashby, 2004).[112]

[111]As done in Landau and Lifshitz (1971), Sec. 90.

For helium, a Lorentz invariant two-fluid model can be built over the usual Landau superfluid hydrodynamics as done by Carter and Khalatnikov (1992) and Lebedev and Khalatnikov (1982).[113] The invariant velocity circulation, the generalization of Eq. (16), reads

$$\int_\Xi \{v'_0 dx^0 + v'_i dx^i\} = n\kappa, \tag{78}$$

where (v'_o, v'_i) is the four-velocity in the rotating frame $(c^2 + \mathbf{v}'_n \cdot \mathbf{v}'_s, -\mathbf{v}'_s)$. The normal fluid velocity v'_n and the superfluid velocity v'_s are very small compared to c so that the timelike component of the four-velocity reduces to c^2. The integration over Ξ is an actual loop integral only for the spacelike components. The corresponding world line is not closed because the time for synchronized clocks varies according to Eq. (77). Upon integration, Eq. (75) is recovered,

$$\oint_\Gamma v'_i dx^i = n\kappa + \int c^2 g_{0i}dx^i/g_{00} \simeq n\kappa - 2\Omega \cdot \mathbf{S}, \tag{79}$$

which establishes the link between superfluid physics and the relativistic clock approach: the true and honest Sagnac effect described by the transported clocks, Eq. (77), and the circulation quantization condition in the rotating frame leading to Eq. (76) are one and the same.[114]

Thus, Einstein-synchronized clocks provide the time standard by which phase differences can be kept track of all studied physical systems. As summarized by Greenberger (1983) for neutron interferometry experiments: "the phase shift (in the rotating interferometer) is seen to be caused by the different rates at which a clock ticks along each of the two beams." The rate at which that clock ticks for helium depends on the chemical potential μ, due to the molecular field of the condensate as shown by Beliaev, and on the Sagnac phase shift.

The helium Sagnac experiments illustrate the reality of matter wave interference in the superfluid helium, a substantially massive coherent field. Coherent means coherence of the quantum phase, giving a wavelike character to a bulky fluid.

B. Landau's two fluids, ODLRO, and macrorealism

Anderson's introductory words to the reprint of his 1966 paper in his book of 1994 are the following[115]: "I feel this is the clearest discussion of superfluidity available. Note that on many points this is contradictory or orthogonal to Landau orthodoxy as pronounced by Khalatnikov. Whether Landau would have agreed was never clarified because of his

[112]Note that this clock transportation experiment was actually performed by Hafele and Keating (1972) who boarded eastward and westward bound commercial jetliners taking as luggage a portable atomic clock.

[113]See Ho and Mermin (1980a).

[114]See Volovik (2003) for an alternate approach and Varoquaux and Varoquaux (2008) for additional references. Equation (11) in the latter reference is misprinted.

[115]See Anderson (1994), p. 165.

accident." This remark poses the problem of the complementarity between the two-fluid model, the description of Bose condensation by the nonvanishing off-diagonal terms of the density matrix over a long range, and the macroscopic wave function approach.

Two crucial aspects of Landau's legacy have been invoked here. The two-fluid model has ruled once and for all on the separation between normal fluid and superfluid components, for both the thermodynamics and the hydrodynamics. As used in this review in its reduced form for incompressible flows, which treats both components as independent, it has allowed one to basically disregard the normal component. There are obviously limits to this high-handed simplification, especially close to the λ point, but it has provided the backbone of the simplified vortex dynamics of Sec. II and subsequent sections on phase-slip processes. The second pillar of Landau's contributions to helium superflow is his criterion that many consider as the genuine *intrinsic* critical velocity in superfluids. This criterion rests on the existence of a sharply defined phonon-roton excitation spectrum, which allows for no low-lying elementary excitations as Landau implicitly postulated.

Landau's foreknowledge was soon put on firm ground by the work of Bogolyubov, Beliaev, Penrose, Onsager, and others. The formal description of the Bose condensate correlations ended up in the concept of off-diagonal long-range order (Yang, 1962) and a formal definition of the single wave function shared by the particles in the condensate. For not-too-complicated superfluids—^{4}He and the B phase of ^{3}He—this wave function, or order parameter, has a definite overall phase.

The role of this phase actually came to the fore when Anderson (1966a) gave it dynamical variable status and universal applicability. In the appendix of his paper, "ODLRO vs macroscopic particle fields," he states explicitly that "recognizing that in principle the relative phase of any two (superfluid) systems may always be measured by a Josephson-type experiment, one immediately has a usable local description" (of those systems).

This local description has been put to good use. It has opened the way to a full understanding of the interaction of quantized vortices and superflow, put on firm classical hydrodynamics footing by Huggins (1970). Sonin (1995) and others further expanded the vortex velocity field idea into a workable scheme for vortex dynamics. More importantly, it has bridged the gap between a predominantly "classical" two-fluid hydrodynamics and the more intimately quantum Josephson effects. The experimental observation of these effects, and, in particular, the detailed way by which dissipative phase slippage, understood first as the nucleation and propagation of vortices, evolves into the purest brand of Josephson hydrodynamics effects, for both ^{3}He and ^{4}He superfluids, has brought new ideas.

Detailed numerical simulations of vortex dynamics have been conducted by Schwarz and others,[116] in particular, for the problems of the vortex in an aperture, or trapped on a thin wire, or else, pinned. Collision between vortices, and the resulting reconnection, their multiplication by vortex mills churning out fresh quantized vorticity, the formation of vortex tangles, and the several ensuing critical velocities, are examples of the improved way of dealing with quantized vortices fostered one way or another by Anderson's considerations, which thus appear complementary to Landau's views. Experimental observations have fully borne out over the years this central concept of a macroscopic quantum phase governing the dynamical behavior of the superfluid.

But this holds for the phase in a single pool of superfluid only. The idea that a given pool, or bucket, or droplet, of superfluid has its own phase has become so common place that the question of knowing if the quantum phase of an isolated droplet of superfluid has a value of its own as compared to another one seems out of place. As stated by Anderson (1986): "Do superfluids that have never seen each other have a well-defined relative phase"?

Before answering by a qualified "yes," it may be useful to consider the new inputs to this problem of the meaning, or reality, of the phase in Bose condensates that have emerged after 1996 from investigations in ultracold atomic systems. This is not the topic of this review, but interference experiments with BEC gases do bear on some aspects of it.

A seemingly curious fact was noted by Javanainen and Yoo (1996) in their numerical simulations of the setting up of an interference pattern between two condensates formed in separate traps and left to overlap with one another.[117] The initial number of particles in each condensate is well defined in this computer experiment. The phases of the condensate wave functions are in no instance invoked in the number crunching sequence describing the interference process. Yet it does appear: the simple statistical count of bosons in separate bins suffices.

This finding is a manifestation for the special case of atoms in cold traps of the well-known tendency of bosons to "bunch" together. This phenomenon was illustrated by Castin and Dalibard (1997) who tackled the same problem analytically. Namely, they studied the evolution of the relative phase of two separate BE condensates of like species of atoms confined into separate traps and left at some instant to interact by leaking two small beams of atoms to a beam splitter. The two outgoing split beams that have been mixed are read by two atom counters.

Following Castin and Dalibard, consider first that only a single atom trap leaks atoms to the beam splitter. Assume the first counting event to occur in counter (+). The probability for this event to take place is $1/2$. Because of the Bose statistics, the next event has a probability $3/4$ to take place in counter (+), in which the first event was recorded, and $1/4$ for counter (−) that has not seen an atom yet (Feynman, Leighton, and Sands, 1965). Iterating for k such events in a row, Castin and Dalibard (1997) found that the probability that the k atoms end up registered by counter (+), and none by counter (−), takes the following form:

$$\mathcal{P}(k,0)=\frac{1}{2}\frac{3}{4}\cdots\frac{2k-1}{2k},$$

[116] See the contributions of D. C. Samuels, O. C. Idowu *et al.*, and M. Tsubota, T. Araki, and S. K. Nemirovskii in Barenghi, Donnelly, and Vinen (2001).

[117] Such an experiment was successfully performed soon after by Andrews *et al.* (1997) and others.

which is quite different from the probability of the same final outcome for atoms with no quantum-statistical correlations, namely, $1/2^k$. The latter becomes rapidly negligible for $k \gg 1$ while the former decreases only as $k^{-1/2}$. Bosons have a strong tendency to crop or bunch together in states where they can find like bosons.

Castin and Dalibard (1997) proceeded to study the case in which the two separate BE condensates are now leaking beams to the beam splitter. If the two incident beams are described by fields with well-defined phases and identical amplitudes, $|\psi_0|e^{i\varphi_A}$ and $|\psi_0|e^{i\varphi_B}$, the mean intensities in the (+) and (−) output channels of the beam splitter are given by

$$I_+ = 2|\psi_0|^2\cos^2(\delta\varphi/2) \quad \text{and} \quad I_- = 2|\psi_0|^2\sin^2(\delta\varphi/2) \tag{80}$$

with $\delta\varphi = \varphi_B - \varphi_A$. This matter wave interferometry measurement allows as expected the determination of the phase difference between the two condensates.

What happens now if the phases are not ascribed to the condensates but instead their particle numbers N_A and N_B are? Assuming $N_B = N_A$ for simplicity [as in the simulations of Javanainen and Yoo (1996)] the two-condensate system is now described by a Fock state $\langle N_A|, |N_A\rangle$. Performing the same interferometry measurement by counting atoms in the (+) and (−) counters should end up yielding result (80). It does, but the interesting thing is how a phase difference arises from the mere statistical count.

The detailed probability $\mathcal{P}(k_+, k_-)$ of counting k_+ events in counter (+) and k_- in counter (−) has been worked out analytically by Castin and Dalibard (1997). The beat pattern given by Eq. (80) is found to emerge gradually from the successive counting events in the (+) and (−) counters. The phase difference can be obtained from the tallied quantities k_+ and k_-: $\delta\varphi \simeq \arctan(\sqrt{k_-/k_+})$. The particlelike description turns into the wavelike description as the counting proceeds. The sequence of measurements brings a definite quantum phase to states for which none had been assumed to start with: In the end, one is left with a state containing $2N_A - k$ atoms and a phase difference known to an accuracy of order $1/k$.

The phase difference is an unpredictable random variable, which takes a different value for any realization of the counting experiment. It appears as a mere by-product of the counting statistics. No direct interaction between the atoms in the condensates has been assumed at any point. The BEC gases are taken as perfect gases. The effect purely originates from the quantum statistics of bosons. As concluded by Castin and Dalibard, "the notion of phase-broken symmetry is therefore not indispensable in order to understand the beating of two condensates."

This conclusion, which has gained wide acceptance,[118] has been illustrated by the experiments of Saba *et al.* (2005). They dropped two condensates of like species out of their traps and, during the course of their free fall and expansion, gently pushed with laser beams a few atoms from one to the other. They dutifully observed the continuous emergence of a fringe pattern in a quintessential form, without beam splitters and interferometers nor destruction of the condensate clouds, thus realizing a nearly noninvasive measurement of their relative phase.

These cold atom gases constitute model systems. They can be studied to their minutest details starting from the basic principles of quantum mechanics. Photons in cavities provide another such instance. Quantum-statistical correlations between indistinguishable bosons play the leading role. Particle interactions play a minor role of decoherence and are neglected. Particle-wave duality is demonstrated to near perfection.

Superfluids differ in a number of respects. The macroscopic wave function introduced by Anderson is defined on the premise that the particle number N and its possible variation δN are sufficiently large so that the uncertainty in φ, expressed by Eq. (11), $\delta N\delta\varphi \sim 1$, is small in most instances. It is then neglected and the operators $\hat{N}$ and $\hat{\varphi}$ are "projected" onto c numbers. They have acquired a value once and for all: the phase is forced to "exist" even if its actual value is not determined by the same token and its absolute meaning uncertain.

The introduction of the superfluid phase resembles a leap of faith: it is there because it is needed to reproduce the hydrodynamics. Leggett and Sols (1991) and Leggett (1995) paid careful attention to this problem of the "existence" of the phase. One of the many points raised by them is that, in order to attribute a well-defined meaning to an *absolute* phase, one has first to consider the *relative* phase of one bucket of superfluid with respect to another—presumably measured by performing a Josephson experiment. The various ways and constraints of such an experiment have been expounded in the previous sections: the "relative" phase between two weakly connected superfluid systems (1) and (2) $\delta\varphi_{12} = \varphi_2 - \varphi_1$ can be measured and indeed possesses a well-defined meaning. Suppose now that systems (1) and (2) are separated and a third system brought in. System (3) can be compared to (1), with the result $\delta\varphi_{13} = \varphi_3 - \varphi_1$: is it possible to infer that the phase difference between (2) and (3) is $\varphi_3 - \varphi_2 = \delta\varphi_{13} - \delta\varphi_{12}$? If yes, then phases can be referred to a "standard" and acquire absolute meaning.

The not-so-trivial answer given by Leggett (1995) is "no" if the systems are left to settle to equilibrium with the environment and the two Josephson phase measurements are independent, but "yes" if they are done simultaneously. In other words, maintaining a superfluid phase standard across the various standards laboratories of the planet would require connecting them with a continuous superfluid duct. The phase information would have to be tapped from this standard at the same time and place, or else a host of corrections, such as that for local gravity or for the Sagnac effect (the synchronization of the Einstein clocks) would have to be performed. If the phase readings are not simultaneous, the correlation between phase measurements for systems (1) and (2) and then (1) and (3) is upset by the sole act of measuring, with a part played by the environment; decoherence takes its toll and phases ultimately randomize (Sols, 1994; Zapata, Sols, and Leggett, 2003).

The situation in simple superfluids such as ^{4}He and ^{3}He-B, in which macroscopic coherence holds over lengths of meters and more, and in which the Planck constant hides at the

[118] See Horak and Barnett (1999) and Nienhuis (2001).

nanometric scale provides a quite extreme example of macroscopic matter field. The fact that the macroscopic field $\Phi(\mathbf{r})$ standing as the single-particle wave function for condensate atoms possesses quantum properties is indisputable—the quantization of velocity circulation and the existence of persistent currents offer concrete examples. However, the sort of coherence shown by ultracold atom condensates does not stand out readily for dense superfluids. The description of the superfluid dynamics in terms of the conjugate variables N and φ belongs more to thermodynamics than to quantum mechanics. The correlation between atoms in the dense helium fluid relies more on their hard-core repulsion than on their Bose statistics.

Yet the quantum interferences by quantum tunneling between macroscopically distinct states in superfluid Josephson junctions, the quantum nucleation of vortices clearly reveals the importance of the latter. In these situations, the coarse-grained average fails and some other procedure, more in line with the basic rules of quantum mechanics, and, in particular, the principle of superposition, is in order. Would it be possible to envision experiments showing actual macroscopic quantum *coherence* as discussed by Leggett (1980, 2002) and Annett (2003)? The superfluid quantum phase would then gain a dual acceptance, actual coherence in the superposition of different states on a very small scale, on the one hand, and, on the other hand, the "rigidity," in the language of F. London, of the velocity potential of the ideal Euler fluid and the quantizsation of the velocity circulation.

The above remarks bring this "essay on criticism" of Anderson's Considerations to a close. At this stage, but one hard conclusion can be drawn: many offshoots have already sprung but more are to grow.

ACKNOWLEDGMENTS

This work has been supported by the Centre National de la Recherche Scientifique and by the Commissariat à l'Énergie Atomique et aux Énergies Alternatives. I owe much to my many colleagues, especially Olivier Avenel and Yuri Mukharsky, who have brought vital contributions to many of the topics discussed in this review.

APPENDIX

What needs to be shown is that the second term on the right-hand side of Eq. (41) corresponds to the variation of the vortex loop self-energy for the infinitesimal deformation $\mathbf{s}(l)$ into $\mathbf{s}(l)+\boldsymbol{\varepsilon}\delta(l-l_0)$. This energy variation can be derived from the functional derivative of $E_v[\mathbf{s}]$, given by Eq. (23), with respect to the deformation $\delta\mathbf{s}$:

$$\left.\frac{\delta E[\mathbf{s}]}{\delta \mathbf{s}}\right|_{l_0} = \frac{\rho_s\kappa_4^2}{8\pi}\left\{-\oint \frac{d\mathbf{s}(l_0)}{dl_0}\cdot\frac{d\mathbf{s}(l_2)}{dl_2}\frac{\mathbf{s}(l_0)-\mathbf{s}(l_2)}{|\mathbf{s}(l_0)-\mathbf{s}(l_2)|^3}dl_2 + \lim_{\varepsilon\to 0}\oint\oint \boldsymbol{\varepsilon}\cdot\frac{d\mathbf{s}(l_2)}{dl_2}\delta'(l_1-l_0)\frac{dl_1dl_2}{|\mathbf{s}(l_1)-\mathbf{s}(l_2)|} + l_1 \Leftrightarrow l_2\right\}. \tag{A1}$$

The first term on the right-hand side of Eq. (A1) results from the differentiation of $1/|\mathbf{s}(l_1)-\mathbf{s}(l_2)|$ with respect to l_1 and integration over the Dirac function representing the deformation at $l_1=l_0$. The integral over the derivative of the Dirac δ function, which comes from the differentiation of $d\mathbf{s}(l_1)/dl_1$, yields the derivative of the integrand evaluated at l_0. The contribution of the integration over l_2 over the same contour with the same deformation is equal to that over l_1, expressed by the first two terms on the right-hand side of Eq. (A1), and yields a factor of 2 in the final result.

Using the notation $\hat{\mathbf{t}}(l)=d\mathbf{s}(l)/dl$ for the unit vector tangent to the vortex loop at location $\mathbf{s}(l)$, Eq. (A1) can be written as

$$\begin{aligned}\left.\frac{\delta E[\mathbf{s}]}{\delta \mathbf{s}}\right|_{l_0} &= \frac{\rho_s\kappa_4^2}{4\pi}\oint\left\{\hat{\mathbf{t}}(l_0)\cdot\frac{\mathbf{s}(l_0)-\mathbf{s}(l_2)}{|\mathbf{s}(l_0)-\mathbf{s}(l_2)|^3}\hat{\mathbf{t}}(l_2) - \hat{\mathbf{t}}(l_0)\cdot\hat{\mathbf{t}}(l_2)\frac{\mathbf{s}(l_0)-\mathbf{s}(l_2)}{|\mathbf{s}(l_0)-\mathbf{s}(l_2)|^3}\right\}dl_2 \\ &= \frac{\rho_s\kappa_4^2}{4\pi}\hat{\mathbf{t}}(l_0)\times\oint\hat{\mathbf{t}}(l_2)\times\frac{\mathbf{s}(l_0)-\mathbf{s}(l_2)}{|\mathbf{s}(l_0)-\mathbf{s}(l_2)|^3}dl_2 \\ &= \rho_s\kappa_4\hat{\mathbf{t}}(l_0)\times\mathbf{v}_v(l_0).\end{aligned} \tag{A2}$$

The double cross product in the second equality of Eq. (A2) appears because of the vector relation $(\mathbf{a}\cdot\mathbf{c})\mathbf{b}-(\mathbf{a}\cdot\mathbf{b})\mathbf{c}=\mathbf{a}\times(\mathbf{b}\times\mathbf{c})$. The last equality is obtained using the Biot-Savart law, Eq. (19), for $\mathbf{v}_v$ the velocity induced by the vortex loop on itself at l_0. The logarithmic divergences for $l_0=l_2$ are cut off at the core radius a_0.[119] The change of the vortex self-energy is then expressed by

$$\begin{aligned}\Delta E_v &= \int_l^{l+\Delta l}\oint_{\text{loop}}\left.\frac{\delta E[\mathbf{s}]}{\delta\mathbf{s}}\right|_{l_0}\cdot\delta\mathbf{x}\delta(l-l_0)dldl_0 \\ &= \int_l^{l+\Delta l}\rho_s\kappa_4\hat{\mathbf{t}}(l_0)\times\mathbf{v}_v\cdot\mathbf{v}_p\Delta t dl_0.\end{aligned}$$

Assuming the integrand constant over the small element $\Delta\mathbf{l}$, Eq. (43) ensues.

[120]Compare with Eqs. (3.7) and (3.15) in Sonin's paper (1987).

REFERENCES

Aarts, R., G. G. Ihas, O. Avenel, and E. Varoquaux, 1994, Physica B (Amsterdam) **194–196**, 493.

Abrikosov, A. A., L. P. Gorkov, and I. E. Dzyaloshinski, 1961, *Methods of Quantum Field Theory in Statistical Physics* (Prentice-Hall, Inc., Englewood Cliffs, NJ), Chap. 5.

Adams, P., M. Cieplak, and W. I. Glaberson, 1985, Phys. Rev. B **32**, 171.

Alpar, M. A., R. Nandkumar, and D. Pines, 1985, Astrophys. J. **288**, 191.

Amar, A., J. C. Davis, R. E. Packard, and R. L. Lozes, 1990, Physica B (Amsterdam) **165–166**, 753.

Amar, A., Y. Sasaki, R. Lozes, J. C. Davis, and R. E. Packard, 1992, Phys. Rev. Lett. **68**, 2624.

Anderson, B. J., B. P. Beecken, and W. Zimmermann, Jr., 1984, in *Proceedings of the Seventeenth International Conference on Low Temperature Physics*, edited by U. Eckern, A. Schmid, W. Weber, and H. Wühl (North-Holland, Amsterdam), Pt. I, p. 313.

Anderson, P. W., 1964, in *Lectures in the Many-Body Problem*, edited by E. Caianello (Academic Press, New York), p. 113.
Anderson, P. W., 1965, in *Some Recent Definitions in the Basic Sciences*, Vol. 2, edited by A. Gelbert (Belfert Graduate School of Science, Yeshiva University, New York), p. 21, reprinted in Anderson (1984).
Anderson, P. W., 1966a, Rev. Mod. Phys. **38**, 298.
Anderson, P. W., 1966b, in *Quantum Fluids*, edited by D. Brewer (North-Holland, Amsterdam), p. 146.
Anderson, P. W., 1984, *Basic Notions of Condensed Matter* (Benjamin/Cummings, Menlo Park, CA).
Anderson, P. W., 1986, in *The Lesson of Quantum Theory*, edited by J. de Boer, E. Dahl, and O. Ulfbeck (Elsevier, New York).
Anderson, P. W., 1994, *A Career in Theoretical Physics* (World Scientific, Singapore).
Anderson, P. W., and W. Brinkman, 1975, in *The Helium Liquids*, edited by J. Armitage and I. Farquhar (Academic Press, London), p. 315.
Anderson, P. W., and P. L. Richards, 1975, Phys. Rev. B **11**, 2702.
Anderson, P. W., and J. M. Rowell, 1963, Phys. Rev. Lett. **10**, 230.
Anderson, P. W., and G. Toulouse, 1977, Phys. Rev. Lett. **38**, 508.
Andreev, A., and L. Melnikovsky, 2004, J. Low Temp. Phys. **135**, 411.
Andrews, M. R., C. G. Townsend, H.-J. Miesner, D. S. Durfee, D. M. Kurn, and W. Ketterle, 1997, Science **275**, 637.
Andronikashvili, E., and Y. Mamaladze, 1966, Rev. Mod. Phys. **38**, 567; **39**, 494(E) (1967).
Annett, J. F., 2003, *Superconductivity, Superfluids and Condensates* (Oxford University Press, New York), Chap. 3.
Asano, Y., 2001, Phys. Rev. B **64**, 224515.
Ashby, N., 2004, *Relativity in Rotating Frames*, Chap. 1, edited by Guido Rizzi and Matteo Ruggiero (Kluwer Academic Publishers, Dordrecht, The Netherlands).
Avenel, O., R. Aarts, G. G. Ihas, and E. Varoquaux, 1994, Physica B (Amsterdam) **194–196**, 491.
Avenel, O., M. Bernard, S. Burkhart, and E. Varoquaux, 1995, Physica B (Amsterdam) **210**, 215.
Avenel, O., P. Hakonen, and E. Varoquaux, 1997, Phys. Rev. Lett. **78**, 3602.
Avenel, O., P. Hakonen, and E. Varoquaux, 1998, J. Low Temp. Phys. **110**, 709.
Avenel, O., G. Ihas, and E. Varoquaux, 1993, J. Low Temp. Phys. **93**, 1031.
Avenel, O., Y. Mukharsky, and E. Varoquaux, 1999, Nature (London) **397**, 484.
Avenel, O., Y. Mukharsky, and E. Varoquaux, 2000, Physica B (Amsterdam) **280**, 130.
Avenel, O., Y. Mukharsky, and E. Varoquaux, 2004, J. Low Temp. Phys. **135**, 745.
Avenel, O., and E. Varoquaux, 1985, Phys. Rev. Lett. **55**, 2704.
Avenel, O., and E. Varoquaux, 1986a, *Proc. ICEC 11, Berlin—1986* (Butterworths, Guilford), p. 587.
Avenel, O., and E. Varoquaux, 1986b, Phys. Rev. Lett. **57**, 921.
Avenel, O., and E. Varoquaux, 1987, Jpn. J. Appl. Phys. **26**, 1798.
Avenel, O., and E. Varoquaux, 1988, Phys. Rev. Lett. **60**, 416.
Avenel, O., and E. Varoquaux, 1989, in *Quantum Fluids and Solids—1989*, edited by G. Ihas and Y. Takano (American Institute of Physics, New York), p. 3.
Avenel, O., and E. Varoquaux, 1996, Czech. J. Phys. **46**, 3319, Issue 6.
Awschalom, D., and K. W. Schwarz, 1984, Phys. Rev. Lett. **52**, 49.
Backhaus, S., S. Pereverzev, R. W. Simmonds, A. Loshak, J. C. Davis, and R. E. Packard, 1998, Nature (London) **392**, 687.
Backhaus, S., S. V. Pereverzev, A. Loshak, J. C. Davis, and R. E. Packard, 1997, Science **278**, 1435.
Barenghi, C., R. Donnelly, and W. Vinen, 2001, Eds., *Quantized Vortex Dynamics and Superfluid Turbulence*, Vol. 571, Lecture Notes in Physics (Springer-Verlag, Berlin).
Bäuerle, C., Y. B. S. Fisher, and H. Godfrin, 2000, *Topological Defects and the Non-equilibrium Dynamics of Symmetry-breaking Phase Transitions* (Kluwer Academic Publishers, Dordrecht), p. 105.
Baym, G., 1969, *Mathematical Methods in Solid State and Superfluid Theory*, Chap. 3, edited by R. C. Clark and G. H. Derrick (Oliver and Boyd Ltd, Edinburgh), p. 134.
Baym, G., and E. Chandler, 1983, J. Low Temp. Phys. **50**, 57.
Beecken, B. P., and W. Zimmermann, Jr., 1987a, Phys. Rev. B **35**, 74.
Beecken, B. P., and W. Zimmermann, Jr., 1987b, Phys. Rev. B **35**, 1630.
Beliaev, S. T., 1958, J. Exp. Theor. Phys. **34**, 417 [Sov. Phys. JETP **7**, 289 (1958)].
Berloff, N. G., and P. H. Roberts, 2001, in *Quantized Vortex Dynamics and Superfluid Turbulence*, edited by C. Barenghi, R. Donnelly, and W. Vinen, Lecture Notes in Physics, Vol. 571 (Springer-Verlag, Berlin), p. 268.
Bogolyubov, N. N., 1947, J. Phys. USSR **11**, 23.
Bonaldi, M., S. Vitale, and M. Cerdonio, 1990, Phys. Rev. B **42**, 9865.
Bowley, R., A. Kirk, and P. King, 1992, J. Low Temp. Phys. **88**, 73.
Bunkov, Y. M., 2010, J. Low Temp. Phys. **158**, 118.
Burkhart, S., 1995, Ph.D. thesis (Université Paris-Sud).
Burkhart, S., M. Bernard, O. Avenel, and E. Varoquaux, 1994, Phys. Rev. Lett. **72**, 380.
Caldeira, A., and A. Leggett, 1983, Ann. Phys. (N.Y.) **149**, 374; **153**, 445(E) (1984).
Carey, R., B. S. Chandrasekhar, and A. J. Dahm, 1973, Phys. Rev. Lett. **31**, 873.
Carter, B., and I. Khalatnikov, 1992, Phys. Rev. D **45**, 4536.
Castin, Y., and J. Dalibard, 1997, Phys. Rev. A **55**, 4330.
Cerdonio, M., and S. Vitale, 1984, Phys. Rev. B **29**, 481.
Chui, T., W. Holmes, and K. Penanen, 2003, Phys. Rev. Lett. **90**, 085301.
Chui, T., and K. Penanen, 2005, Phys. Rev. B **71**, 132509.
Cohen-Tannoudji, C., and C. Robilliard, 2001, C. R. Acad. Sci. Paris **2** (Série IV), 445.
Coleman, S., 1977, Phys. Rev. D **15**, 2929.
Crooker, B., 1984, Ph.D. thesis (Cornell University).
Cross, M. C., 1983, in *Quantum Fluids and Solids—1983*, edited by E. D. Adams and G. G. Ihas (American Institute of Physics, New York).
Cross, M., 1974, Phys. Rev. A **10**, 1442.
Dalfovo, F., 1992, Phys. Rev. B **46**, 5482.
Dalfovo, F., S. Giorgini, L. P. Pitaevskii, and S. Stringari, 1999, Rev. Mod. Phys. **71**, 463.
Davis, J. C., J. D. Close, R. Zieve, and R. E. Packard, 1991, Phys. Rev. Lett. **66**, 329.
Davis, J. C., and R. E. Packard, 2002, Rev. Mod. Phys. **74**, 741.
Deaver, B. S., and J. M. Pierce, 1972, Phys. Lett. **38A**, 81.
Dobbs, E., 2000, *Helium Three* (Oxford University Press, New York), Sec. 27.3, and references therein.
Donev, L. A. K., L. Hough, and R. J. Zieve, 2001, Phys. Rev. B **64**, 180512.
Donnelly, J., 1991, *Quantized Vortices in Helium* (Cambridge University Press, Cambridge, England).
Duan, J.-M., 1994, Phys. Rev. B **49**, 12381.

Duan, J.-M., and A. Leggett, 1992, Phys. Rev. Lett. **68**, 1216.
Eckart, C., 1938, Phys. Rev. **54**, 920.
Ellis, F. M., and L. Li, 1993, Phys. Rev. Lett. **71**, 1577.
Eltsov, V., M. Krusius, and G. Volovik, 2005, in *Progress in Low Temperature Physics*, Vol. XV, edited by W. Halperin, Chap. 1 (Elsevier, New York), p. 1.
Eltsov, V. B., T. W. B. Kibble, M. Krusius, V. M. H. Ruutu, and G. E. Volovik, 2000, Phys. Rev. Lett. **85**, 4739.
Enz, C. P., 1974, Rev. Mod. Phys. **46**, 705.
Eska, G., S. Gladchenko, and S. V. Pereverzev, 2010, Europhys. Lett. **89**, 26009.
Essèn, H., and M. C. N. Fiolhais, 2012, Am. J. Phys. **80**, 164.
Fetter, A., 1965, Phys. Rev. **138**, A429.
Fetter, A., 1972, Phys. Rev. A **6**, 402.
Fetter, A., and S. Ullah, 1988, J. Low Temp. Phys. **70**, 515.
Fetter, A. L., 1976, in *The Physics of Liquid and Solid Helium—Part 1*, Chap. 3, edited by K. H. Benneman and J. B. Ketterson (Wiley-Interscience, New York), p. 238.
Feynman, R., 1955, in *Progress in Low Temperature Physics*, Vol. I, Chap. II, edited by C. J. Gorter (North-Holland, Amsterdam), p. 17;
Feynman, R., 1972, *Statistical Mechanics* (Benjamin/Cummings, Reading, MS), Chap. 11.
Feynman, R., R. Leighton, and M. Sands, 1965, *The Feynman Lectures on Physics: Quantum Mechanics* (Addison-Wesley, Reading, MA), Vol. III, Sec. 4.3.
Feynman, R. P., 1953a, Phys. Rev. **91**, 1291.
Feynman, R. P., 1953b, Phys. Rev. **91**, 1301.
Feynman, R. P., 1954, Phys. Rev. **94**, 262.
Finne, A. P., V. B. Eltsov, R. Hänninen, N. B. K. J. Kopu, M. Krusius, M. Tsubota, and G. E. Volovik, 2006, Rep. Prog. Phys. **69**, 3157.
Fischer, U. R., 2000, Ann. Phys. (Berlin) **9**, 523.
Flaten, J., C. T. Borden, C. Lindensmith, and W. Zimmermann, Jr., 2006, J. Low Temp. Phys. **142**, 753.
Flaten, J., C. Lindensmith, and W. Zimmermann, Jr., 2006, J. Low Temp. Phys. **142**, 725.
Frisch, T., Y. Pomeau, and S. Rica, 1992, Phys. Rev. Lett. **69**, 1644.
Gammel, P. L., T.-L. Ho, and J. D. Reppy, 1985, Phys. Rev. Lett. **55**, 2708.
Gamota, G., 1973, Phys. Rev. Lett. **31**, 517.
Gamota, G., 1974, Phys. Rev. Lett. **33**, 1428.
Glaberson, W., and R. Donnelly, 1966, Phys. Rev. **141**, 208.
Glaberson, W., and R. Donnelly, 1986, in *Progress in Low Temperature Physics*, edited by D. F. Brewer (Elsevier Science, Amsterdam), Vol. IX, Chap. 1.
Glyde, H., 1993, J. Low Temp. Phys. **93**, 861.
Glyde, H., 2013, J. Low Temp. Phys. **172**, 364.
Golubov, A. A., M. Y. Kupriyanov, and E. Il'ichev, 2004, Rev. Mod. Phys. **76**, 411.
Grabert, H., 1988, Phys. Rev. Lett. **61**, 1683.
Grabert, H., P. Olschowski, and U. Weiss, 1987, Phys. Rev. B **36**, 1931.
Greenberger, D., 1983, Rev. Mod. Phys. **55**, 875.
Gregory, D., 1972, Ph.D. thesis (University of California—San Diego), unpublished.
Greiter, M., 2005, Ann. Phys. (Amsterdam) **319**, 217.
Griffin, A., 1987, Can. J. Phys. **65**, 1368.
Griffin, A., 1993, *Excitations in a Bose-Condensed Liquid* (Cambridge University Press, Cambridge, England).
Griffin, A., 1999, "Bose-Einstein condensation in atomic gases," arXiv:cond-mat/9901123.
Gross, E., 1961, Nuovo Cimento **20**, 454.
Guernsey, R., 1971, in *Proceedings of the 12th International Conference on Low Temperature Physics*, edited by E. Kanda (Keigahn, Tokyo), p. 79.
Hafele, J. C., and R. E. Keating, 1972, Science **177**, 168.
Hakonen, P., O. Avenel, and E. Varoquaux, 1998, Phys. Rev. Lett. **81**, 3451.
Hakonen, P., K. Nummila, J. Simola, L. Skrbek, and G. Mamniashvili, 1987, Phys. Rev. Lett. **58**, 678.
Hall, H., 1960, Adv. Phys. **9**, 89.
Hall, H., and J. Hook, 1986, in *Progress in Low Temperature Physics*, Vol. IX, edited by D. Brewer (North-Holland, Amsterdam), p. 143.
Halperin, B. I., P. C. Hohenberg, and E. D. Siggia, 1976, Phys. Rev. B **13**, 1299.
Hänggi, P., P. Talkner, and M. Borkovec, 1990, Rev. Mod. Phys. **62**, 251.
Hasselbach, F., and M. Niklaus, 1993, Phys. Rev. A **48**, 143.
Heitler, W., 1954, *The Quantum Theory of Radiation* (Oxford University Press, Oxford), Chap. II, Sec. 7.
Hendry, P., N. Lawson, P. McClintock, C. Williams, and R. Bowley, 1988, Phys. Rev. Lett. **60**, 604.
Hess, G., 1977, Phys. Rev. B **15**, 5204.
Hess, G., 1992, Nature (London) **359**, 192.
Ho, T.-L., 1978, Phys. Rev. B **18**, 1144.
Ho, T.-L., and N. D. Mermin, 1980a, Phys. Rev. B **21**, 5190.
Ho, T. L., and N. D. Mermin, 1980b, Phys. Rev. Lett. **44**, 330.
Hohenberg, P. C., and B. I. Halperin, 1977, Rev. Mod. Phys. **49**, 435.
Hook, J. R., 1987, Jpn. J. Appl. Phys. **26**, 159.
Horak, P., and S. M. Barnett, 1999, J. Phys. B **32**, 3421.
Hoskinson, E., Y. Sato, I. Hahn, and R. E. Packard, 2006, Nat. Phys. **2**, 23.
Hoskinson, E., Y. Sato, and R. Packard, 2006, Phys. Rev. B **74**, 100509.
Huggins, E. R., 1970, Phys. Rev. A **1**, 332.
Hulin, J., D. D'Humières, B. Perrin, and A. Libchaber, 1974, Phys. Rev. A **9**, 885.
Hulin, J., C. Laroche, A. Libchaber, and B. Perrin, 1972, Phys. Rev. A **5**, 1830.
Hulin, J., B. Perrin, C. Laroche, and A. Libchaber, 1971, in *Proceedings of the 12th International Conference on Low Temperature Physics*, edited by E. Kanda (Keigahn, Tokyo), p. 83.
Idowu, O. C., D. Kivotides, C. F. Barenghi, and D. C. Samuels, 2000, J. Low Temp. Phys. **120**, 269.
Idowu, O. C., A. Willis, C. F. Barenghi, and D. C. Samuels, 2000, Phys. Rev. B **62**, 3409.
Ihas, G., O. Avenel, R. Aarts, R. Salmelin, and E. Varoquaux, 1992, Phys. Rev. Lett. **69**, 327.
Javanainen, J., and S. M. Yoo, 1996, Phys. Rev. Lett. **76**, 161.
Josephson, B., 1962, Phys. Lett. **1**, 251.
Josephson, B., 1965, Adv. Phys. **14**, 419.
Josephson, B. D., 1964, Rev. Mod. Phys. **36**, 216.
Josephson, B. D., 1966, Phys. Lett. **21**, 608.
Josserand, C., and Y. Pomeau, 1995, Europhys. Lett. **30**, 43.
Josserand, C., Y. Pomeau, and S. Rica, 1995, Phys. Rev. Lett. **75**, 3150.
Kadanoff, L. P., 2013, J. Stat. Phys. **152**, 805.
Karn, P. W., D. R. Starks, and J. W. Zimmermann, 1980, Phys. Rev. B **21**, 1797.
Khalatnikov, I., 1965, *An Introduction to the Theory of Superfluidity* (W. A. Benjamin, New York).
Khorana, B. M., 1969, Phys. Rev. **185**, 299.

Khorana, B. M., and B. S. Chandrasekhar, 1967, Phys. Rev. Lett. **18**, 230.
Kopnin, N., 1978, Pis'ma Zh. Eksp. Teor. Fiz. **27**, 417 [JETP Lett. **27**, 390 (1978)].
Kopnin, N., 1986, Pis'ma Zh. Eksp. Teor. Fiz. **43**, 541 [JETP Lett. **43**, 700 (1986)].
Kopnin, N., 1995, Physica B (Amsterdam) **210**, 267.
Kopnin, N., and M. Salomaa, 1990, Phys. Rev. B **41**, 2601.
Kopnin, N., P. Soininen, and M. Salomaa, 1991, Physica B (Amsterdam) **169**, 535.
Kopnin, N., P. Soininen, and M. Salomaa, 1992, Phys. Rev. B **45**, 5491.
Kramers, H., 1940, Physica (Utrecht) **7**, 284.
Krusius, M., J. Korhonen, Y. Kondo, and E. Sonin, 1993, Phys. Rev. B **47**, 15113.
Kurkijärvi, J., 1988, Phys. Rev. B **38**, 11184.
Lamb, S. H., 1945, *Hydrodynamics* (Cambridge University Press, Cambridge, England).
Landau, L., 1941, Zh. Eksp. Teor. Fiz. **11**, 592 [J. Phys. USSR **5**, 71 (1941)].
Landau, L., 1947, J. Phys. USSR **11**, 91.
Landau, L., and E. Lifshitz, 1958, *Quantum Mechanics* (Pergamon Press, Oxford).
Landau, L., and E. Lifshitz, 1959, *Fluid Mechanics* (Pergamon Press, Oxford).
Landau, L., and E. Lifshitz, 1971, *Classical Theory of Fields* (Pergamon Press, Oxford), Sec. 89.
Langer, J., 1968, Phys. Rev. **167**, 183.
Langer, J., and M. Fisher, 1967, Phys. Rev. Lett. **19**, 560.
Langer, J., and J. Reppy, 1970, in *Progress in Low Temperature Physics*, edited by C. J. Gorter (North-Holland, Amsterdam), Vol. 6, Chap. 1, p. 1.
Langevin, P., 1921, C.R. Acad. Sci. (Paris) **173**, 831 (in French).
Langevin, P., 1935, C.R. Acad. Sci. (Paris) **200**, 48 (in French).
Langevin, P., 1937, C.R. Acad. Sci. (Paris) **205**, 304 (in French) [http://gallica.bnf.fr].
Langlois, D., 2000, "Superfluidity in relativistic neutron starts," arXiv:astro-ph/0008161.
Larkin, A., K. Likharev, and Y. Ovchinnikov, 1984, Physica B+C (Amsterdam) **126**, 414.
Lebedev, V. V., and I. M. Khalatnikov, 1982, Zh. Eksp. Teor. Fiz., **56**, 1601 Sov. Phys. JETP **56**, 923 (1982)].
Lee, D. M., and R. C. Richardson, 1978, in *Physics of Liquid and Solid Helium*, edited by K. H. Bennemann and J. B. Ketterson (Wiley, New York), Pt. II, p. 287.
Leggett, A. J., 1975, Rev. Mod. Phys. **47**, 331; **48**, 357(E) (1976).
Leggett, A. J., 1980, Prog. Theor. Phys. Suppl. **69**, 80.
Leggett, A. J., 1995, in *Bose Einstein Condensation*, edited by A. Griffin, D. W. Snoke, and S. Stringari, Chap. 19 (Cambridge University Press, Cambridge, England).
Leggett, A. J., 2002, J. Phys. Condens. Matter **14**, R415.
Leggett, A. J., and F. Sols, 1991, Found. Phys. **21**, 353.
Leiderer, P., and F. Pobell, 1973, Phys. Rev. A **7**, 1130.
Li, Y.-H., and T.-L. Ho, 1988, Phys. Rev. B **38**, 2362.
Lifshitz, E. M., and L. P. Pitaevskii, 1980, *Statistical Physics Part 2* (Pergamon, Oxford), Sec. 24, p. 93.
Likharev, K. K., 1979, Rev. Mod. Phys. **51**, 101.
Likharev, K. K., 1986, *Dynamics of Josephson Junctions and Circuits* (Gordon and Breach, New York).
London, F., 1938, Nature (London) **141**, 643.
London, F., 1954, *Superfluids*, Vol. II (John Wiley, New York), reprinted by Dover Publications.
Lounasmaa, O. V., M. T. Manninen, S. A. Nenonen, J. P. Pekola, R. G. Sharma, and M. S. Tagirov, 1983, Phys. Rev. B **28**, 6536.
Madison, K. W., F. Chevy, V. Bretin, and J. Dalibard, 2001, Phys. Rev. Lett. **86**, 4443.
Manninen, M., and J. Pekola, 1983, J. Low Temp. Phys. **52**, 497.
Marchenkov, A., R. W. Simmonds, S. Backhaus, A. Loshak, J. C. Davis, and R. E. Packard, 1999, Phys. Rev. Lett. **83**, 3860.
Martinis, J., and H. Grabert, 1988, Phys. Rev. B **38**, 2371.
Martinis, J. M., M. H. Devoret, and J. Clarke, 1987, Phys. Rev. B **35**, 4682.
McClintock, P. V. E., and R. M. Bowley, 1991, "Vortex creation in superfluid helium-4," *Excitations in Two-Dimensional and Three-Dimensional Quantum Fluids*, edited by A. F. G. Wyatt and H. J. Lauter (Plenum Press, New York), p. 567.
McClintock, P., and R. Bowley, 1995, in *Progress in Low Temperature Physics*, edited by W. Halperin (Elsevier, New York), Vol. XIV, p. 1.
Mel'nikov, V., 1991, Phys. Rep. **209**, 1.
Monien, H., and L. Tewordt, 1986, J. Low Temp. Phys. **62**, 277.
Monien, H., and L. Tewordt, 1987, Can. J. Phys. **65**, 1388.
Muirhead, C., W. Vinen, and R. Donnelly, 1984, Phil. Trans. R. Soc. A **311**, 433.
Muirhead, C., W. Vinen, and R. Donnelly, 1985, Proc. R. Soc. A **402**, 225.
Mukharsky, Y., 2004, J. Low Temp. Phys. **134**, 731.
Mukharsky, Y., O. Avenel, and E. Varoquaux, 2004, Phys. Rev. Lett. **92**, 210402.
Musinski, D., 1973, J. Low Temp. Phys. **13**, 287.
Musinski, D. L., and D. H. Douglass, 1972, Phys. Rev. Lett. **29**, 1541.
Narayana, S., and Y. Sato, 2010, Phys. Rev. Lett. **105**, 205302.
Narayana, S., and Y. Sato, 2011, Phys. Rev. Lett. **106**, 055302.
Neumann, I. H., and R. J. Zieve, 2014, Phys. Rev. B **89**, 104521.
Neutze, R., and F. Hasselbach, 1998, Phys. Rev. A **58**, 557.
Nienhuis, G., 2001, in *Modern Challenges in Quantum Optics: Selected Papers of the First International Meeting in Quantum Optics, Santiago, Chile, August 2000*, edited by M. Orszag and J. C. Retamal, Lecture Notes in Physics Vol. 575 (Springer-Verlag, Berlin), p. 95.
Nishida, M., N. Hatakenaka, and S. Kurihara, 2002, Phys. Rev. Lett. **88**, 145302.
Nore, C., C. Huepe, and M. Brachet, 2000, Phys. Rev. Lett. **84**, 2191.
Nozières, P., and D. Pines, 1990, *The Theory of Quantum Liquids* (Addison-Wesley, Redwood City, CA), Vol. II, Chap. 5.
Onsager, L., 1949, Nuovo Cimento Suppl. **6**, 279, http://bookos.org/book/653790 and reprinted in *The Collected Works of Lars Onsager*, edited by P. C. Hemmer, H. Holden, and S. Kjelstrup Ratkje (World Scientific, Singapore, 1996).
Osheroff, D. D., W. J. Gully, R. C. Richardson, and D. M. Lee, 1972, Phys. Rev. Lett. **29**, 920.
Packard, R. E., 1972, Phys. Rev. Lett. **28**, 1080.
Packard, R. E., 1998, Rev. Mod. Phys. **70**, 641.
Packard, R. E., 2004, J. Low Temp. Phys. **135**, 471.
Packard, R. E., and S. Vitale, 1992, Phys. Rev. B **46**, 3540.
Parts, Ü., E. V. Thuneberg, G. E. Volovik, J. H. Koivuniemi, V. M. H. Ruutu, M. Heinilä, J. M. Karimäki, and M. Krusius, 1994, Phys. Rev. Lett. **72**, 3839.
Pekker, D., R. Barankov, and P. M. Goldbart, 2007, Phys. Rev. Lett. **98**, 175301.
Penrose, O., 1951, Philos. Mag. **42**, 1373.
Penrose, O., and L. Onsager, 1956, Phys. Rev. **104**, 576.
Pereverzev, S. V., and G. Eska, 2001, J. Low Temp. Phys. **124**, 383.

Perron, J. K., M. O. Kimball, K. P. Mooney, and F. M. Gasparini, 2013, Phys. Rev. B **87**, 094507.
Pitaevskii, L., 1961, J. Exp. Theor. Phys. USSR **40**, 646 [Sov. Phys. JETP, **13**, 451 (1961)].
Pomeau, Y., and S. Rica, 1993, Phys. Rev. Lett. **71**, 247.
Putterman, S., 1974, *Superfluid Hydrodynamics* (North-Holland, Amsterdam) in the Preface.
Putterman, S., and I. Rudnick, 1971, Phys. Today **24**, No. 8, 39.
Rainer, D., and P. A. Lee, 1987, Phys. Rev. B **35**, 3181.
Rayfield, G. W., and F. Reif, 1964, Phys. Rev. **136**, A1194.
Reppy, J., and C. Lane, 1965, Phys. Rev. **140**, A106.
Rica, S., 2001, in *Quantized Vortex Dynamics and Superfluid Turbulence*, edited by C. Barenghi, R. Donnelly, and W. Vinen, Lecture Notes in Physics, Vol. 571 (Springer-Verlag, Berlin), p. 258.
Richards, P. L., 1970, Phys. Rev. A **2**, 1532.
Richards, P. L., and P. W. Anderson, 1965, Phys. Rev. Lett. **14**, 540.
Rips, I., and E. Pollak, 1990, Phys. Rev. A **41**, 5366.
Rizzi, G., and M. L. Ruggiero, 2004, *Relativity in Rotating Frames* (Springer-Verlag, Heidelberg), p. 179, http://digilander.libero.it/solciclos/.
Rizzi, G., and M. L. Ruggiero, 2003a, Gen. Relativ. Gravit. **35**, 1745.
Rizzi, G., and M. L. Ruggiero, 2003b, Gen. Relativ. Gravit. **35**, 2129.
Roberts, P. H., and R. J. Donnelly, 1970, Phys. Lett. **31A**, 137.
Roberts, P. H., and J. Grant, 1971, J. Phys. A: Gen. Phys. **4**, 55.
Rudnick, I., 1973, Phys. Rev. A **8**, 1969.
Saba, M., T. A. Pasquini, C. Sanner, Y. Shin, W. Ketterle, and D. E. Pritchard, 2005, Science **307**, 1945.
Saffman, P. G., 1992, *Vortex Dynamics* (Cambridge University Press, Cambridge, England).
Salomaa, M. M., and G. E. Volovik, 1987, Rev. Mod. Phys. **59**, 533.
Salomaa, M. M., and G. E. Volovik, 1988, Phys. Rev. B **37**, 9298.
Sato, Y., 2014, C.R. Phys. **15**, 898.
Sato, Y., E. Hoskinson, and R. E. Packard, 2006, Phys. Rev. B **74**, 144502.
Sato, Y., E. Hoskinson, and R. E. Packard, 2007, J. Low Temp. Phys. **149**, 222.
Sato, Y., A. Joshi, and R. E. Packard, 2008, Phys. Rev. Lett. **101**, 085302.
Sato, Y., and R. E. Packard, 2012, Rep. Prog. Phys. **75**, 016401.
Schofield, Jr., G., 1971, Ph.D. thesis (University of Michigan—Ann Arbor), unpublished.
Schwab, K., N. Bruckner, and R. E. Packard, 1997, Nature (London) **386**, 585.
Schwab, K., N. Bruckner, and R. E. Packard, 1998, J. Low Temp. Phys. **110**, 1043.
Schwab, K., J. C. Davis, and R. E. Packard, 1996, Czech. J. Phys. **46**, 2739, Pt. 5.
Schwab, K., J. Steinhauer, J. C. Davis, and R. E. Packard, 1996, J. Microelectromech. Syst. **5**, 180.
Schwarz, K. W., 1978, Phys. Rev. B **18**, 245.
Schwarz, K. W., 1981, Phys. Rev. Lett. **47**, 251.
Schwarz, K. W., 1983, Phys. Rev. Lett. **50**, 364.
Schwarz, K. W., 1985, Phys. Rev. B **31**, 5782.
Schwarz, K. W., 1990, Phys. Rev. Lett. **64**, 1130.
Schwarz, K. W., 1992, Phys. Rev. Lett. **69**, 3342.
Schwarz, K. W., 1993a, J. Low Temp. Phys. **93**, 1019.
Schwarz, K. W., 1993b, Phys. Rev. Lett. **71**, 259.
Schwarz, K. W., and J. R. Rozen, 1991, Phys. Rev. B **44**, 7563.
Shapiro, S., 1963, Phys. Rev. Lett. **11**, 80.
Shifflett, G., and G. Hess, 1995, J. Low Temp. Phys. **98**, 591.
Silaev, M. A., 2012, Phys. Rev. Lett. **108**, 045303.
Silveri, M., T. Turunen, and E. Thuneberg, 2014, Phys. Rev. B **90**, 184513.
Simmonds, R. W., A. Marchenkov, S. Vitale, J. C. Davis, and R. E. Packard, 2000, Phys. Rev. Lett. **84**, 6062.
Smerzi, A., S. Raghavan, S. Fantoni, and S. Shenoy, 2001, Eur. Phys. J. B **24**, 431.
Soininen, P. I., N. Kopnin, and M. Salomaa, 1991, Europhys. Lett. **14**, 49.
Soininen, P. I., N. Kopnin, and M. Salomaa, 1992a, Europhys. Lett. **17**, 429.
Soininen, P. I., N. Kopnin, and M. Salomaa, 1992b, Physica B (Amsterdam) **178**, 318.
Sols, F., 1994, Physica B (Amsterdam) **194–196**, 1389.
Sonin, E., 1987, Rev. Mod. Phys. **59**, 87.
Sonin, E., 1994, J. Low Temp. Phys. **97**, 145.
Sonin, E., 1995, Physica B (Amsterdam) **210**, 234.
Sonin, E., 1997, Phys. Rev. B **55**, 485.
Sonin, E., V. Geshkenbein, A. van Otterlo, and G. Blatter, 1998, Phys. Rev. B **57**, 575.
Sonin, E., and M. Krusius, 1994, in *The Vortex State*, edited by N. Bontemps *et al.* (Kluwer Academic Publishers, Dordrecht), p. 193.
Sonin, E. B., 2015, "Dynamics of quantised vortices in superfluids" (unpublished).
Stedman, G. E., 1997, Rep. Prog. Phys. **60**, 615.
Steinhauer, J., K. Schwab, Y. Mukharsky, J. Davis, and R. E. Packard, 1995, Phys. Rev. Lett. **74**, 5056.
Stirling, W. G., R. Scherm, P. A. Hilton, and R. A. Cowley, 1976, J. Phys. C **9**, 1643.
Stringari, S., 2001, Phys. Rev. Lett. **86**, 4725.
Sudraud, P., P. Ballongue, E. Varoquaux, and O. Avenel, 1987, J. Appl. Phys. **62**, 2163.
Sukhatme, K., Y. Mukharsky, T. Chui, and D. Pearson, 2001, Nature (London) **411**, 280.
Svistunov, B., 1995, Phys. Rev. B **52**, 3647.
Thuneberg, E., 1988, Europhys. Lett. **7**, 441.
Thuneberg, E., 2005, "Theory of Josephson phenomena in superfluid 3He," arXiv:cond-mat/0509504.
Thuneberg, E. V., J. Kurkijärvi, and J. Sauls, 1990, Physica B (Amsterdam) **165&166**, 755.
Tilley, D., and J. Tilley, 1990, *Superfluidity and Superconductivity* (IOP Publishing Ltd, Bristol), 3rd ed.
Tisza, L., 1938a, Nature (London) **141**, 913.
Tisza, L., 1938b, Compt. Rend. Acad. Sciences (Paris) **207**, 1035.
Tisza, L., 1938c, Compt. Rend. Acad. Sciences (Paris) **207**, 1186.
Trela, W., and W. Fairbank, 1967, Phys. Rev. Lett. **19**, 822.
Tsubota, M., T. Araki, and S. K. Nemirovskii, 2000, Phys. Rev. B **62**, 11751.
Tsubota, M., and M. Kobayashi, 2009, *Progress in Low Temperature Physics* (Elsevier, Amsterdam), Vol. IX, Chap. 1, and references therein.
Tsubota, M., and S. Maekawa, 1994, Physica B (Amsterdam) **194–196**, 721.
Ullah, S., and A. Fetter, 1989, Phys. Rev. B **39**, 4186.
Varoquaux, E., 2000, in *Topological Defects and the Non-Equilibrium Dynamics of Symmetry Breaking Phase Transitions*, edited by Y. Bunkov and H. Godfrin (Kluwer Academic Publishers, Dordrecht), p. 303.
Varoquaux, E., 2001, in *Bose-Einstein Condensates and Atom Lasers*, edited by A. Aspect and J. Dalibard, C.R. Acad. Sci. Paris, t.2, Série IV (Elsevier, Paris), p. 531.
Varoquaux, E., 2006, C.R. Phys. **7**, 1101.
Varoquaux, E., and O. Avenel, 1994, Physica B (Amsterdam) **197**, 306.

Varoquaux, E., and O. Avenel, 1996a, Phys. Rev. Lett. **76**, 1180.
Varoquaux, E., and O. Avenel, 1996b, Czech. J. Phys. **46**, Suppl. S1, 41.
Varoquaux, E., and O. Avenel, 2003, Phys. Rev. B **68**, 054515.
Varoquaux, E., O. Avenel, M. Bernard, and S. Burkhart, 1995, J. Low Temp. Phys. **101**, 821.
Varoquaux, E., O. Avenel, P. Hakonen, and Y. Mukharsky, 1998, Physica B (Amsterdam) **255**, 55.
Varoquaux, E., O. Avenel, P. Hakonen, and Y. Mukharsky, 1999, in *Quantum Coherence and Decoherence—ISQM—Tokyo '98*, edited by Y. Ono and K. Fujikawa (Elsevier Science B.V., Amsterdam), p. 287.
Varoquaux, E., O. Avenel, P. Hakonen, and Y. Mukharsky, 2000, Physica B (Amsterdam) **284–288**, 87.
Varoquaux, E., O. Avenel, G. Ihas, and R. Salmelin, 1992, Physica B (Amsterdam) **178**, 309.
Varoquaux, E., O. Avenel, and M. Meisel, 1987, Can. J. Phys. **65**, 1377.
Varoquaux, E., O. Avenel, Y. Mukharsky, and P. Hakonen, 2001, in *Quantized Vortex Dynamics and Superfluid Turbulence*, edited by C. Barenghi, R. Donnelly, and W. Vinen, Lecture Notes in Physics Vol. 571 (Springer-Verlag, Berlin), p. 36.
Varoquaux, E., G. Ihas, O. Avenel, and R. Aarts, 1993, Phys. Rev. Lett. **70**, 2114.
Varoquaux, E., M. Meisel, and O. Avenel, 1986, Phys. Rev. Lett. **57**, 2291.
Varoquaux, E., and G. Varoquaux, 2008, Usp. Fiz. Nauk **178**, 217 [Phys. Usp. **51**, 205 (2008)].
Varoquaux, E., W. Zimmermann, Jr., and O. Avenel, 1991, "Phase-slippage studies of the critical velocity in Helium-4," *Excitations in Two-Dimensional and Three-Dimensional Quantum Fluids*, edited by A. F. G. Wyatt and H. J. Lauter (Plenum Press, New York), p. 343.
Verbeek, H., E. V. Spronsen, H. Mars, H. V. Beelen, R. D. B. Ouboter, and K. W. Taconise, 1974, Physica (Utrecht) **73**, 621.
Viljas, J., and E. Thuneberg, 1999, Phys. Rev. Lett. **83**, 3868.
Viljas, J., and E. Thuneberg, 2002a, J. Low Temp. Phys. **129**, 423.
Viljas, J., and E. Thuneberg, 2002b, Phys. Rev. B **65**, 064530.
Viljas, J. K., 2005, Phys. Rev. B **71**, 064509.
Viljas, J. K., and E. V. Thuneberg, 2004a, Phys. Rev. Lett. **93**, 205301.
Viljas, J. K., and E. V. Thuneberg, 2004b, J. Low Temp. Phys. **136**, 329.
Vinen, W., 1961, Proc. R. Soc. A **260**, 218.
Vinen, W., 1963, in *Liquid Helium*, edited by G. Careri (Academic Press, New York), p. 336.
Vinen, W., 1966, in *Quantum Fluids* edited by D. F. Brewer (North-Holland, Amsterdam), p. 74.
Vinen, W., 1968, Rep. Prog. Phys. **31**, 61.
Vollhardt, D., and P. Wölfle, 1990, *The Superfluid Phases of Helium 3* (Taylor & Francis, London).
Volovik, G. E., 1972, Zh. Eksp. Teor. Fiz. **15**, 116 [JETP Lett. **15**, 81 (1972)].
Volovik, G., 1997, JETP Lett. **65**, 217.
Volovik, G. E., 2003, *The Universe in a Helium Droplet* (Oxford University Press, Oxford), Chap. 31.
Waxman, D., and A. Leggett, 1985, Phys. Rev. B **32**, 4450.
Wheatley, J., 1975a, Rev. Mod. Phys. **47**, 415.
Wheatley, J., 1975b, in *The Helium Liquids*, edited by J. Armitage and I. Farquhar (Academic Press, London), p. 241.
Whitmore, S., and W. Zimmermann, Jr., 1968, Phys. Rev. **166**, 181.
Wilks, J., 1967, *The Properties of Liquid and Solid Helium* (Clarendon Press, Oxford).
Wirth, F. H., and W. Zimmermann, Jr., 1981, Physica B+C (Amsterdam) **107**, 579.
Yang, C. N., 1962, Rev. Mod. Phys. **34**, 694.
Yang, C. N., 2003, Int. J. Mod. Phys. A **18**, 1.
Yip, S.-K., 1999, Phys. Rev. Lett. **83**, 3864.
Zapata, I., F. Sols, and A. J. Leggett, 2003, Phys. Rev. A **67**, 021603.
Zhang, W., and Z. D. Wang, 2001, Phys. Rev. B **64**, 214501.
Zieve, R. J., Y. Mukharsky, J. D. Close, J. C. Davis, and R. E. Packard, 1992, Phys. Rev. Lett. **68**, 1327.
Ziff, R. M., G. E. Uhlenbeck, and M. Kac, 1977, Phys. Rep. **32**, 169.
Zimmermann, Jr., W., 1993a, J. Low Temp. Phys. **91**, 219.
Zimmermann, Jr., W., 1993b, J. Low Temp. Phys. **93**, 1003.
Zimmermann, Jr., W., 1994, Physica B (Amsterdam) **194–196**, 585.
Zimmermann, Jr., W., 1996, Contemp. Phys. **37**, 219.
Zimmermann, Jr., W., O. Avenel, and E. Varoquaux, 1990, Physica B (Amsterdam) **165–166**, 749.
Zimmermann, Jr., W., C. A. Lindensmith, and J. A. Flaten, 1998, J. Low Temp. Phys. **110**, 497.